

5. SITE 1264¹

Shipboard Scientific Party²

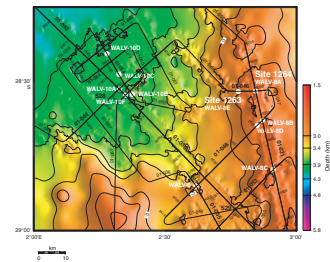
INTRODUCTION

Site 1264 (proposed Site WALV-8A; seismic lines GeoB 01-031, common depth point [CDP] 7884, and GeoB 01-046, CDP 1047) is located at a water depth of 2507 m near the crest of a north-south-trending segment of Walvis Ridge (Fig. F1). The site is ~52 m deeper than Deep Sea Drilling Project (DSDP) Site 525 to the southwest, where a 574-m-thick sedimentary sequence was recovered during previous drilling (Moore, Rabinowitz, et al., 1984). All sediments in the sequence are rich in biogenic carbonate. The Neogene section at Site 525 is truncated by a hiatus at 270 meters below seafloor (mbsf) so that upper Oligocene sediments overlie middle Eocene sediments. The upper Oligocene–Pleistocene sequence consists of nannofossil- and foraminifer-bearing nannofossil ooze. The Paleogene section includes nannofossil- and foraminifer-bearing nannofossil ooze and chalk and extends to 452 mbsf. DSDP Site 525 was drilled using a combination of the hydraulic piston corer and rotary drilling.

Our main objective for this site was the recovery of undisturbed upper Oligocene–Pleistocene sediments with the emphasis on the recovery of Neogene sediments to complement the recovery of a Paleogene section at nearby Site 1263. The combined sections from Sites 1263 and 1264 thus cover the Cenozoic at the shallow end of the Leg 208 depth transect. We planned to recover 100% of the sedimentary section in multiple holes to make it possible to establish a cyclostratigraphy and develop an astronomically tuned timescale. We aimed to fully document the thermal and chemical evolution of the South Atlantic during the Neogene, including the early Miocene Climatic Optimum.

To this end, Site 1264 was located in an area where total sediment thickness is estimated to be 621 m (velocity = 1.9 m/ms; 650 ms two-way travelttime [TWT] below seafloor). The seismic profiles show a series of reflectors ($R_{O/M}$, R_1 , $R_{P/E}$ and $R_{K/P}$) that can be traced from Site 525 to Sites 1264 and 1263 and indicate that the Eocene/Oligocene (E/O) un-

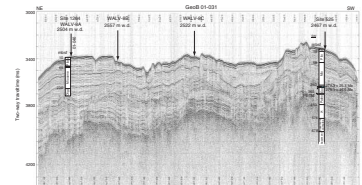
F1. Locations of Sites 1263 and 1264 and alternate sites, p. 22.



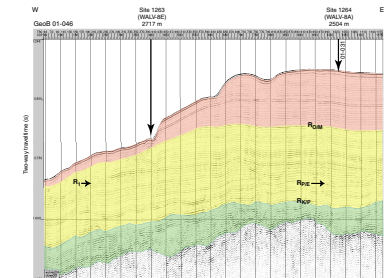
conformity (R_1) disappears laterally away from Site 525 (Figs. F2, F3). The E/O unconformity at Site 525 is represented in seismic line GeoB 01-031 as a zone of high amplitude and truncated reflectors. This zone tapers or fades toward Sites 1264 and 1263. At Site 1264, the shallowest of the distinct reflectors, $R_{O/M}$ (250 ms TWT below seafloor), is just below the Oligocene/Miocene (O/M) boundary. Deeper in the profile, $R_{P/E}$ (484 ms TWT below seafloor) represents the Paleocene/Eocene (P/E) boundary and $R_{K/P}$ (580 ms TWT below seafloor) represents the Cretaceous/Paleogene (K/P) boundary. The correlation of reflectors from DSDP Site 525 suggests the E/O boundary is at ~380 mbsf (velocity = 1.8 m/ms; 400 ms TWT below seafloor), indicating a thick upper Paleogene–Neogene sequence at Site 1264.

Coring in two holes at Site 1264 yielded a 280-m-thick sequence of carbonate-rich lower Oligocene to Pleistocene pelagic sediments (see “Site 1264,” p. 18 in “Site Summaries” in the “Leg 208 Summary” chapter). With the exception of a condensed interval in the middle Miocene and an unconformity in the upper Miocene, the 273-m-thick section is stratigraphically complete and exhibits subtle bedding cycles (expressed in core logs) throughout. The O/M boundary was recovered intact at 230 mbsf.

F2. Site 1264 on line GeoB 01-031, p. 23.



F3. Line GeoB 01-046 and Sites 1263 and 1264 with ages, p. 24.



OPERATIONS

The vessel was positioned at Site 1264 (proposed Site WALV-8A) at 1310 hr on 5 April 2003. Coring intervals, times, nominal recovery rates, core barrels that required drillover to be released from the sediment, and the deployments of the Advanced Piston Corer Temperature (APCT) tool, Tensor core orientation tool, and nonmagnetic core barrel are listed in Table T1.

Hole 1264A

The bit was placed at a depth of 2518 meters below rig floor (mbrf), and Hole 1264A was initiated with the advanced piston corer (APC) at 1505 hr on 5 April. The estimated seafloor depth calculated from the recovery of Core 208-1264A-1H was 2518.2 mbrf. The APC advanced without incident to the target depth of 280.7 mbsf (Table T1). One interval was advanced by recovery (256.3–261.7 mbsf; Core 208-1264-28H). The bit was pulled clear of the seafloor at 2155 hr on 6 April, and the vessel moved 20 m north of Hole 1264A.

Hole 1264B

Prior to initiating Hole 1264B, a bottom water temperature measurement was obtained with the APCT at 2513 mbrf. Core 208-1264B-1H was cored with the bit placed at 2513 mbrf. The estimated seafloor depth calculated from the recovery of the first core was 2515.2 mbrf. Piston coring advanced without incident to the target depth of 282.8 mbsf. The bit cleared the seafloor at 0350 hr on 8 April.

Hole 1264C

Hole 1264C was drilled to confirm the seafloor depth. Core 208-1264C-1H was retrieved at 0430 hr on 8 April, with the bit at 2509 mbrf. The calculated seafloor depth, based upon a 3.0-m recovery, was

T1. Coring summary, p. 54.

2515.5 mbrf, only 0.3 m deeper than the calculated seafloor depth from Core 208-1264B-1H.

The cored interval at Site 1264 was 566 m, and the recovered interval was 564 m (average nominal recovery = 99%). Six downhole temperature measurements (Hole 1264A: 38–123 mbsf and Hole 1264B: 102–197 mbsf) and one bottom water temperature measurement (Hole 1262B) taken with the APCT yielded an initial temperature gradient estimate of 1.5°C/100 m. The vessel left Site 1264 at 1140 hr on 8 April.

COMPOSITE DEPTH

Magnetic susceptibility (MS) and point sediment lightness (L^*) data collected from Holes 1264A and 1264B at 2.5-cm intervals were used to construct the composite section for Site 1264 (Figs. F4, F5). The 600 nm (orange) to 450 nm (blue) ratio of the color reflectance data was primarily used for core-to-core correlation and to construct the composite section in the carbonate-rich sediments from ~25–130 meters composite depth (mcd). The depth offsets that define the composite section for Site 1264 are given in Table T2.

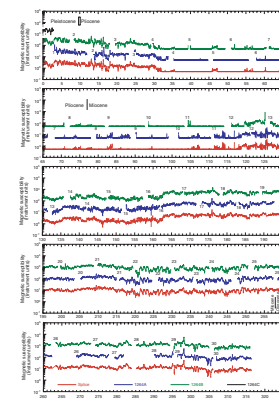
The composite depths of Cores 208-1264A-26H, 208-1264B-27H, 208-1264A-28H, and 208-1264B-29H were calculated using 11% and 12% growth rates for the mcd scale relative to the mbsf scale of Holes 1264A and 1264B, respectively (Fig. F6). This rate is based on the correlation of Cores 208-1264A-1H through 25H and 208-1264B-1H through 25H in the depth interval from 0 to 260 mcd. The composite data show that the cores from Site 1264 provide an almost continuous sequence from the seafloor down to 316.5 mcd, the lower Oligocene (Core 208-1264A-30H). Following construction of the composite depth section for Site 1264, a single spliced record was assembled from the aligned core intervals from the two parallel holes (Table T3). The presence of short cores (208-1264A-25H, 27H, and 28H) and a lack of overlap between the base of Core 208-1264A-29H and the top of Core 208-1264B-30H cause four gaps to occur in the spliced record. These gaps were bridged by applying the average growth rate of 14% to the core-top depths in mbsf. Most of the cores were not significantly stretched, squeezed, or disturbed by the coring process, and as a result, the color and MS cycles were reasonably well aligned between holes (e.g., Fig. F4), although the mcd values of the same stratigraphic horizon in alternate holes may not be exactly the same.

The O/M boundary interval in the composite was taken from Core 208-1264B-25H. The Site 1264 splice (Table T3) can be used as a guide to sample a single sedimentary sequence between the seafloor and 316 mcd and was used to plot other data sets from this site.

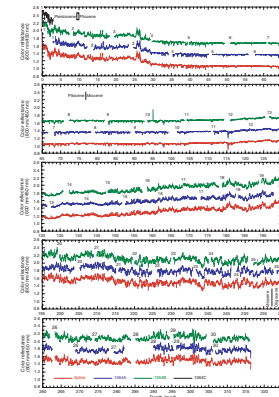
LITHOSTRATIGRAPHY

Three holes were drilled at Site 1264. Hole 1264A was drilled to a depth of 316.5 mcd (280.9 mbsf); Hole 1264B was drilled to a depth of 316.1 mcd (283.2 mbsf). One core was taken in Hole 1264C to a depth of 3.1 mcd (3.0 mbsf) to recover the mudline. The major lithologies include nannofossil ooze, foraminifer-bearing nannofossil ooze, foraminifer nannofossil ooze, and nannofossil foraminifer ooze. Clay-bearing nannofossil ooze and foraminifer-bearing nannofossil chalk are present

F4. MS data, p. 25.

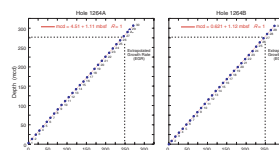


F5. Color reflectance data, p. 26.



T2. Composite depth scale, p. 56.

F6. Mcd growth rates, p. 27.



T3. Splice tie points, p. 57.

as minor lithologies. Ash-bearing nannofossil ooze and oxide-bearing nannofossil ooze are present as accessory lithologies. Based on visual core descriptions, color reflectance, smear slide descriptions, MS, and compressional wave (*P*-wave) velocity measurements, the sediments at Site 1264 are divided into two lithostratigraphic units, with the lower unit further divided into two subunits (Table T4; Fig. F7). Physical property data obtained from whole rounds, split cores, and smear slide data support the lithostratigraphic subdivisions (Figs. F8, F9, F10, F11, F12, F13, F14). The boundaries between lithostratigraphic units are gradational; therefore, boundary depths are approximate. Bioturbation appears rare to moderate but may not be visible in some intervals because of subtle color contrast. Measurements of natural gamma radiation (NGR), grain density, bulk density, and porosity show only minor variations downhole (Figs. F8, F11). Homogeneity of the sediments is also reflected by minor downhole variation in grain density and *P*-wave velocity. Bulk density and porosity are well correlated, indicating that bulk density variations are controlled by porosity (Fig. F12). In these carbonate-rich sediments, L^* is not controlled by the carbonate content (Fig. F9) but, rather, by other factors. For example, at Site 1264, chromaticity a^* covaries with the Mn concentration of interstitial water, implying that the quantity of trace components such as Mn oxides is exerting a strong influence on color (Fig. F14).

Description of Lithostratigraphic Units

Unit I

Interval: 208-1264A-1H-1, 0 cm, through 3H-4, 21 cm; 208-1264B-1H-1, 0 cm, through 4H-1, 29 cm; 208-1264C-1H-1, 0 cm, through 1H-CC, 18 cm

Depth: Hole 1264A: 0.0–23.5 mbsf (3.0–29.4 mcd); Hole 1264B: 0.0–26.6 mbsf (0.0–30.0 mcd); Hole 1264C: 0.0–3.0 mbsf (0.1–3.1 mcd)

Age: Pleistocene to early Pliocene

Lithology: foraminifer-bearing nannofossil ooze, foraminifer nannofossil ooze, and nannofossil foraminifer ooze

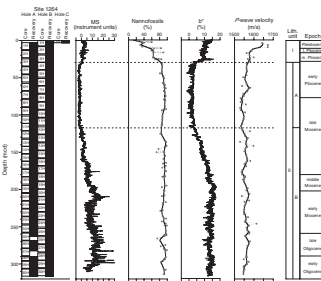
Unit I consists of pale brown nannofossil foraminifer ooze, foraminifer nannofossil ooze, and foraminifer-bearing nannofossil ooze. Based on the smear slide descriptions, the foraminifer content decreases downhole from 80% to 10% (Fig. F10) and nannofossil content shows a complementary increase. The sediment L^* and carbonate content increase downhole in accordance with the higher nannofossil content (Fig. F9). The average carbonate content is 94.6 wt%. Unit I exhibits a downhole change in color from pale brown to very pale brown, as indicated by decreasing color reflectance values on both the a^* -axis (red-green chromaticity) and b^* -axis (yellow-blue chromaticity). In addition to color change, MS, NGR, porosity, and *P*-wave velocity values all slightly decrease downhole through Unit I (Figs. F7, F8).

Unit II

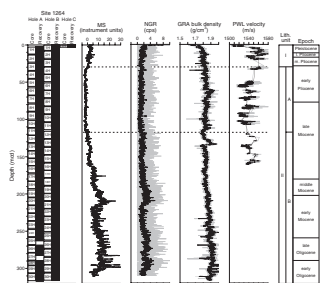
Interval: 208-1264A-3H-4, 21 cm, through 30H-CC, 15 cm; 208-1264B-4H-1, 29 cm, through 30H-CC, 12 cm

T4. Lithostratigraphic subdivisions, p. 58.

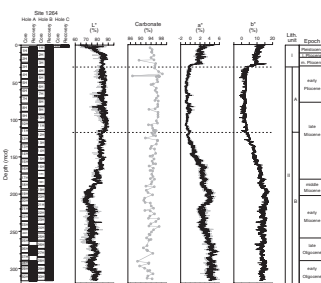
F7. Parameters used to define lithostratigraphic units, p. 28.



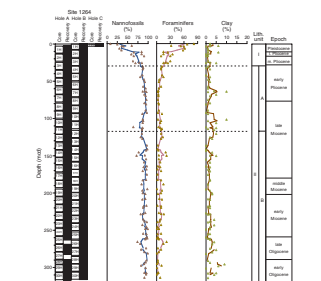
F8. MS, gamma ray attenuation bulk density, and *P*-wave velocity values, p. 29.



F9. Lightness, carbonate, and chromaticity, p. 30.



F10. Smear slide components, p. 31.



Depth: Hole 1264A: 23.5–280.9 mbsf (30.0–316.5 mcd); Hole 1264B: 26.6–283.2 mbsf (29.4–316.2 mcd)

Age: early Pliocene to early Oligocene

Lithology: nannofossil ooze and foraminifer-bearing nannofossil ooze

Unit II is characterized by high nannofossil content >75%. Dominant lithologies include nannofossil ooze and foraminifer-bearing nannofossil ooze. Clay-bearing nannofossil ooze and nannofossil chalk are reported as minor lithologies. Volcanic ash and oxides are present throughout and are occasionally abundant enough to form accessory lithologies such as ash-bearing nannofossil ooze and oxide-bearing nannofossil ooze. Density profiles show little variation except for three abrupt steps in grain density and porosity at ~135, ~165, and ~235 mcd (Fig. F11). Dramatic changes in interstitial water Fe and Mn concentrations suggest a diagenetic origin for these features. Downhole variations in chromaticity values a^* and b^* exhibit profiles similar to the interstitial water Mn content (Fig. F14). The white lithology of Subunit IIA is characterized by high Fe concentrations in the interstitial waters, whereas interstitial waters of the brownish colored Subunit IIB are characterized by high Mn concentrations.

Subunit IIA

Interval: 208–1264A-3H-4, 21 cm, through 11H-4, 109 cm; 208–1264B-4H-1, 29 cm, through 12H-2, 45 cm

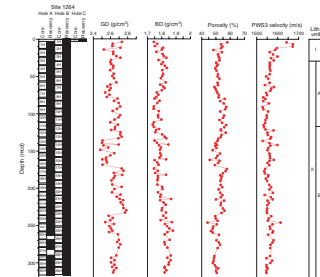
Depth: Hole 1264A: 23.5–100.4 mbsf (30.0–117.0 mcd); Hole 1264B: 26.6–103.3 mbsf (29.4–117.0 mcd)

Age: early Pliocene to late Miocene

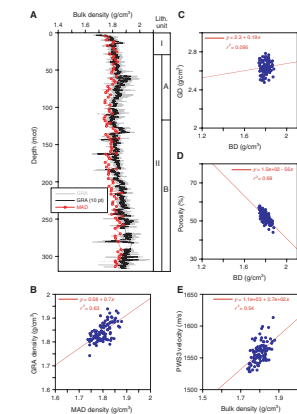
Lithology: nannofossil ooze and foraminifer-bearing nannofossil ooze.

Subunit IIA is composed of white nannofossil ooze with light bluish-gray bands alternating at a centimeter to decimeter scale (Fig. F15). Foraminifer-bearing nannofossil ooze is present as a minor lithology. The color banding likely reflects either differences in the concentration of oxides related to sediment diagenesis or a variation in clay content resulting from the balance of carbonate production vs. preservation. Contacts between colored bands and the white ooze range from sharp to slightly diffuse, and the contacts are sometimes sharp at the base and gradual at the top. In general, the banding is well preserved with only minor to moderate disruption by the drilling process. Visible bioturbation features are rare, pointing to either sediment homogeneity or post-depositional diagenetic color changes that obscured the bioturbational features. Despite obvious color oscillations in Subunit IIA, the lithologic composition and physical properties are relatively invariant. Nannofossil content is consistently >80%. The resulting high carbonate content (average = 96.1 wt%) is reflected by negative MS values (Figs. F7, F15). MS, sediment L*, and chromaticity a^* and b^* values are less variable than those in either Unit I or Subunit IIB. Despite the overall constancy of sediment properties, quasi-periodic oscillations are common within this subunit (Fig. F15). At the highest frequency, individual centimeter-scale gray bands may represent short-term orbital (precessional) or even sub-orbital cycles. Clusters of gray bands on a decimeter scale as expressed by the L* oscillations in Figure F15 may be related to precessional or oblique

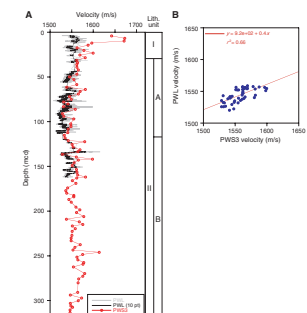
F11. Grain density, bulk density, porosity, and P -wave velocity, p. 32.



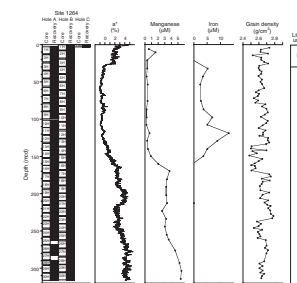
F12. Physical property measurements, p. 33.



F13. P -wave velocity data, p. 34.



F14. Chromaticity, dissolved Mn and Fe, and grain density, p. 35.



uity cycles. Lower-frequency oscillations in the MS values are very low and not reliable for frequency analysis in this interval.

Subunit IIB

Interval: 208-1264A-11H-4, 109 cm, through 30H-CC, 15 cm; 208-1264B-12H-2, 45 cm, through 30H-CC, 12 cm

Depth: Hole 1264A: 100.4–280.9 mbsf (117.0–316.5 mcd); Hole 1264B: 103.3–283.2 mbsf (117.0–316.2 mcd)

Age: late Miocene to early Oligocene

Lithology: nannofossil ooze and foraminifer-bearing nannofossil ooze

Subunit IIB is characterized by an alternation of nannofossil ooze and foraminifer-bearing nannofossil ooze on a decimeter to meter scale. Compositional changes are accompanied by color variations; slightly darker intervals are foraminifer rich. L* generally decreases downhole. Within the upper part of this subunit (117–190 mcd), a color change from light gray to pale brown is accompanied by increases in MS, NGR, and chromaticity (a* and b*) values (Figs. F8, F9). Disseminated oxide is present in trace amounts throughout this interval and persists downcore. Oxide-enriched zones are represented in several ways within the core: gray banding, gray halos surrounding mostly pale pinkish brown-colored blebs, and black concretions of oxides. X-ray diffraction analysis of Sample 208-1264A-26H-5, 25 cm, indicates that these oxide concretions comprise calcite and the Mn oxide, lithiophorite ($\text{Al}, \text{Li}\text{MnO}_2(\text{OH})_2$) (Fig. F16).

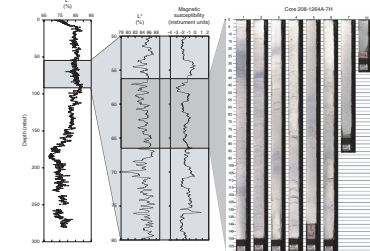
The interval from 190 to 220 mcd is dominated by pale brown foraminifer-bearing nannofossil ooze. MS, NGR, and chromaticity a* and b* values all peak in this interval (~210 mcd), whereas the mean carbonate content exhibits a subtle drop to a low average of 92.3 wt% (Fig. F9). Below 220 mcd, alternation of foraminifer-bearing nannofossil ooze and nannofossil ooze continues on a decimeter to meter scale. The color of this interval changes slightly from very pale brown within the foraminifer-rich layers to pinkish gray in the nannofossil-dominated sediments. The observed alternation of color in Subunit IIB may reflect cyclic production/preservation oscillations on orbital timescales (Fig. F17).

After the sharp decrease at ~220 mcd, MS, NGR, gamma ray attenuation bulk density, and chromaticity a* values begin to increase, whereas L* and b* values show weak trends downhole (Figs. F8, F9). This may reflect a change in the terrigenous sediment component rather than in carbonate preservation. Between 295 and 316.5 mcd, MS and NGR values decrease abruptly (Fig. F8).

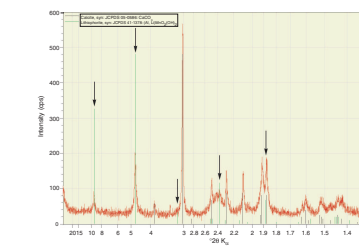
BIOSTRATIGRAPHY

Pleistocene through lower Oligocene carbonate-rich sediments were recovered at Site 1264. All samples contain nannofossils with moderate to good preservation. Planktonic foraminifers with generally good preservation are abundant. Well-preserved benthic foraminifers are rare in all samples. Preservation for all fossil groups deteriorates in the lower part of the record. Several upper Miocene nannofossil and planktonic foraminifer markers are missing because of the temperate environmental conditions at this site. Oligocene benthic foraminifer assemblages

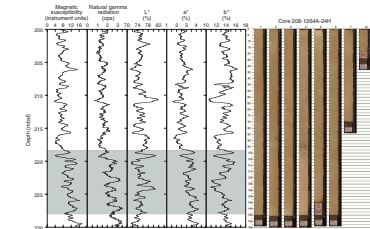
F15. L* and cyclic oscillations in L* and MS, p. 36.



F16. X-ray diffraction pattern, p. 37.



F17. Cyclic oscillations in MS, NGR, lightness, and chromaticity, p. 38.



show downslope transport and reworking. Benthic foraminifers indicate upper abyssal depths (2000–3000 m) during the late Oligocene through Pleistocene and possibly lower bathyal depths (~2000 m) during the early Oligocene.

Shipboard examination of calcareous nannofossils and planktonic foraminifers permitted preliminary zonal and stage assignments (Fig. F18; Tables T5, T6). Biochronological ages plotted against mcd delineate overall sedimentation rates (Fig. F19) (see “Age Model and Mass Accumulation Rates,” p. 19). A nearly complete Neogene and upper Oligocene section is present and was deposited at variable sedimentation rates. An upper Miocene unconformity representing ~0.6 m.y. occurs between 76.8 and 77.2 mcd. The middle Miocene is condensed and is represented between 177.3 and 203.6 mcd. The records of Sites 1263 and 1264 can be correlated over the interval 28–30 Ma, jointly providing a “complete” coverage for the last 58 m.y.

Calcareous Nannofossils

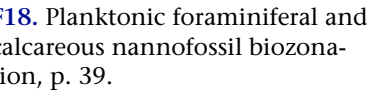
Calcareous nannofossil assemblages taken from core catcher samples of all holes and additional discrete (toothpick) samples from critical intervals were examined. The nannofossil biostratigraphy suggests that the recovered section represents an almost complete record from the upper Pleistocene–Holocene (Zones CN15 and NN21b) through the upper part of the lower Oligocene (approximately at the Zone CP18/CP17 boundary). Depth and age estimates of key biostratigraphic markers are shown in Table T5. Table T7 shows a distribution chart of the core catcher samples. Nannofossils are present throughout the section and have generally good preservation. Lower Oligocene and middle Miocene discoasterids (from 110 mcd to the bottom of the section) are overgrown with secondary calcite.

Pleistocene (0–10 mcd)

The complete succession of Pleistocene nannofossil assemblages is present in Sections 208-1264A-1H-1 through 1H-5, 208-1264B-1H, and 208-1264C-1H, including the events based on the size change of *Gephyrocapsa*. Sample 208-1264C-1H-1, 0–2 cm, has an upper Pleistocene assemblage belonging to Zone CN15 (Subzone NN21b). The Pliocene/Pleistocene boundary is placed between 9.7 and 11.4 mcd (between Samples 208-1264A-1H-5, 70 cm, and 1H-6, 70 cm) between the lowest occurrence of medium *Gephyrocapsa* spp. and the highest occurrence of *Discoaster brouweri*.

Pliocene (11–77 mcd)

Pliocene assemblages mainly consist of reticulofenestrids, sphenoliths, and discoasterids. Helicoliths and ceratholiths belonging to the genus *Amaurolithus* are common, whereas representatives of the genus *Ceratholithus* are very rare. The middle and upper Pliocene assemblages are dominated by small placoliths (2–4 µm), mainly small *Reticulofenestra* spp. and *Pseudoemiliania lacunosa* (Cores 208-1264A-2H, 3H, and 208-1264B-2H and 3H). The consistent presence of *D. brouweri*, *Discoaster brouweri* var. *triradiatus*, *Discoaster pentaradiatus*, *Discoaster surculus*, *Discoaster tamalis*, and *Discoaster asymmetricus* provided a detailed biostratigraphic subdivision of the middle–upper Pliocene (Subzones CN12d–CN12aA; Zones NN18–NN16).

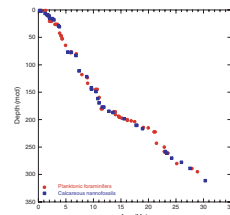


The figure is a stratigraphic column for Site 1294, spanning from the Paleocene to the Recent. The vertical axis represents Depth (m) from 0 to 300. The horizontal axis represents time, with major ticks for Paleocene, Eocene, Oligocene, Miocene, Pliocene, Pleistocene, and Holocene. The column is divided into several lithological units: Paleocene (L1), Eocene (L2-L4), Oligocene (L5-L7), Miocene (L8-L10), Pliocene (L11-L13), and Holocene (L14-L15). Biostratigraphic zones are indicated by brackets above the column, including the Paleocene (P1-P4), Eocene (E1-E4), Oligocene (O1-O4), Miocene (M1-M4), Pliocene (Pl1-Pl4), and Holocene (H1-H4). The column also shows the presence of various fossil groups: Foraminifera (F1-F15), Nannofossils (N1-N15), Radiolaria (R1-R15), and Ostracodes (O1-O15). Environmental events are marked with arrows: 'B.C. sea-levelstand' at ~150m depth, 'High subsidence of basins' at ~250m depth, and 'Resedimentation and downslope transport' at the bottom. A legend on the right defines symbols for core locations (Core, Hole A, Hole B, Hole C), Lithology (Lith.), Epoch (Epoch), Biostratigraphic Zone (Biostrat.), and Fossil Group (Foram., Nanno., Radiol., Ostrac.).

T5. Selected calcareous nannofossil datums, p. 59.

T6. Selected planktonic foraminiferal datums, p. 60.

F19. Sedimentation rates, p. 40.



T7. Range and abundance of calcareous nannofossils, p. 61.

An expanded lower Pliocene section is present between 29.4 and 77.0 mcd (Sections 208-1264A-3H-4 through 7H-6 and 208-1264B-4H-CC through 8H-CC), corresponding to Zone CN11 and Subzone CN10c (NN13–NN15). The discoasterid assemblage is characterized by *Discoaster variabilis* gr., *D. pentaradiatus*, *Amaurolithus delicatus*, and *Amaurolithus primus* and by common to abundant *Scyphosphaera* spp. The Miocene/Pliocene boundary marker *Ceratolithus acutus* is present in Sample 208-1264A-7H-6, 80 cm, and the uppermost Miocene ceratolith marker *Nicklithus amplificus* occurs in Sample 208-1264A-7H-7, 20 cm. This indicates the presence of an unconformity in Core 208-1264A-7H (within Section 6 or 7) at the Miocene–Pliocene transition, spanning a time interval of at least 0.63 m.y. and corresponding to Subzones CN10a and CN9bC.

Miocene (77 to ~258 mcd)

Miocene nannofossil assemblages are rich and diverse, and most of the Miocene zonal boundaries can be recognized (Fig. F18). The upper Miocene is characterized by the presence of common *A. primus* and *A. delicatus* (Cores 208-1264A-8H through 10H), by the absence interval (“paracme”) of *Reticulofenestra pseudoumbilicus* (Cores 208-1264A-10H and 11H), and by the presence of abundant *Minylitha convallis* and *Calcidiscus* spp. (Cores 208-1264A-11H through 13H). The upper and middle Miocene *Discoaster* assemblages are rich in species and compose a large part of the total nannofossil assemblage at Site 1264. Nevertheless, the upper Miocene *Discoaster* marker species *Discoaster quinqueramus* and *Discoaster berggrenii* are missing in the area. Therefore, the upper Miocene zonal boundaries CN10a/CN9 (NN12/NN11) and CN9/CN8 (NP11/NP10), marked by the last occurrence of *D. quinqueramus* and the first occurrence of *D. berggrenii*, respectively, were not recognized. Other discoasterid markers are present with atypical morphotypes (e.g., *Discoaster hamatus*).

The range of common *Discoaster kugleri* (11.6–11.88 Ma; Backman and Raffi, 1997) provides a distinct middle Miocene biostratigraphic marker that is consistently isochronous between low and middle latitudes (Hilgen et al., 2000). The lowest common occurrence and highest common occurrence of this species could not be determined in detail because the events occur within the break between Cores 208-1264A-16H and 17H. In the middle Miocene (~180 to ~202 mcd), the Zone CN4/CN3 (NN5/NN4) boundary was not defined because the marker *Helicosphaera ampliaperta* is absent. In the lower Miocene, *Triquetrorhabdulus carinatus* is very rare or absent; *Discoaster druggii* is missing; and the zonal boundaries NN3/NN2 and CN1c/CN1a+b (NN2/NN1) could therefore not be recognized.

The presence of *Sphenolithus disbelemnos* in Core 208-1264A-24H and the range of *Sphenolithus delphix* in Core 25H indicate that the O/M boundary is between Section 208-1264A-24H-CC and Sample 25H-1, 10 cm, and Sections 208-1264B-25H-3 and 25H-CC at ~258 mcd.

Oligocene (258–316 mcd)

The lower section of Site 1264 is placed in the upper Oligocene and the upper part of the lower Oligocene (Cores 208-1264A-25H through 30H and Sections 208-1264B-25H-CC through 28H-CC). Key elements in the observed low-diversity assemblages are the Oligocene markers *Sphenolithus ciperoensis* and *Sphenolithus distentus*. These small spheno-

liths define the bases of Zones NP24 and NP25 (Subzones CP19a and CP19b). A nannofossil assemblage with abundant *Braarudosphaera bigelowii* occurs in distinct layers in Sections 208-1264A-29H-3 and 29H-4 (299.7 and 300.8 mcd). The “*Braarudosphaera* layers” are a typical feature of the lower upper Oligocene in the South Atlantic Ocean (Roth, 1974). The assemblages mainly consist of *B. bigelowii*, with the secondary components *Dictyococcites bisectus*, *Sphenolithus predistentus*, *S. dis-*
tentus, *Sphenolithus moriformis*, *Zygrhablithus bijugatus*, and *Cyclicar-*
golithus abiseptus. The high relative abundance of *B. bigelowii* has been related to low salinity (Takayama, 1972) or eutrophication (Cuhna and Shimabukuro, 1996).

Planktonic Foraminifers

Planktonic foraminifers were examined in all core catcher samples from Holes 1264A, 1264B, and 1264C and in additional samples around critical intervals in Holes 1264A and 1264B (Tables T6, T8). Generally, planktonic foraminifers are abundant and well preserved. Reworking of planktonic foraminiferal specimens is rare, except for specimens in Sections 208-1264A-1H-CC and 30H-CC.

T8. Range and abundance of planktonic foraminifers, p. 62.

Pleistocene (0–11 mcd)

Sample 208-1264C-1H-1, 0–2 cm (mudline), contains a mixture of well-preserved subtropical and temperate Pleistocene species. The fauna is dominated by *Globorotalia crassaformis*, *Globorotalia truncatulinoides*, *Globorotalia tumida*, *Globoconella inflata*, *Globigerinoides ruber*, *Globigerinoides sacculifer*, *Globigerinella siphonifera*, *Hirsutella scitula*, *Menardella menardii*, and *Orbulina universa*.

The uppermost occurrence (top) of *Globorotalia tosaensis* (base of Subzone PT1b; 0.65 Ma) is between Samples 208-1264C-1H-1, 0–1 cm (0.1 mcd), and 1H-2, 0–1 cm (1.5 mcd). The Pliocene/Pleistocene boundary is between Sections 208-1264B-1H-CC and 208-1264A-1H-CC (7.3–12.3 mcd). We used the uppermost occurrence of *Globigerinoides extremus* to approximate the boundary because *Globigerinoides fistulosus* is absent.

Pliocene (11–77 mcd)

Many of the tropical/subtropical age-diagnostic taxa used to subdivide the upper Pliocene are missing because of the temperate environmental conditions. Boreal species (e.g., *Globoconella crassaformis*, *Globoconella conomiozea*, and *Globoconella conoidea*) dominate the assemblage. Although menardellids are extremely rare, the boundary between PL5 and PL6 could be defined by the highest occurrence of *Menardella mio-*
cenica (Kennett and Srinivasan, 1983). We did not define Subzone PL1b because the highest occurrence of *Hirsutella cibaoensis* (base of Subzone PL1b) is, according to Lourens et al. (in press), younger than the highest occurrence of *Globigerina nepenthes* (Zone PL2). Our data confirm that the highest occurrence of *H. cibaoensis* (47.3 mcd) is above the highest occurrence of *Globoturborotalita nepenthes* (52.7 mcd). All other zonal boundaries could be recognized (Fig. F18). *Dentoglobigerina altispira* and *Sphaeroidinellopsis seminulina* both have their highest occurrence in Sections 208-1264A-2H-CC and 208-1264B-3H-CC, which makes it impossible to resolve Zone PL4 (160 k.y.).

The middle/upper Pliocene boundary is between Sections 208-1264B-2H-CC and 208-1264A-2H-CC (20.8 mcd), and the lower/middle

Pliocene boundary is between Sections 208-1264A-2H-CC (23.4 mcd) and 3H-CC (26.7 mcd).

Miocene (77–258 mcd)

G. conoidea, *G. conomiozea*, *Globigerina apertura*, and *Globoturborotalita nepenthes* are typical and frequent species in the upper Miocene. The absence of *Neogloboquadrina acostaensis* prevented a division of Zones M13 and M12. The boundary between the middle and upper Miocene is between Sections 208-1264B-17-CC (178.0 mcd) and 208-1264A-17H-CC (182.5 mcd).

Middle Miocene assemblages are dominated by *Globoquadrina dehisces*, *Globorotalia archeomenardii*, and the *Praeorbulina*-*Orbulina* lineage. The tropical/subtropical zonation between ~13.45 and 8.91 Ma is not applicable because most members of the *Fohsella* lineage are missing, which is typical for this latitude (Puig, 1983; Boersma, 1984). *Fohsella peripheroacuta* and *Fohsella peripheroronda* are the only representatives of this lineage. *Menardella praemenardii* and *Menardella archeomenardii* are the only representatives of the menardellids. The absence of menardellids and foehsellids before ~11.6 Ma (below 180.3 mcd) might indicate either more subtropical conditions or a wider ecological tolerance of the founders of the lineages. Consequently, we used the transitional austral zonation (see “**Planktonic Foraminifers**,” p. 15, in “Biostratigraphy” in the “Explanatory Notes” chapter) for the middle and upper Miocene (Fig. F18). Below this level, sedimentation rates drop significantly, especially in a condensed interval between 196 and 204 mcd (corresponding to 14.7–17.5 Ma). The completeness of the sequence of foraminiferal events in this interval (especially the *Praeorbulina*-*Orbulina* lineage) points to a reduced sedimentation rate and not an unconformity. The lower/middle Miocene boundary is between Samples 208-1264B-20H-2, 78–80 cm, and 208-1264A-19H-6, 32–34 cm (202.0–202.5 mcd).

Lower Miocene assemblages contain *G. dehiscens*, *Globigerina venezuelana*, *Globigerina angustumilicata*, *Globigerina praebulloides*, *Catapsydrax dissimilis*, *Paragloborotalia pseudokugleri*, and *Paragloborotalia kugleri*. *Globigerinatella insueta* s.s. is missing, which prevents the definition of the base of Zone M3. The O/M boundary is between Section 208-1264A-24H-CC and Sample 25H-1, 32–34 cm (257.7 and 258.9 mcd).

Oligocene (258–316 mcd)

The lowermost Miocene to uppermost Oligocene sediments are potentially condensed, with 2.9 m of sediment corresponding to the time interval from 22.9 to 24.3 Ma. The tentative age model must be refined to ascertain this observation. Upper Oligocene assemblages are dominated by *G. venezuelana*, *G. praebulloides*, *Globigerina euapertura*, *G. angustumilicata*, *Paragloborotalia opima*, and *C. dissimilis*. The upper/lower Oligocene boundary is between Sections 208-1264B-27H-CC and 28H-CC (284.0–294.4 mcd). Section 208-1264A-30H-CC contains some reworked Eocene to Paleocene specimens.

Benthic Foraminifers

All core catcher samples from Hole 1264A were semiquantitatively investigated for benthic foraminifers. In addition, samples from the up-

per core in Holes 1264B and 1264C (0.1–7.3 mcd) and samples in the lower Miocene of Hole 1264B were studied (Table T9).

In all samples, benthic foraminifers are rare compared to planktonic foraminifers. Preservation is good in most samples, with the exception of Sections 208-1264A-24H-CC through 30H-CC (below 257 mcd to the bottom of the section). These contain specimens of variable preservation, with some reworked from upper Paleocene through Eocene and some indicative of downslope transport. Benthic foraminiferal assemblages indicate deposition at upper abyssal depths (2000–3000 m). Sections 208-1264A-28H-CC through 30H-CC (below 295 mcd) were probably deposited close to the upper abyssal/lower bathyal boundary (~2000 m), but paleodepth assignment is difficult because of reworking of specimens indicative of middle to lower bathyal depths.

Samples 208-1264C-1H-1, 0–2 cm, and 1H-CC (0–3 mcd) contain assemblages with common *Globocassidulina subglobosa*, *Cibicidoides wuellerstorfi*, *Cibicidoides mundulus*, *Oridorsalis umbonatus*, and *Pyrgo* spp., with varying relative abundances of the *Uvigerina peregrina* group, *Pullenia* spp., and minor *Osangularia culter*, *Bulimina rostrata*, *Bolivinita pseudothalmani*, and *Gyroidinoides* spp. These samples do not contain pleurostomellid and siphonodosariid species and were probably deposited after the “*Stilostomella* extinction” at 0.65 Ma (Hayward, 2002). At present, similar assemblages occur along Walvis Ridge between ~2000 and 3300 m (Schmiedl et al., 1997), with common *G. subglobosa* indicative of locations on the slopes of ridges. At these depths, bottom waters are derived from northern sources (North Atlantic Deep Water), as indicated by the common presence of *C. wuellerstorfi*.

Assemblages between 7 and 172 mcd (Sections 208-1264B-1H-CC through 208-1264A-16H-CC) are very similar to those in the upper samples but contain pleurostomellid and siphonodosariid species in addition to those listed (Table T9). The upper Miocene *incertae sedis* “*Bulava indica*” (probably a pteropod) occurs in Section 208-1264A-16H-CC (172 mcd).

C. wuellerstorfi has its lowest occurrence between Sections 208-1264A-16H-CC and 17H-CC (172 and 183 mcd; 11.0–11.9 Ma). This first appearance of *C. wuellerstorfi* at Site 1264 is considerably later than its first appearance in the Atlantic Ocean at ~13.7 Ma (e.g., Thomas, 1986; age recalculated to the Leg 208 timescale). Therefore the first appearance of common *C. wuellerstorfi* at Site 1264 probably indicates that northern source deep water reached this location at that time.

The benthic foraminiferal assemblages show a gradual turnover in species composition between Sections 208-1264A-17H-CC and 19H-CC (183–204 mcd) at a time of global deep-sea benthic foraminiferal assemblage change (upper lower through middle Miocene; e.g., Boltovskoy and Boltovskoy, 1989). Above this transition, typical middle Miocene and younger species such as *Laticarinina pauperata*, the *U. peregrina* group, *B. rostrata*, miliolid species (mainly *Pyrgo* spp.), and *Melonis* spp. are present, whereas below the transition, species typical of deposits older than middle Miocene occur (e.g., *Buliminella grata*, *Nonion havanense*, *Vulvulina spinosa*, and *Bolivinoides huneri*) and the abundance of siphonodosariid taxa is high (van Morkhoven et al., 1986; Thomas, 1986).

Between 258 and 282 mcd, evidence for reworking is convincing in some samples because they contain broken and worn specimens of *Nuttallides truempyi*, which has its uppermost appearance in the Eocene. In other samples there are no specimens older than Oligocene, but reworking is indicated by the presence of very large broken, bored, and

T9. Selected benthic foraminifers, p. 63.

abraded specimens of long-lived, thick-shelled specimens (e.g., *O. umbonatus*, various nodosarids, and *Siphonodosaria pomuligera*).

Between 210 and 212 mcd (Samples 208-1264B-21H-1, 78–80 cm, and 21H-2, 78–80 cm), benthic foraminiferal assemblages contain high relative abundances (>75%) of small smooth-walled bolivinid species. These occurrences reflect an unusual event in benthic foraminiferal faunas in the eastern Atlantic and western Indian Oceans, which is called the high abundance of bolivinids (HAB) event (Smart and Murray, 1994; Smart and Ramsay, 1995). The HAB event is coeval with the range of the calcareous nannofossil *Sphenolithus belemnos* (18.92–17.89 Ma in the Leg 208 timescale) at North Atlantic Site 608 (Thomas, 1987). The cause of this benthic event is not understood because in the present oceans, such high relative abundances of bolivinids occur within oxygen minimum zones in regions of upwelling and high productivity and the sedimentary record shows no indication of low-oxygen conditions during the HAB event.

Sections 208-1264A-28H-CC through 30H-CC (below 295 mcd) contain typical upper abyssal to lower bathyal upper Eocene through Oligocene assemblages with *Bulimina semicostata*, *Bulimina elongata*, *C. mundulus*, *O. umbonatus*, *Gyroidinoides* spp., *N. havanense*, common *Siphonodosaria* spp., as well as unilocular, laevidentalinid, and pleurosatomellid taxa and rare *V. spinulosa*. These samples contain specimens indicating downslope transport and reworking as described above for Sections 208-1264A-24H-CC through 27H-CC. As a result of this reworking, the paleodepth assignment to the boundary between upper abyssal and lower bathyal is not certain.

PALEOMAGNETISM

Drilling and Core Orientation

Every other core at Site 1264 was recovered with a nonmagnetic core barrel until the first barrel had to be drilled over (see Table T1; “[Operations](#),” p. 2). As at other sites, we noticed no obvious differences in the magnetic data between sediments recovered with the nonmagnetic core barrel and those with a standard barrel. All APC cores taken in Holes 1264A and 1264B were successfully oriented with the Tensor tool, with the exception of the top two cores in each hole (see “[Operations](#),” p. 2; Table T1).

Archive-Half Measurements

The archive halves of 61 cores from Holes 1264A, 1264B, and 1264C were measured in the pass-through magnetometer. Natural remanent magnetization (NRM) was measured on all cores. Most cores were demagnetized at 10 and 15 mT. As at the other sites, a strong vertical overprint is largely removed in most cases by demagnetization to 10 mT. Both the archive and working halves of Section 208-1264A-24H-4 were demagnetized to 15 mT as part of an experiment to determine the source of bias in the declination data (see “[Paleomagnetism](#),” p. 20, in the “Explanatory Notes” chapter).

Remanent Magnetization Intensity

After alternating-field (AF) demagnetization to 15 mT, the depositional remanent magnetization (DRM) of sediments varies with depth between 10^{-4} and 10^{-5} A/m in the upper 30 mcd (lithostratigraphic Unit I) and between 10^{-4} and 10^{-5} A/m from 30 to 120 mcd (lithostratigraphic Subunit IIA) and is on the order of 10^{-2} A/m below 120 mcd (lithostratigraphic Subunit IIB) (Fig. F20). In lithostratigraphic Subunit IIA, the average intensity of the sediments is roughly two orders of magnitude lower than the average from the remainder of the section (Fig. F20). These low intensities are just above the stated resolution of the pass-through magnetometer for split cores ($\sim 2 \times 10^{-5}$ A/m), resulting in erratic directions and intensities. This interval is also characterized by negative initial MS values (Fig. F21), reflecting the dominance of diamagnetic calcite of the MS signal.

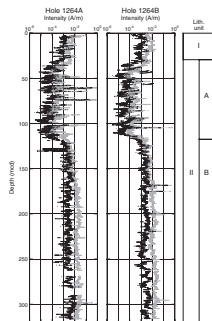
Lithostratigraphic Subunit IIB (below ~120 mcd) can be subdivided on the basis of magnetic parameters such as DRM normalized by MS (nDRM_{15 mT}) and the differential component of magnetization (dDRM), reflecting the low-coercivity fraction (≤ 10 or ≤ 15 mT). The interval between 120 and 164 mcd is characterized by nDRM_{15 mT} values nearly an order of magnitude greater than the interval below 164 mcd (Fig. F22). This appears to result primarily from lower MS values in the upper interval (Fig. F21). The upper interval is also characterized by a significant decrease in the low-coercivity (<15 mT) component (Fig. F20) when compared to the interval below. Together, these observations imply a change in magnetic mineralogy and/or grain size (probably resulting from diagenesis), rather than a long-term change in the average geomagnetic field intensity.

Further evidence for diagenetic changes can be observed in the transition (~155–170 mcd) between the two intervals in Subunit IIB described above. Downhole records of the interstitial water iron and manganese concentrations, grain density, and color reflectance exhibit changes in the same interval (see Fig. F14; “Lithostratigraphy,” p. 3). Diagenesis can result in the partial dissolution of iron oxide minerals (especially magnetite) and the formation of iron manganese oxides (such as jacobsite) or iron sulfide minerals (such as pyrite, pyrrhotite, or greigite). This interpretation may explain the increase in interstitial water iron combined with a decrease in manganese in this interval (see Fig. F14; “Lithostratigraphy,” p. 3). However, constraints on magnetic mineralogy await shore-based analysis of discrete samples.

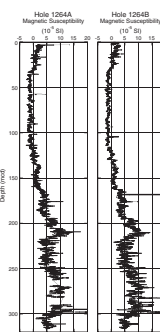
Magnetostratigraphy

As at Site 1263, the magnetostratigraphy at Site 1264 is difficult to interpret. In the upper 30 m, it is possible to make preliminary chron assignments for the Pliocene–Pleistocene (Fig. F23A; Table T10). These assignments correspond (in depth) to the available biostratigraphic datums (Tables T5, T15). No magnetostratigraphic interpretations were made for the interval of low magnetization from 30 to 120 mcd, where the directional record is extremely erratic. Below this interval of low magnetization, the inclination record becomes less erratic (Fig. F23B, F23C, F23D) but shows a bias toward negative values (normal polarity), as at Site 1263. Some tentative chron assignments have been made largely based on biostratigraphic datums, but, in general, little confidence is placed in the inclination record at this site below the Pliocene.

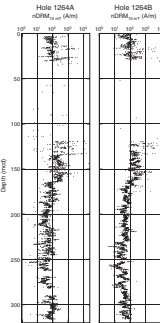
F20. Intensities, 0- and 15-mT demagnetization, p. 41.



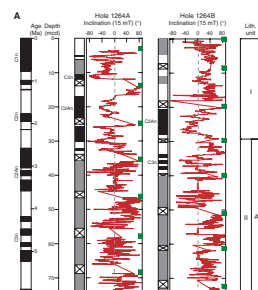
F21. Downhole variation in initial MS, p. 42.



F22. Downhole variation of nDRM_{15 mT}, p. 43.



F23. Magnetostratigraphic interpretation, p. 44.



T10. Magnetostratigraphic age-depth tie points, p. 65.

GEOCHEMISTRY

Volatile Hydrocarbons

The concentration of CH₄ (C₁) in 28 headspace samples analyzed from Site 1264 was at an atmospheric background level (range = 1.6–2.0 µL/L), and no hydrocarbon gases higher than C₁ were detected.

Interstitial Water Chemistry

Interstitial waters from 29 samples were collected at Site 1264: 28 from Hole 1264A (10.4–314.2 mcd) and 1 from Hole 1264B (5.9 mcd). Chemical constituents were determined according to the procedures outlined in “Geochemistry,” p. 23, in the “Explanatory Notes” chapter. Results of the chemical analyses are presented in Table T11.

T11. Pore water analyses, p. 66.

pH, Salinity, Alkalinity, Chloride, and Sodium

The pH of pore waters at Site 1264 ranges from 7.3 to 7.6 (average = 7.4 ± 0.1) (Table T11). All values are lower than the average seawater value of 8.1, and the data exhibit no depth-dependent trend. Salinity values range from 34.5 to 35.5 g/kg.

Alkalinity decreases slightly from 2.6 mM in the shallowest sample at 5.9 mcd to 2.3 mM at 303.7 mcd (Fig. F24A). Two samples had values of 3.3 mM at 10.4 and 53.6 mcd.

The pore water chloride concentration generally increases with depth from a minimum value of 559 mM (5.9 mcd) to 573 mM (292.2 mcd) (Fig. F24B), although it shows significant variability about the mean of 565 mM (standard deviation = 5 mM). One sample contains a lower chloride value of 555 mM (212.6 mcd).

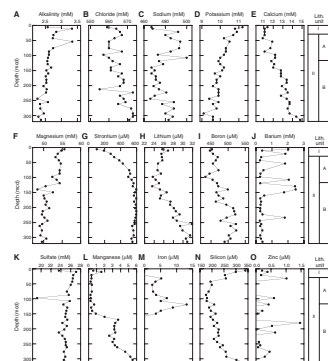
Sodium concentrations increase from 467 to 492 mM from 5.9 to 21.0 mcd and remain high (~485–500 mM) down to 107.5 mcd (Fig. F24C). The pore water sodium concentration decreases to 467 mM from 107.5 to 140.0 mcd. Below 140.0 mcd, the sodium concentration gradually increases to 483 mM at the base of the profile (314.2 mcd).

Potassium, Calcium, Magnesium, Strontium, and Lithium

Site 1264 downhole trends in potassium, calcium, and magnesium are consistent with those resulting from exchange with basaltic basement at depth (Gieskes, 1981), with potassium and magnesium decreasing and calcium increasing slightly with depth (Fig. F24D, F24E, F24F). Pore water potassium concentrations decrease slightly from 11.2 mM (5.9 mcd) to 9.6 mM (314.2 mcd) (Fig. F24D). Calcium values generally increase from 11.4 mM (5.9 mcd) to 14.8 mM (314.2 mcd) (Fig. F24E). The magnesium profile (Fig. F24F) is characterized by a general decrease with depth from 55.6 mM in the shallowest sample (5.9 mcd) to 49.5 mM at the base of the section (314.2 mcd).

The strontium concentration increases from 101 µM (5.9 mcd) to 595 µM (169.5 mcd). Below this depth, strontium values remain high (>530 µM) down to the base of the analyzed record (314.2 mcd). The profile exhibits a slight decrease over the interval from 223.2 to 314.2 mcd (Fig. F24G). These high pore water concentrations may be related to carbonate diagenesis, in which dissolution of biogenic calcite and subsequent reprecipitation of inorganic diagenetic calcite supplies dissolved strontium to the interstitial waters (e.g., Baker et al., 1982).

F24. Chemical constituents in interstitial water, p. 48.



The lithium concentration profile shows a decrease from 25.7 to 23.6 μM over the interval from 5.9 to 129.0 mcd then increases gradually to 30.9 μM at the base of the section (314.2 mcd) (Fig. F24H). This trend suggests a shallow subsurface sink for dissolved lithium and a deeper source of lithium from the sediment into the pore waters.

Boron and Barium

Boron values exhibit a general increase with depth from 453 μM (5.9 mcd) to 490 μM (314.2 mcd) (Fig. F24I). Pore water barium concentrations range between background values of <0.5 and ~2 μM (Fig. F24J). Elevated barium concentrations do not correlate with any decrease in pore water sulfate concentrations that might suggest enhanced barite solubility.

Sulfate, Manganese, and Iron

The pore water profile at Site 1264 is characterized by a general decrease in sulfate from 27.1 mM (10.4 mcd) to 24.6 mM (303.7 mcd) (Fig. F24K). Samples 208-1264B-1H-4, 140–150 cm (23.6 mM), and 208-1264A-9H-5, 140–150 cm (19.2 mM), yielded lower, and possibly spurious, values. The relatively high concentrations of sulfate (mean = 25.22 \pm 0.77 mM) reflect the very low organic matter content of the sedimentary section recovered at Site 1264 (see “[Carbonate and Organic Carbon](#),” p. 16, in “Sediment Geochemistry”).

The manganese pore water profile exhibits low and relatively uniform values (less than ~1.0 μM) down to 140.0 mcd. Below this depth, values increase from 0.44 μM (140.0 mcd) to 3.34 μM (212.6 mcd) and increase further to 5.5 μM (303.7 mcd) toward the base of the profile (Fig. F24L).

The pore water concentration of dissolved iron is below detection limit throughout much of the interval analyzed (Fig. F24M). However, concentrations rise from 0 to 5.2 μM at 32.1 mcd and peak at 13.1 μM (118.8 mcd). Dissolved iron concentrations then decrease back to 0 μM at 160.0 mcd. Interestingly, maximum iron concentrations occur above the increase in dissolved manganese concentrations, and the maximum value corresponds to the division between lithostratigraphic Subunits IIA and IIB. This sedimentary interval contains abundant iron oxide “bands” that may have contributed dissolved iron to the pore waters (see “[Lithostratigraphy](#),” p. 3).

Silicon and Zinc

Pore water silicon concentrations (Fig. F24N) decrease from the shallowest value of 339 μM (5.9 mcd) to 175 μM (86.8 mcd) then generally increase to 340 μM at the base of the profile (314.2 mcd). Zinc concentrations in pore waters from Site 1264 were low and variable, ranging from below detection to 1.4 μM (Fig. F24O).

Summary of Interstitial Water Chemistry

The Site 1264 pore water profiles of potassium, calcium, and magnesium reflect the diffusional gradient between seawater and basalt. In contrast, the profiles of strontium, lithium, boron, and parts of the manganese and iron records are dominated by sedimentary contributions of dissolved ions to the pore waters. Little evidence of microbial

influence exists in these profiles, as reflected in the sulfate, manganese, and iron profiles.

Sediment Geochemistry

Carbonate and Organic Carbon

Carbonate determinations by coulometry were made for a total of 115 samples from Site 1264 (Table T12). Samples were selected to provide a measure of the carbonate content within different units and to assess the influence of carbonate content on color reflectance. The carbonate values in Unit I average 94.6 wt%. Below Unit I, carbonate contents remain relatively high but decrease gradually. Values in Unit II are slightly higher than those in Unit I (mean = 96.1 wt%) (Table T12; Fig. F25). Subunit IIB carbonate content averages 94.2 wt%, whereas the carbonate values of Subunits IIC and IID are slightly lower and more variable (mean = 92.3 and 93.0 wt%, respectively).

Elemental analysis of C indicates generally low concentrations of organic matter in Site 1264 sediments (Table T12). Several of the samples analyzed contained organic carbon concentrations slightly greater than zero, with values ranging from 0.0 to 0.3 wt%. None of the analyzed samples contained measurable nitrogen.

Extractable Hydrocarbons

Extraction of organic matter (12 hr) was performed on Samples 208-1264A-1H-5, 145–150 cm; 9H-5, 140–150 cm; and 24H-5, 140–150 cm, after squeezing out the interstitial water.

The chromatogram for Sample 208-1264A-1H-5, 145–150 cm (10.4 mcd), was dominated by *n*-C₁₄ through *n*-C₁₈ alkanes with a minor component of branched isoprenoids (with the exception of pristane and phytane) (Fig. F26). The extracts from Samples 208-1264A-9H-5, 140–150 cm, and 24H-5, 140–150 cm (97.6 and 255.1 mcd, respectively), display a similar *n*-alkane abundance and distinct peaks of pristane and phytane; however, branched isoprenoids were more abundant than those in Sample 208-1264A-1H-5, 145–150 cm. The results indicate that the majority of sedimentary organic matter originates from photosynthetic algae.

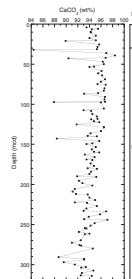
A comparison of the Neogene samples from Site 1264 with the Paleogene samples from Site 1263 reveals a significant difference. Branched isoprenoids, especially anteiso-alkanes in Sample 208-1263A-17H-5, 140–150 cm, were dominant compounds in earlier eluates at *m/z* 85 (Fig. F26) on the mass chromatogram, suggesting a greater contribution of cyanobacterial products to the sedimentary organic matter. These results suggest a shift in major primary producers from cyanobacteria to photosynthetic algae between the middle Eocene and earliest Miocene.

Sediment Elemental Content

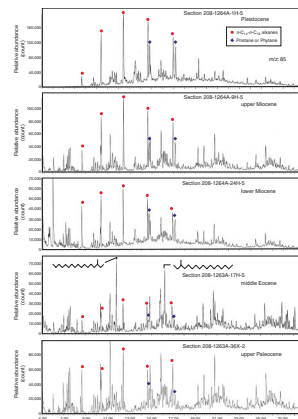
A total of 55 squeeze cake samples (sediments remaining after interstitial water samples have been squeezed) from Sites 1263 and 1264 were analyzed shipboard by inductively coupled plasma-atomic emission spectroscopy following the method outlined in “Geochemistry,” p. 23, in the “Explanatory Notes” chapter. These analyses were intended to provide bulk carbonate chemical data, but the resulting calcium contents (Tables T13, T14) clearly demonstrate that phases other

T12. Calcium carbonate and total and organic carbon, p. 67.

F25. Sedimentary carbonate contents, p. 49.



F26. Chromatograms, p. 50.



T13. Sediment dissolution analyses, Site 1263, p. 69.

T14. Sediment dissolution analyses, Site 1264, p. 70.

than carbonate have also been dissolved and analyzed (the average calcium content of the leachates is 51.1 wt% for Site 1263 and 49.7% for Site 1264, whereas the calcium content of pure CaCO_3 is only 40 wt%). Therefore, these data (Tables T13, T14) are not useful for assessing the partitioning of elements between the pore waters and carbonates as intended but provide information about the chemical composition of acid-leachable components (carbonate plus some clay components of the sediment).

No lithium peaks were observed during analysis, suggesting that the 2000-fold diluted samples contained lithium at levels below the detection limit. Silicon concentrations in the leachates could not be determined because the silicon blank levels in the nitric acid dilution matrix used were too high.

Generally the sediment leachate data (Tables T13, T14) display no relationship with the corresponding pore water profiles with the exceptions of boron and strontium (discussed below). Calcium, potassium, and magnesium concentrations in Site 1263 leachates show no downhole trend and fluctuate between 54.4–49.6 wt%, 36.3–13.4 mM, and 77.7–43.9 mM, respectively. At Site 1264, leachate calcium, potassium, and magnesium concentrations also exhibit no downhole trend and fluctuate between 52.5–46.3 wt%, 25.5–9.3 mM, and 59.6–40.4 mM, respectively. The lack of a relationship between the calcium, potassium, and magnesium content of the leachates and the associated pore waters supports the interpretation that the clear downhole increase in pore water calcium and decrease in pore water potassium and magnesium at Sites 1263 and 1264 is the result of diffusion between seawater and basement basalt.

Iron concentrations in the leachates fluctuate between 55.5 and 15.3 mM in Site 1263 samples and between 50.3 and 17.9 mM in Site 1264 samples. There is no downhole trend or noticeable relationship with associated pore water iron concentrations for either Site 1263 or 1264.

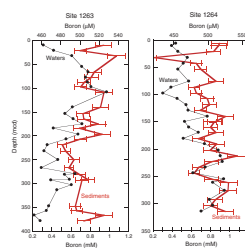
Manganese concentrations in the leachates vary between 6.46–1.28 and 4.80–1.71 mM in Site 1263 and 1264 samples, respectively. No general downhole trend or relationship with pore water manganese is observed for either site.

Sodium concentrations in the leachates fluctuate between 193–66 and 225–129 mM in Site 1263 and 1264 samples, respectively. No downhole trend or relationship with pore water sodium is apparent at either site.

Barium concentrations in the leachates display no consistent downhole relationship with pore water barium in either Site 1263 or 1264 samples. In Site 1263 sediments, barium concentrations increase downhole from 0.92 mM at the top of the section (10.2 mcd) to peak at a value of 9.44 mM at 250.2 mcd before dropping to a value of 3.39 mM at the base of the section (378.2 mcd). In Site 1264 sediments, barium concentrations decrease downhole from 2.93 mM at 10.4 mcd to a minimum of 0.23 mM at 180.6 mcd before increasing to values >1 mM below 212.6 mcd.

Boron concentrations of leachates from Sites 1263 and 1264 follow the downhole fluctuations of pore water boron throughout the majority of both sections (Fig. F27). In the Site 1263 section, the sediment and pore water boron profiles show no relationship above ~75 mcd and below ~300 mcd, but throughout the interval between ~75 and ~300 mcd, the sediment and pore water profiles trace each other. The lack of a relationship between the sediment and pore water boron above ~75 mcd can be attributed to the downward diffusion of seawater into the

F27. Boron from sediment dissolution and pore waters, p. 51.

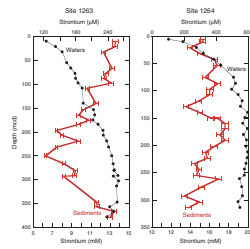


sediments. Below 292.6 mcd, Site 1263 samples were recovered using the extended core barrel coring system, which could increase seawater contamination of the pore water samples (see “[Geochemistry](#),” p. 17, in the “Site 1263” chapter). At Site 1264, all cores were recovered using the APC system, which produces the most undisturbed cores with minimum seawater contamination, and the sediment and pore water boron profiles trace each other down to the base of the section (314.2 mcd). However, in the upper ~100 m (especially the top 50 m) of the Site 1264 section, the sediment and pore water boron profiles exhibit little or no relationship, which is again suggestive of seawater diffusion into the sediments from above. Laboratory experiments under controlled temperatures and pressures have shown that boron is leached from terrigenous sediments into fluids (e.g., James et al., 2003), and a study of Leg 186 interstitial water samples concluded that the removal of boron from clays and volcanic ash was responsible for boron enrichment in the pore waters (Deyhle and Kopf, 2002). The strong relationship between the sediment and pore water boron profiles at Sites 1263 and 1264 supports the notion that the concentrations of boron in the pore waters are related to the amount of boron in the sediments. Interestingly, the pore water profiles of other elements (e.g., calcium, potassium, and magnesium) indicate that diffusion of dissolved species through the sediments has occurred, which would potentially mask the association of pore water boron to that of sediment boron concentrations through the smoothing of pore water boron concentration gradients. For the structure of the pore water boron profile to remain unaltered by such diffusion requires the ongoing release of boron from sediments to occur on timescales smaller than that at which diffusion is effective.

Strontium concentrations in the leachates of Site 1263 samples generally decrease downhole from 13.5 mM at the top of the section (10.2 mcd) to a minimum of 6.3 mM at 250.2 mcd before increasing down-hole to values >13 mM near the base of the section (378.2 mcd) (Fig. F28). The Site 1263 pore water strontium profile increases downhole and peaks at values >250 µM below ~250 mcd and thus is inversely related to the sediment strontium profile to a depth of ~250 mcd. Such a relationship is explained by carbonate dissolution and recrystallization being focused around ~250 mcd, which releases strontium to the pore waters and produces inorganic calcite with substantially lower strontium concentrations than the original biogenic calcite (e.g., Baker et al., 1982). Below ~250 mcd, the strontium concentration of the leachates increases with no associated change in the strontium pore water profile. It is unlikely that carbonate dissolution and recrystallization has occurred at ~250 mcd and not in the sediments below. This is supported by the continuation of enhanced pore water strontium below ~250 mcd. Instead, the increase in the sediment strontium profile below ~250 mcd suggests a noncarbonate sedimentary strontium component, which does not release strontium to the pore waters and increases in abundance with depth below ~250 mcd, enhancing the strontium content of the sediments.

The sediment strontium concentrations in Site 1264 samples fluctuate downhole between 17.6 and 13.4 mM (Fig. F28) and exhibit no relationship with the associated pore water strontium profile. This is consistent with minimal carbonate dissolution and recrystallization in the Site 1264 section, as the sediment strontium values remain much higher (>13 mM) than those measured in the interval suspected to exhibit inorganic carbonate characteristics in Site 1263 sediments (6.3

F28. Strontium from sediment dissolution and pore waters, p. 52.



mM). However, below ~100 mcd, the Site 1264 pore water strontium values are consistently more than twice the maximum values observed in the Site 1263 pore waters, suggesting that a noncarbonate sedimentary component rich in strontium is leaching strontium to the pore waters below ~100 mcd. These interpretations are not necessarily exclusive, as the influence of a strontium-rich noncarbonate sedimentary component could mask the signal of carbonate dissolution and recrystallization. Further work is required to assess the strontium chemistry of only the carbonate fraction and to diagnose the true extent of carbonate diagenesis in the sediments of Sites 1263 and 1264.

AGE MODEL AND MASS ACCUMULATION RATES

A 316.5-mcd-thick (280.9 mbsf) lower Oligocene (~31 Ma) to Pleistocene pelagic sediment sequence was recovered at Site 1264. A total of 92 biostratigraphic datums and 6 magnetostratigraphic polarity reversals (Table T15) were used to construct an age-depth model for this site (Table T16; Fig. F29). Linear sedimentation rates (LSRs), total mass accumulation rates (MARs), and carbonate MARs were calculated at 1-m.y. intervals (see “Age Model and Mass Accumulation Rates,” p. 33, in the “Explanatory Notes”).

Age-Depth Model

The main objective of Site 1264 was to recover a complete and well-resolved Neogene section representative of the Walvis Ridge transect. The sediment section at Site 1264 is fairly complete, although the interval from 17.5 to 14 Ma (204–186 mcd) is condensed and an unconformity exists in the uppermost Miocene and lowermost Pliocene (5.9–5.2 Ma; ~77 mcd) (see “Biostratigraphy,” p. 6). Biostratigraphic and magnetic reversal datums are in general agreement for most of the section (Fig. F29). The most significant discrepancies between nannofossil and planktonic foraminiferal datums exist in the Pliocene–Pleistocene, and we relied on calcareous nannofossils and magnetostratigraphy to define the age model in that interval.

Linear Sedimentation and Mass Accumulation Rates

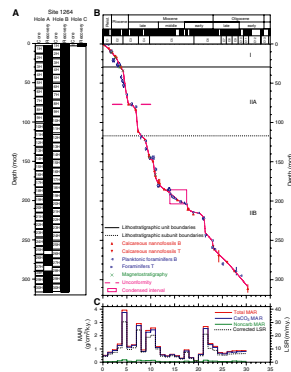
LSRs range between <1 and 30 m/m.y., and total MARs range from <0.1 to 3.9 g/cm²/k.y. Total MAR fluctuations essentially represent variations in carbonate MAR. Our 1-m.y. resolution record shows large fluctuations in LSRs and carbonate MARs with little overall trend. Low to moderate and relatively constant rates were calculated for the Oligocene; the lower part of the lower Miocene has significantly higher rates, followed by near-zero accumulation rates based on a planktonic foraminifer-based age-depth model. The LSRs and MARs remained low through the middle Miocene and increased significantly in the late Miocene to early Pliocene, punctuated by a 0.6-m.y hiatus not resolved in this age model (see “Biostratigraphy,” p. 6). The rates declined steadily in the Pliocene–Pleistocene to low values for the top of the Site 1264 sediment section.

In general, averaged noncarbonate MARs are low (<0.2 g/cm²/k.y.) throughout the section, and the small fluctuations reported here are probably representative of the analytical uncertainty rather than environmental changes.

T15. Age-depth model, LSRs, and MARs, p. 71.

T16. Datum levels, p. 73.

F29. Age-depth model, p. 53.



REFERENCES

- Backman, J., and Raffi, I., 1997. Calibration of Miocene nannofossil events to orbitally tuned cyclostratigraphies from Ceara Rise. In Shackleton, N.J., Curry, W.B., Richter, C., and Bralower, T.J. (Eds.), *Proc. ODP, Sci. Results*, 154: College Station, TX (Ocean Drilling Program), 83–99.
- Baker, P.A., Gieskes, J.M., and Elderfield, H., 1982. Diagenesis of carbonates in deep-sea sediments—evidence from $\text{Sr}^{2+}/\text{Ca}^{2+}$ ratios and interstitial dissolved Sr^{2+} data. *J. Sediment. Petrol.*, 52:71–82.
- Boersma, A., 1984. Cretaceous–Tertiary planktonic foraminifera from the southeastern Atlantic, Walvis Ridge area, Deep Sea Drilling Project Leg 74. In Moore, T.C., Jr., Rabinowitz, P.D., et al., *Init. Repts. DSDP*, 74: Washington (U.S. Govt. Printing Office), 501–523.
- Boltovskoy, E., and Boltovskoy, D., 1989. Paleocene–Pleistocene benthic foraminiferal evidence of major paleoceanographic events in the eastern South Atlantic (DSDP Site 525, Walvis Ridge). *Mar. Micropaleontol.*, 14:283–316.
- Cande, S.C., and Kent, D.V., 1995. Revised calibration of the geomagnetic polarity timescale for the Late Cretaceous and Cenozoic. *J. Geophys. Res.*, 100:6093–6095.
- Cunha, A.S., and Shimabukuro, S., 1996. Evidence of *Braarudosphaera* blooms and anomalous enrichment of *Nannoconus*: evidence from the Turonian South Atlantic, Santos Basin, Brazil. *J. Nannoplankton Res.*, 19:51–55.
- Deyhle, A., and Kopf, A., 2002. Strong B-enrichment and anomalous boron isotope geochemistry in the Japan forearc. *Mar. Geol.*, 183:1–15.
- Gieskes, J.M., 1981. Deep-sea drilling interstitial water studies: implications for chemical alteration of the oceanic crust, layers I and II. In Warme, J.E., Douglas, R.G., and Winterer, E.L. (Eds.), *The Deep Sea Drilling Project: A Decade of Progress*. Spec. Publ.—Soc. Econ. Paleontol. Mineral., 32:149–167.
- Hayward, B.W., 2002. Late Pliocene to middle Pleistocene extinctions of deep-sea benthic foraminifera (“*Stilostomella* extinction”) in the southwest Pacific. *J. Foraminiferal Res.*, 32:274–307.
- Hilgen, F.J., Krijgsman, W., Raffi, I., Turco, E., and Zachariasse, W.J., 2000. Integrated stratigraphy and astronomical calibration of the Serravallian/Tortonian boundary section at Monte Gibliscemi (Sicily, Italy). *Mar. Micropaleontol.*, 38:181–211.
- James, R.H., Allen, D.E., and Seyfried, W.E., Jr., 2003. An experimental study of alteration of oceanic crust and terrigenous sediments at moderate temperatures (51 to 350°C): insights as to chemical processes in near-shore ridge-flank hydrothermal systems. *Geochim. Cosmochim. Acta*, 67:681–691.
- Kennett, J.P., and Srinivasan, M.S., 1983. *Neogene Planktonic Foraminifera: A Phylogenetic Atlas*. Stroudsburg, PA (Hutchinson Ross).
- Lourens, L.J., Hilgen, F.J., Laskar, J., Shackleton, N.J., and Wilson, D., in press. The Neogene period. In Gradstein, F.M., Ogg, J., and Smith, A.G. (Eds.), *A Geological Time Scale 2004*. Cambridge (Cambridge Univ. Press).
- Moore, T.C., Jr., Rabinowitz, P.D., et al., 1984. *Init. Repts. DSDP*, 74: Washington (U.S. Govt. Printing Office).
- Pujol, C., 1983. Cenozoic planktonic foraminiferal biostratigraphy of the Southwest Atlantic (Rio Grande Rise), Deep Sea Drilling Project Leg 72. In Barker, P.F., Carlson, R.L., Johnson, D.A., et al., *Init. Repts. DSDP*, 72: Washington (U.S. Govt. Printing Office), 623–673.
- Roth, P.H., 1974. Calcareous nannofossils from the northwestern Indian Ocean Leg 24, Deep Sea Drilling Project. In Fisher, R.L., Bunce, E.T., et al., *Init. Repts. DSDP*, 24: Washington (U.S. Govt. Printing Office), 969–994.
- Schmiedl, G., Mackensen, A., and Müller, P.J., 1997. Recent benthic foraminifera from the eastern South Atlantic Ocean: dependence on food supply and water masses. *Mar. Micropaleontol.*, 32:249–287.

- Smart, C.W., and Murray, J.W., 1994. An early Miocene Atlantic-wide foraminiferal/palaeoceanographic event. *Palaeogeogr., Palaeoclimatol., Palaeoecol.*, 108:139–148.
- Smart, C.W., and Ramsay, A.T.S., 1995. Benthic foraminiferal evidence for the existence of an early Miocene oxygen-depleted oceanic water mass? *J. Geol. Soc. (London, UK)*, 152:735–738.
- Takayama, T., 1972. A note on the distribution of *Braarudosphaera bigelowii* (Gran and Braarud) Deflandre in the bottom sediments of Sendai Bay, Japan. *Paleontol. Soc. Jpn., Trans. Proc. N. S.*, 87:429–435.
- Thomas, E., 1986. Changes in composition of Neogene benthic foraminiferal faunas in equatorial Pacific and North Atlantic. *Palaeogeogr., Palaeoclimatol., Palaeoecol.*, 53:47–61.
- _____, 1986. Early to middle Miocene benthic foraminiferal faunas from DSDP Sites 608 and 610, North Atlantic. In Summerhayes, C.P., and Shackleton, N.J. (Eds.), *North Atlantic Palaeoceanography*. Geol. Soc. Spec. Publ., 21:205–218.
- van Morkhoven, F.P.C.M., Berggren, W.A., and Edwards, A.S., 1986. *Cenozoic Cosmopolitan Deep-Water Benthic Foraminifera*. Bull. Cent. Rech. Explor.—Prod. Elf-Aquitaine, Mem. 11.

Figure F1. Meteor Cruise M49/1 track chart showing the locations of Site 1263 (proposed Site WALV-8E), Site 1264 (proposed Site WAL-8A), and alternate sites (WALV-8B and WALV8C) on lines GeoB 01-046 and GeoB 01-031.

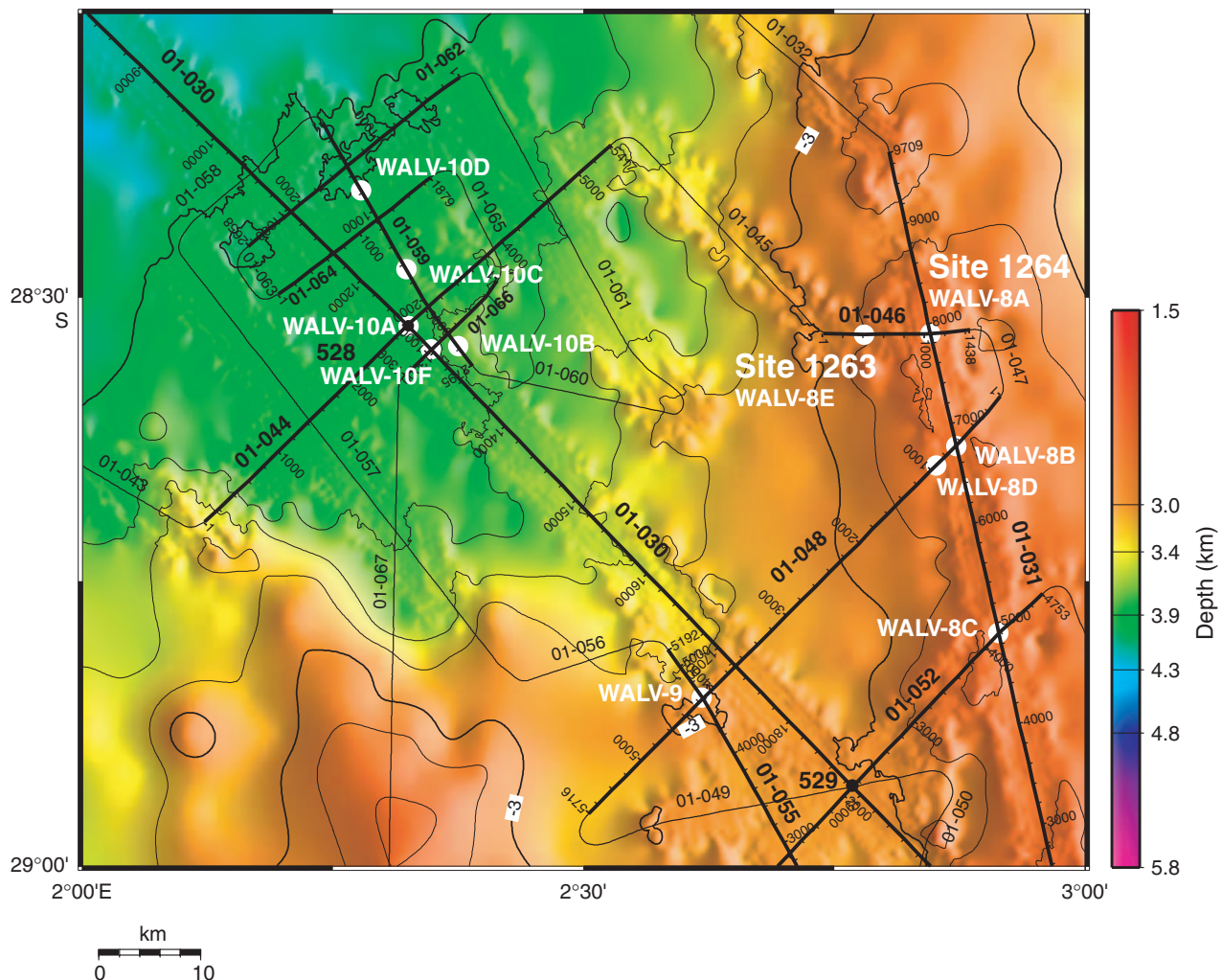


Figure F2. Site 1264 on line GeoB 01-031 (Part 1) with the location of crossing line GeoB 01-046. Also shown are the locations of proposed Sites WALV-8B, WALV-8C, and DSDP Site 525. w.d. = water depth. PETM = Paleocene/Eocene Thermal Maximum. K = Cretaceous.

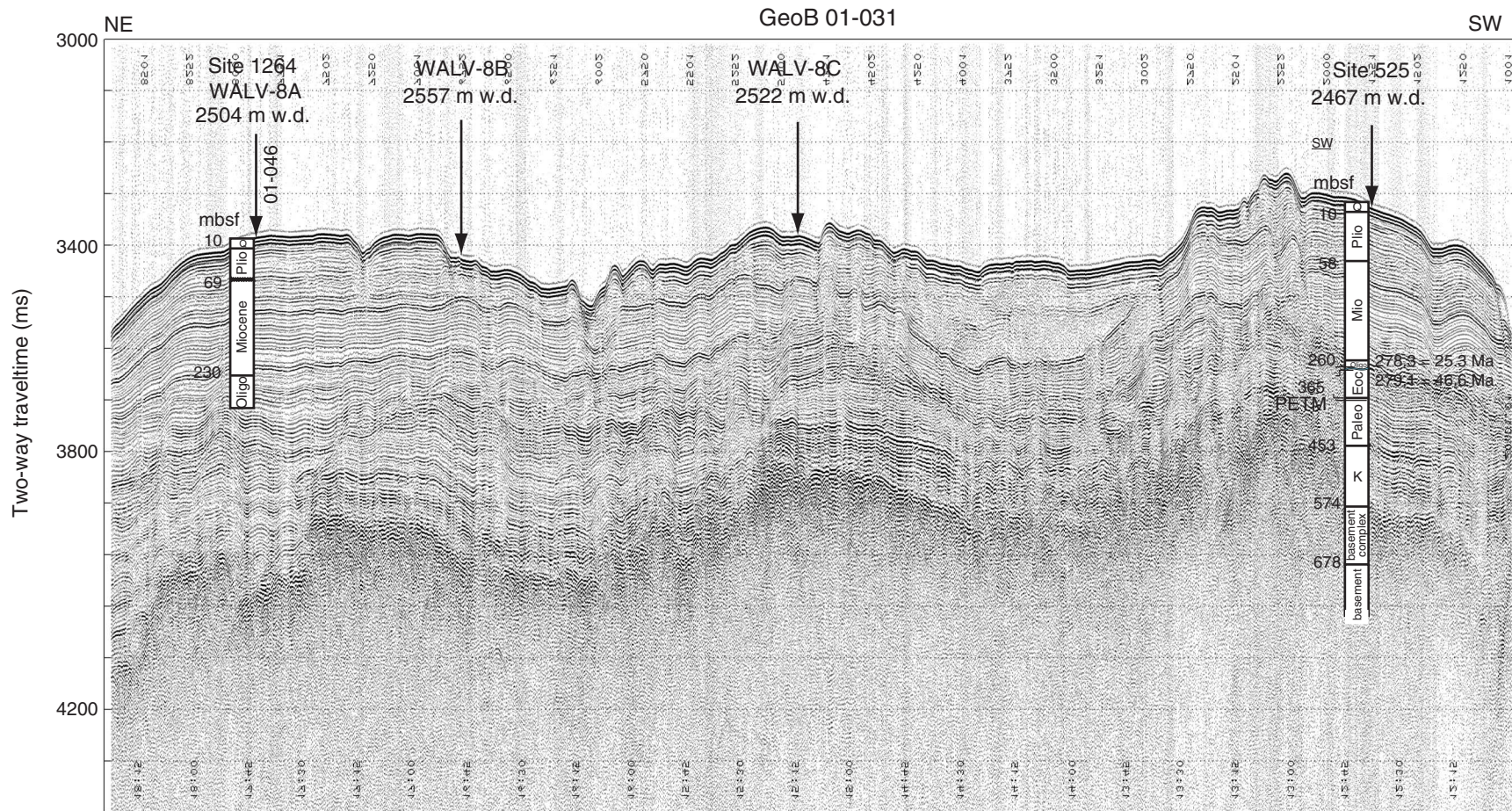


Figure F3. Line GeoB 01-046 and Sites 1263 and 1264 plotted with age estimates of prominent reflectors. $R_{O/M}$ = the Oligocene/Miocene boundary reflector. R_1 = a regional reflector associated with an erosional unconformity. The Paleocene/Eocene boundary reflector ($R_{P/E}$) beneath Site 1264 is estimated to be at 460 mbsf. $R_{K/P}$ = the Cretaceous/Paleogene boundary reflector.

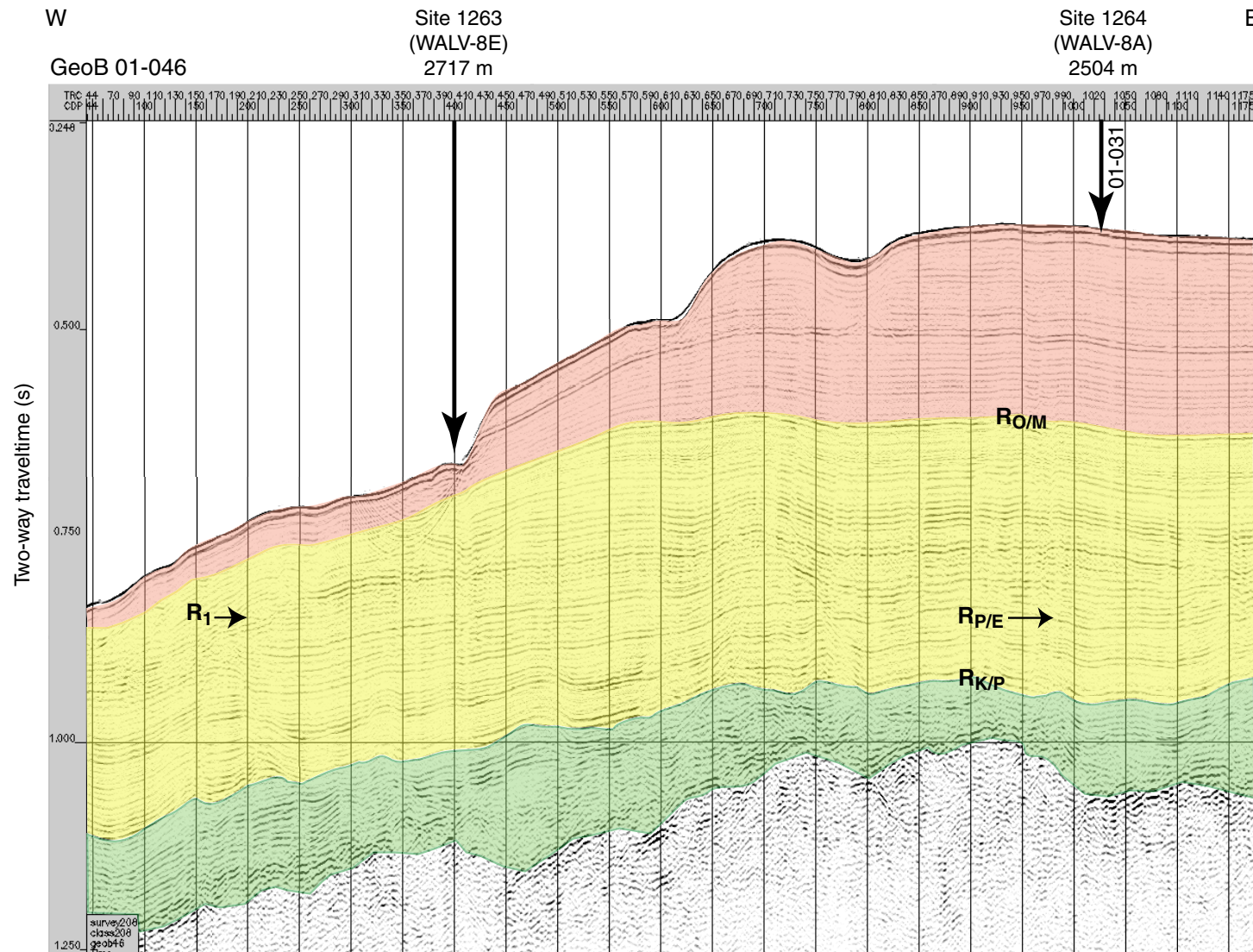


Figure F4. Magnetic susceptibility data from 0 to 316 mcd at Site 1264. Data from Holes 1264A and 1264B are offset from the spliced record by 10 and 100 times their values, respectively. Magnetic susceptibility values less than -1 instrument units were cut off at -1, and all values lower than 2 were multiplied by 0.5 and incremented by 1. Numbers near the tops of the individual core records refer to the core numbers.

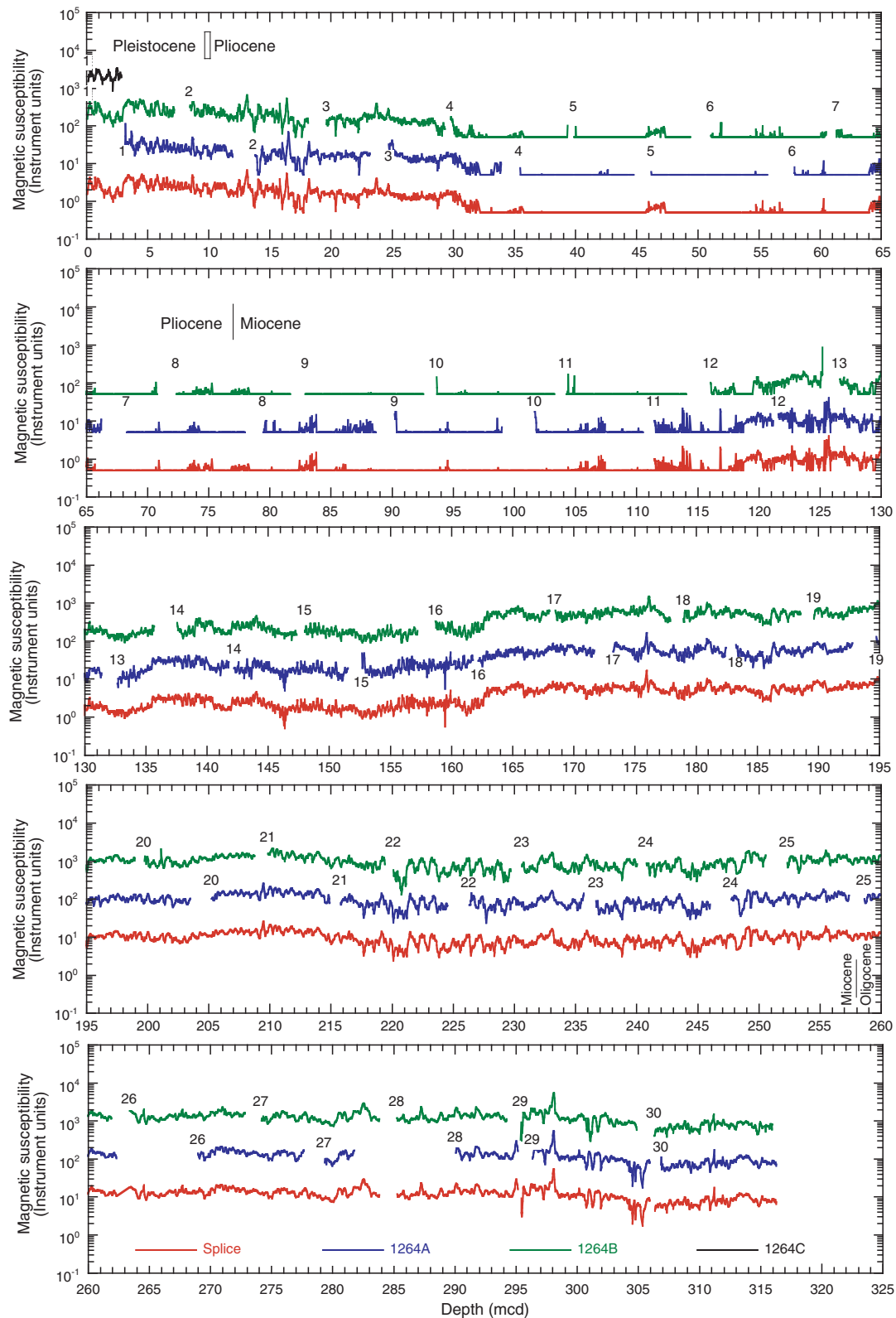


Figure F5. Orange (600 nm) to blue (450 nm) ratio from 0 to 312 mcd of Site 1264. Data from Holes 1264A and 1264B are offset from the spliced record by 0.3 and 0.6, respectively. Numbers near the tops of the individual core records refer to the core numbers.

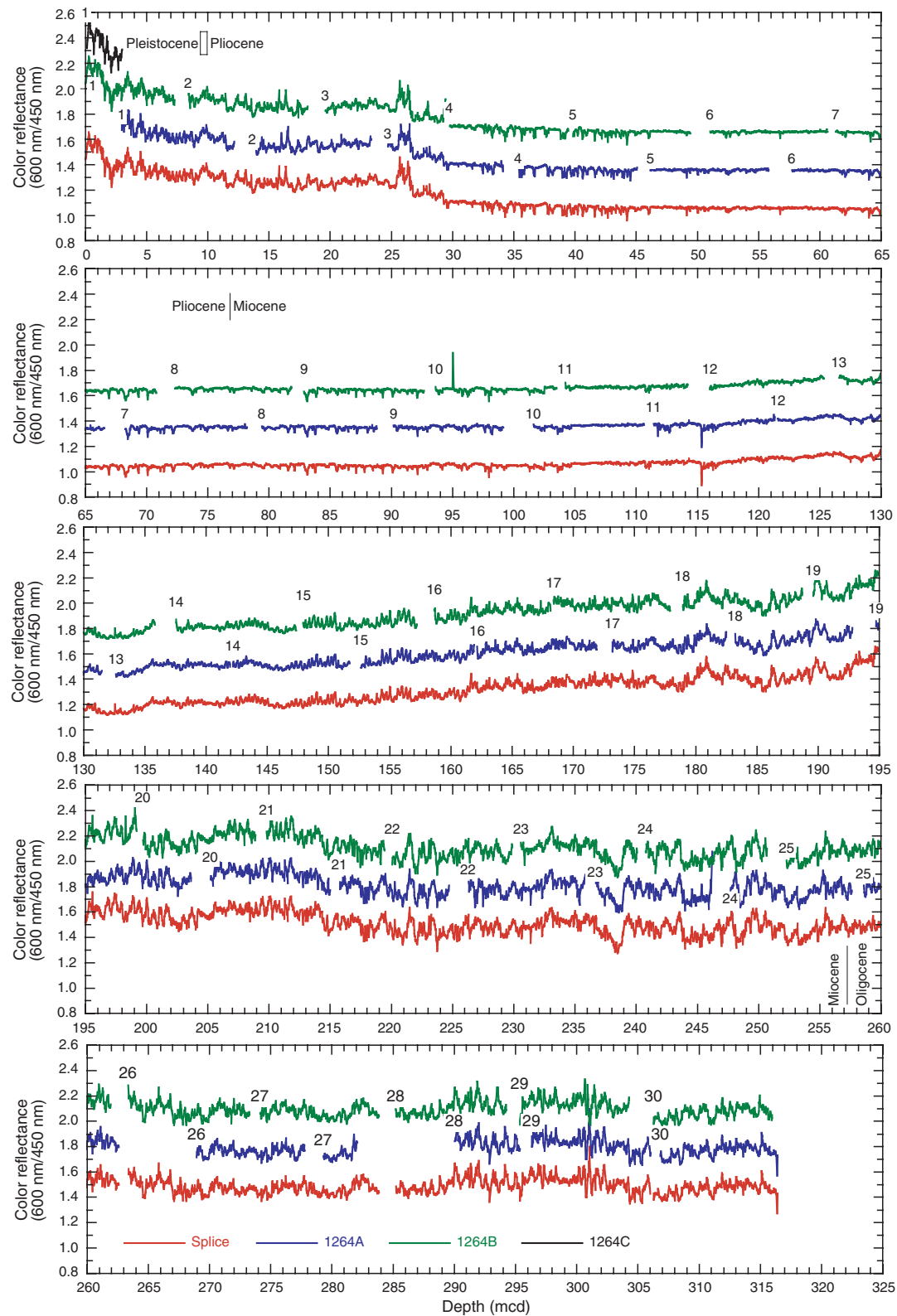


Figure F6. Mcd growth rates for Holes 1264A and 1264B.

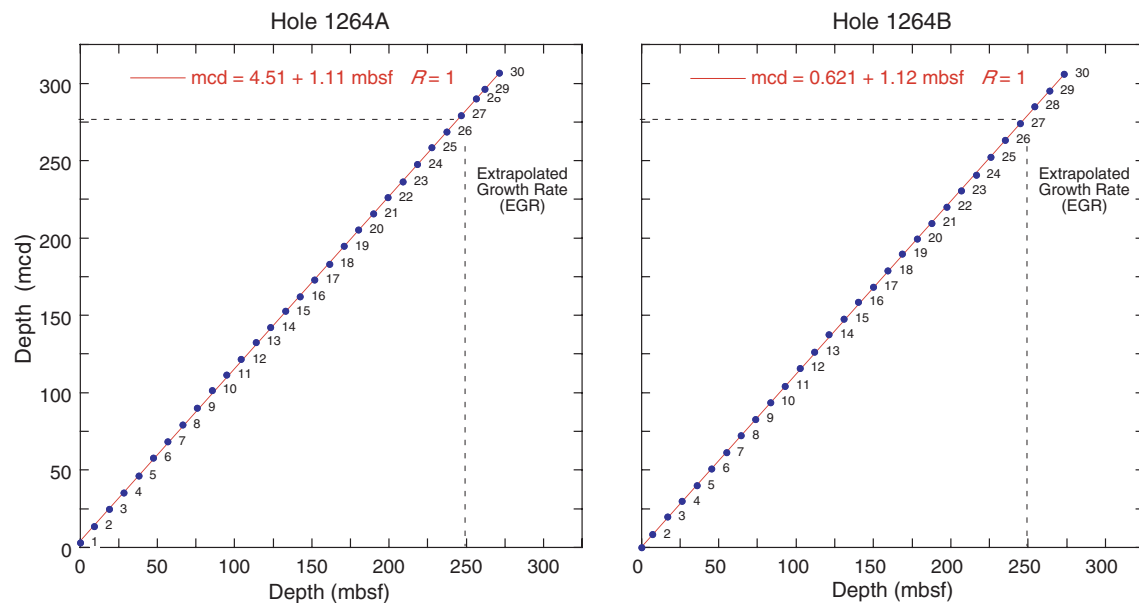


Figure F7. Site 1264 lithostratigraphic composite illustrating stratigraphic variation in parameters used to define lithostratigraphic units, including magnetic susceptibility (MS), nannofossil content, color reflectance (b^* , blue-yellow chromaticity value), and P -wave velocity. MS and chromaticity data are smoothed with a 5-point moving average. Nannofossil content and P -wave velocity are smoothed with a 5% weighted average.

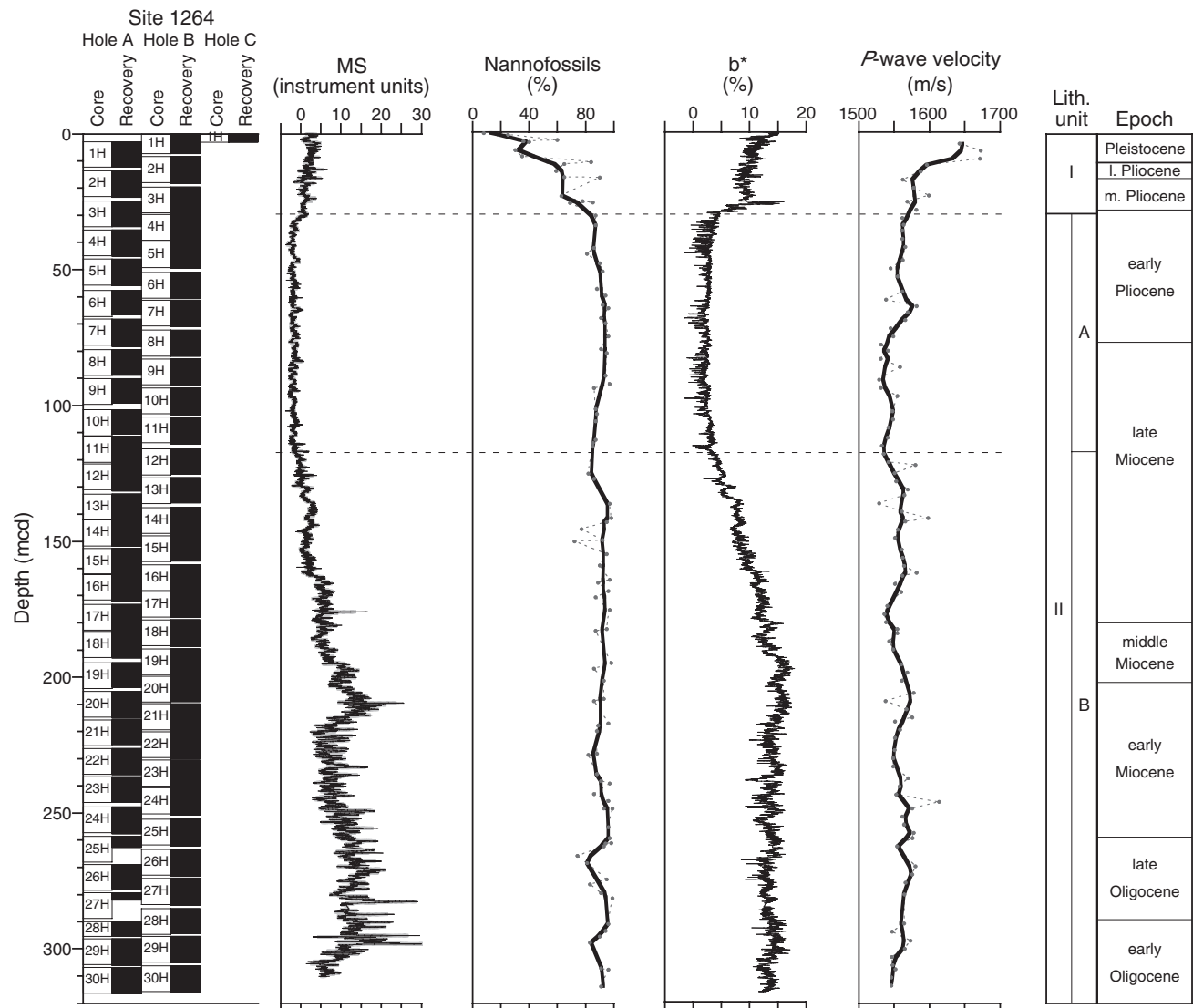


Figure F8. Site 1264 lithostratigraphic composite illustrating stratigraphic variation in whole-core MST measurements of magnetic susceptibility (MS), gamma ray attenuation (GRA) bulk density, and *P*-wave velocity logger (PWL) values. Natural gamma radiation (NGR) data are smoothed with a 10-point moving average; all other data are smoothed with a 5-point moving average.

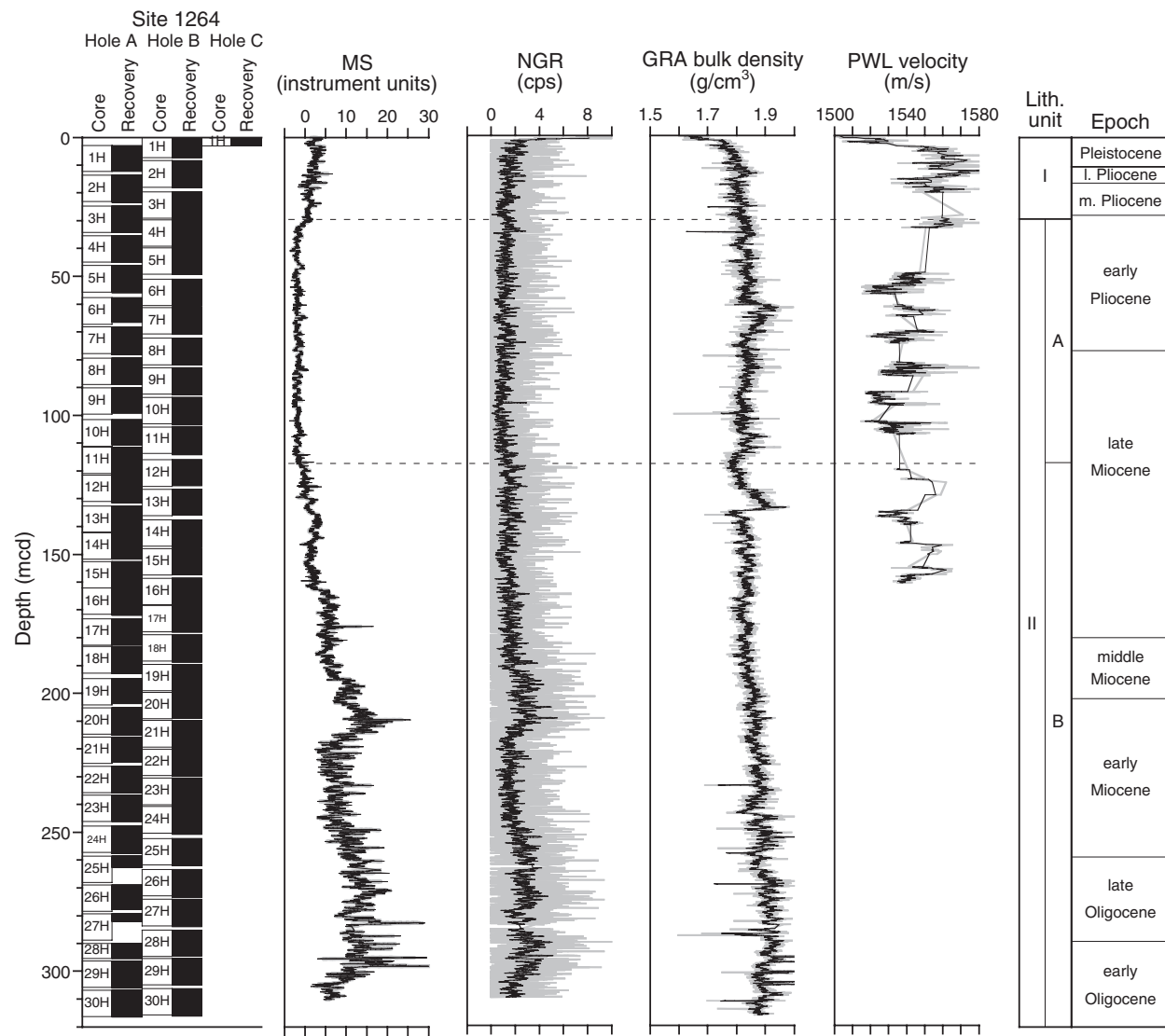


Figure F9. Site 1264 lithostratigraphic composite illustrating stratigraphic variation in sediment lightness (L^*), carbonate content, and chromaticity (a^* and b^*).

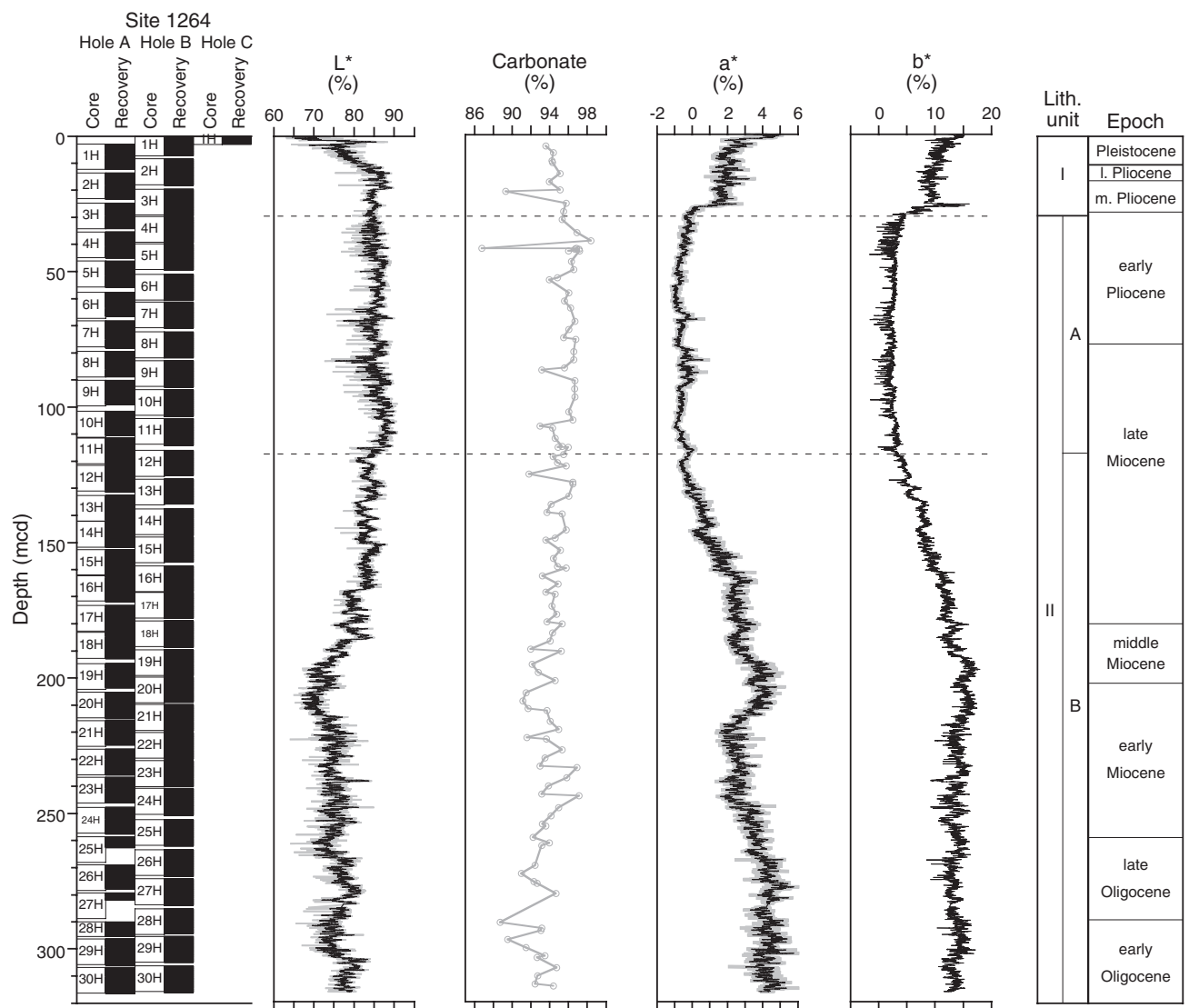


Figure F10. Site 1264 lithostratigraphic composite illustrating stratigraphic variation in predominant and accessory smear slide components from Holes 1264A, 1264B, and 1264C (single points), smoothed with a 3-point moving average (solid lines).

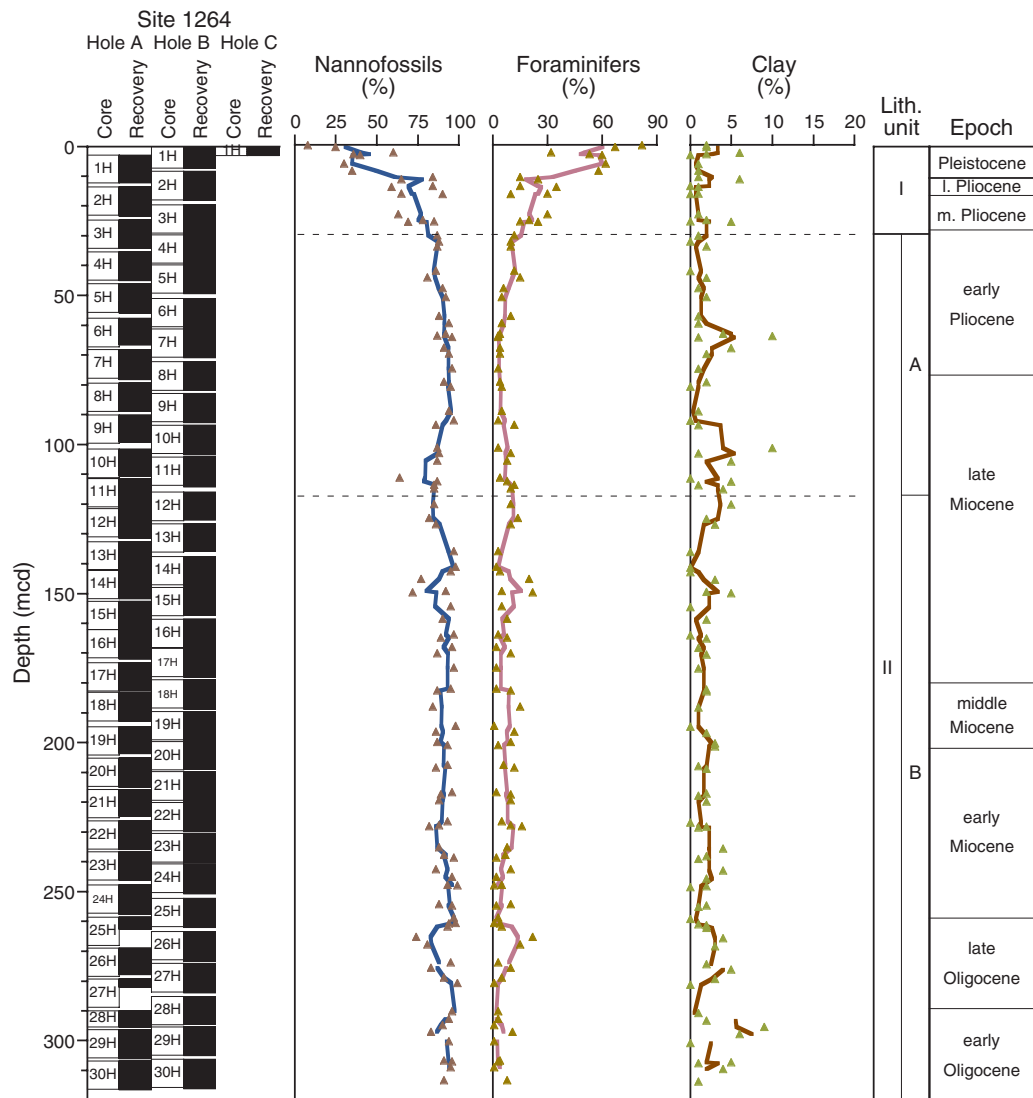


Figure F11. Site 1264 lithostratigraphic composite illustrating stratigraphic variations in grain density (GD), bulk density (BD; MAD method), porosity, and P-wave velocity sensor 3 (PWS3) measurements.

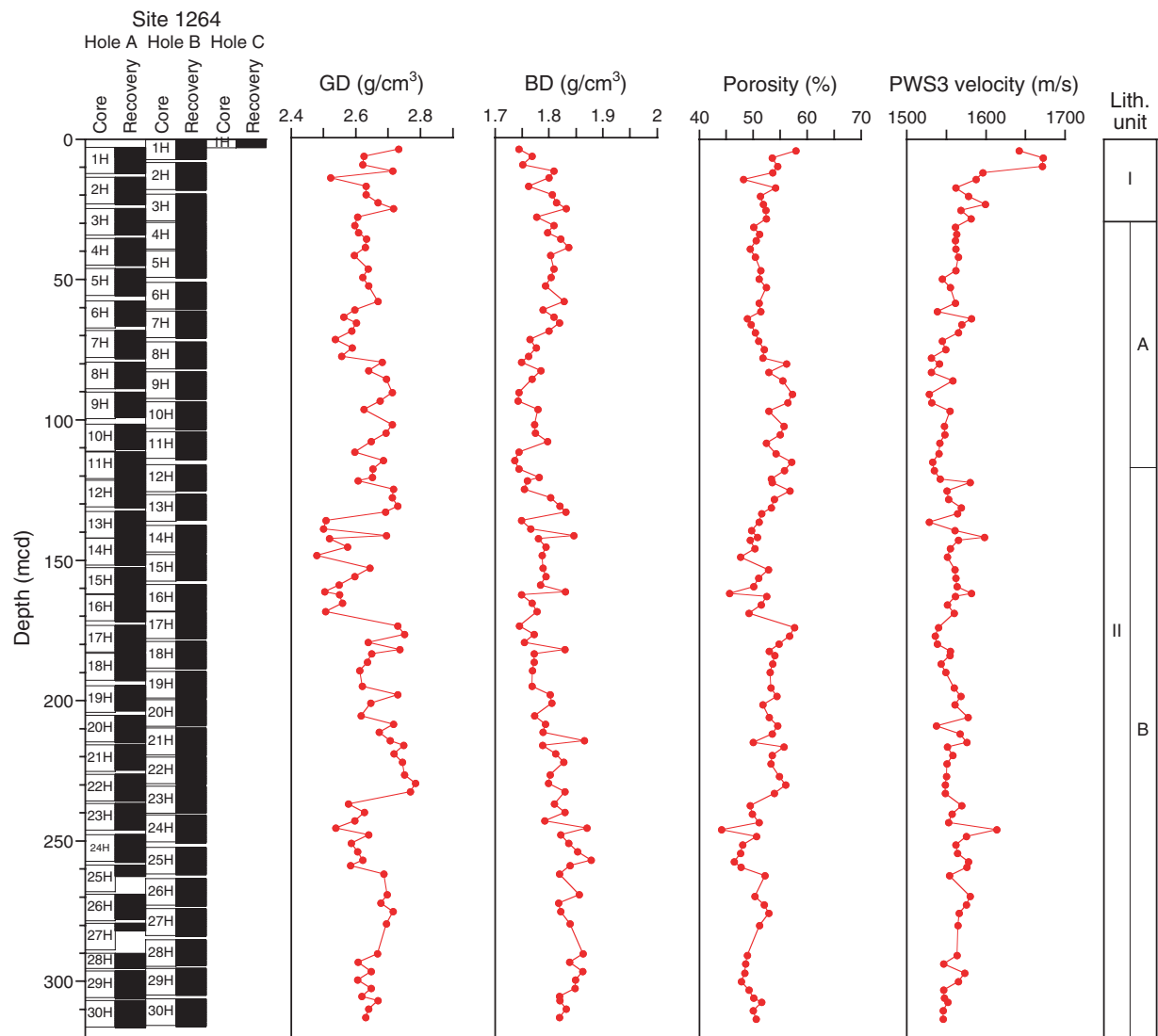


Figure F12. A, B. Comparison between bulk density measured by gamma ray attenuation (GRA) and moisture and density (MAD) methods. C. Correlation of grain density (GD) with bulk density (BD; MAD method). D. Correlation of porosity with BD (MAD method). E. Correlation of *P*-wave velocity sensor 3 (PWS3) and BD (MAD method) measurements.

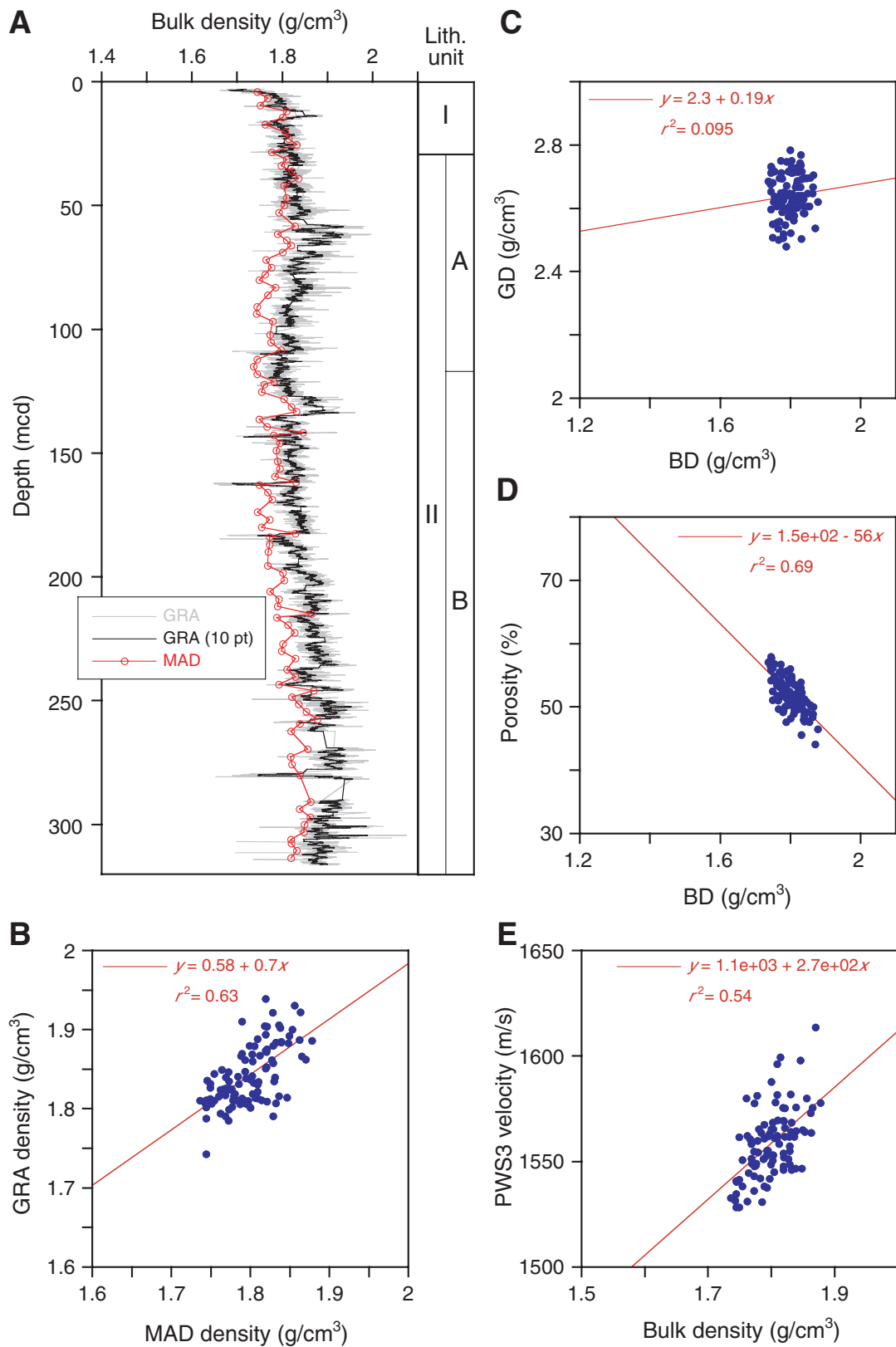


Figure F13. A. Comparison of *P*-wave velocities measured on the whole-core MST *P*-wave logger (PWL) and the split-core *P*-wave sensor 3 (PWS3). B. Scatterplot of PWL vs. PWS3 data.

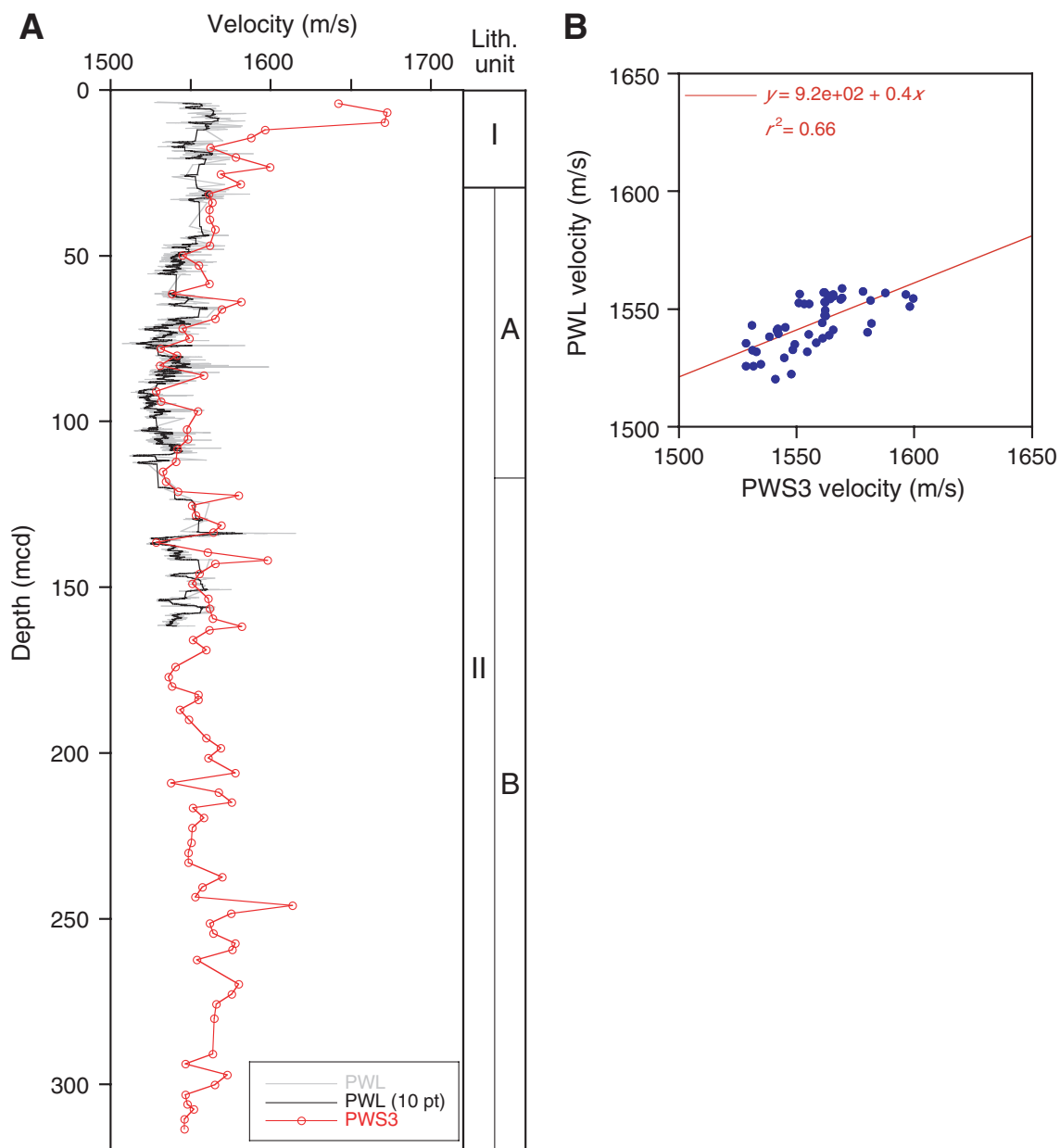


Figure F14. Site 1264 lithostratigraphic composite illustrating chromaticity (a^*) and manganese and iron concentrations in the interstitial waters and grain density in Hole 1264A. Gray lines at ~135, ~165, and ~235 mcd mark slight but abrupt steps in grain density associated with dramatic changes in the interstitial water Mn and Fe concentrations.

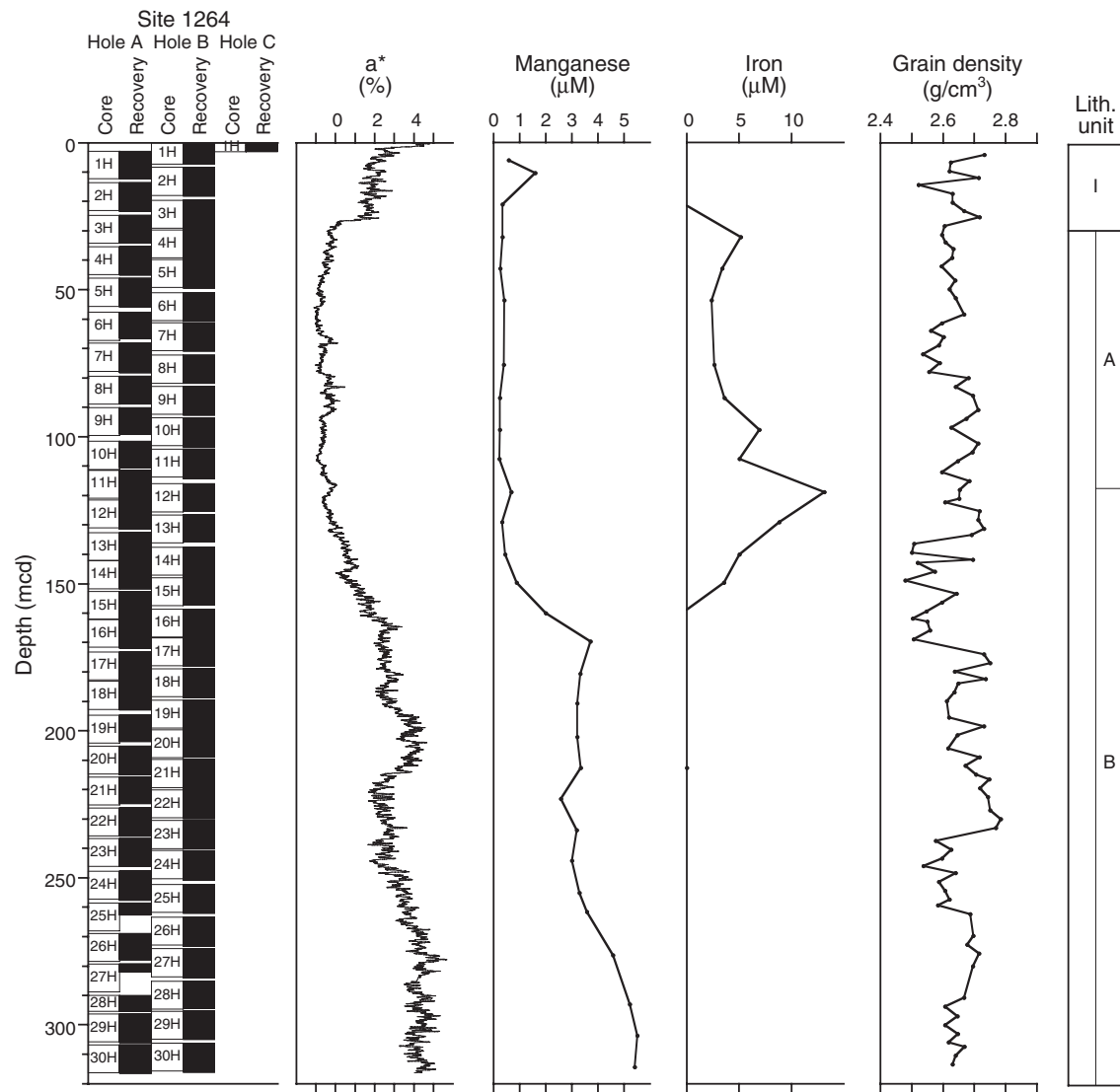


Figure F15. Downhole variation in sediment lightness (L^*) (9-point moving average) in Hole 1264A sediments with a close-up of cyclic oscillations in L^* and magnetic susceptibility (9-point moving average) between 50 and 80 mbsf (60.41–94.37 mcd). Typical cyclicity is shown in the digital image of Core 208-1264A-7H (56.80–66.59 mbsf; 68.25–78.03 mcd).

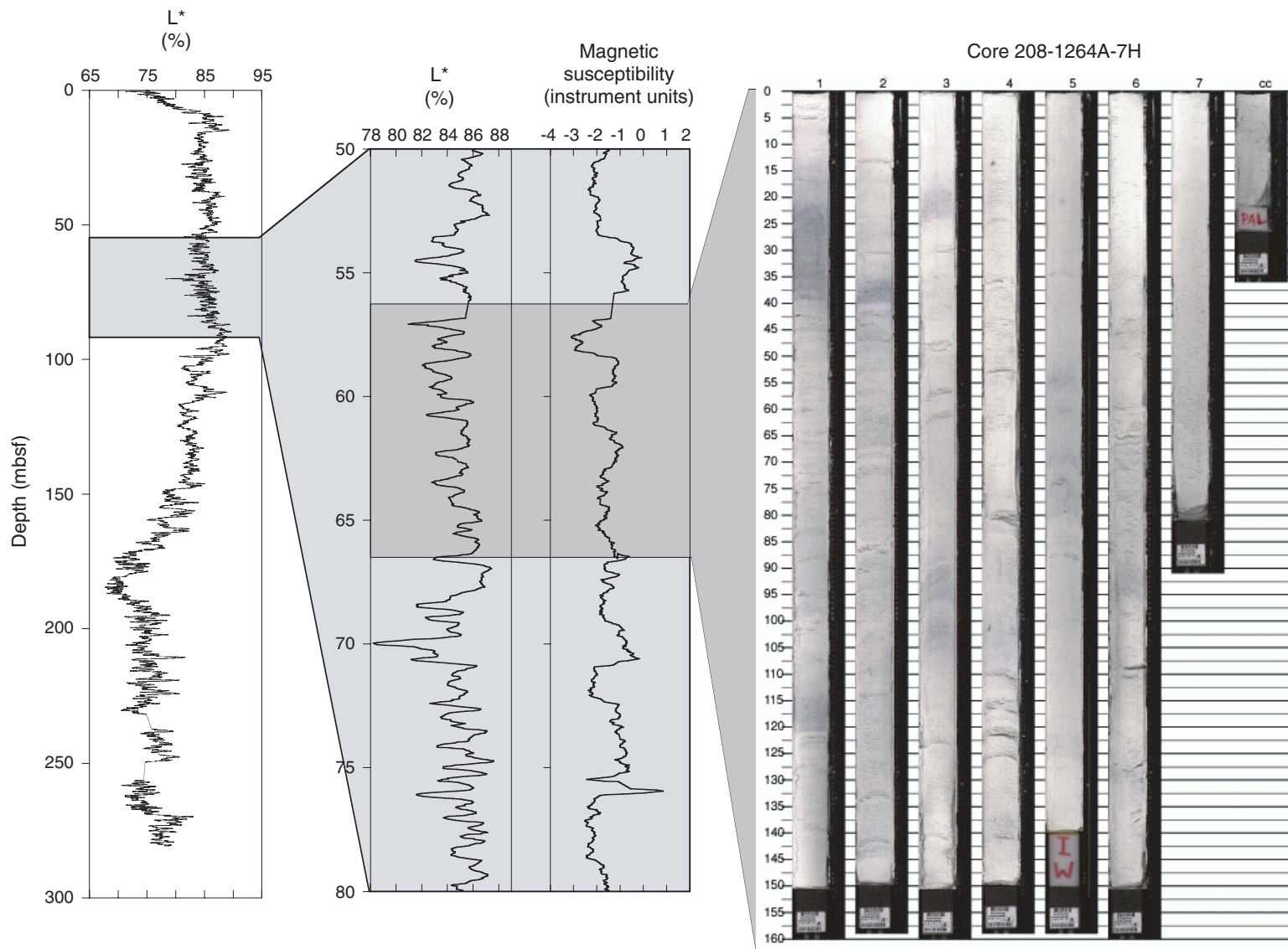


Figure F16. X-ray diffraction pattern from Sample 208-1264A-26H-5, 25 cm. Arrows highlight the positions of lithiophorite peaks.

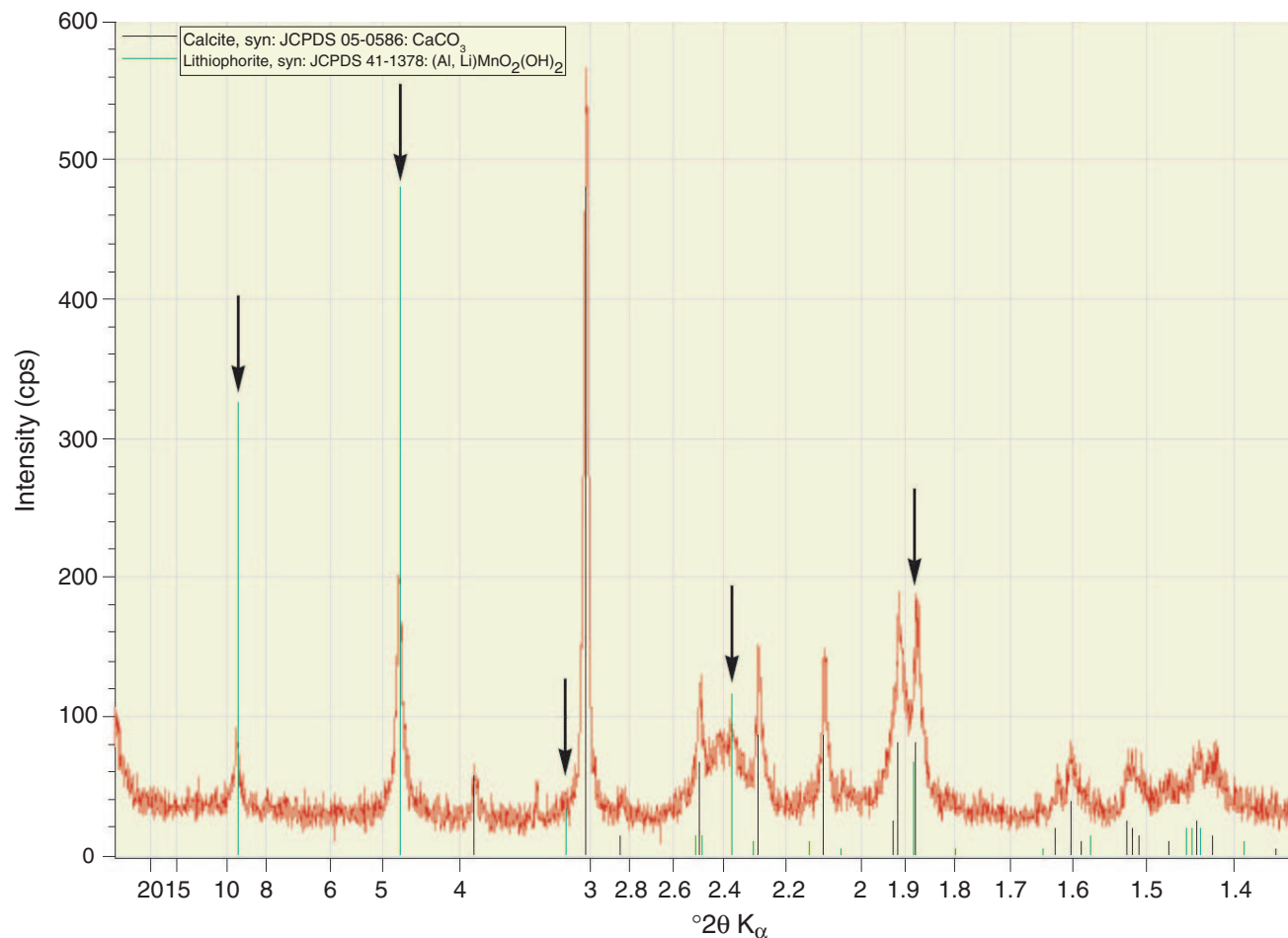


Figure F17. Downhole cyclic oscillations in magnetic susceptibility, natural gamma radiation, sediment lightness (L^*), and chromaticity (a^* and b^*) in the interval 200–230 mbsf (226.97–260.78 mcd) from Hole 1264A. Data have been smoothed with a 9-point running average. Cyclicity typical of Subunit IIB is shown in a digital image of Core 208-1264A-24H (218.30–228.05 mbsf; 247.10–257.45 mcd).

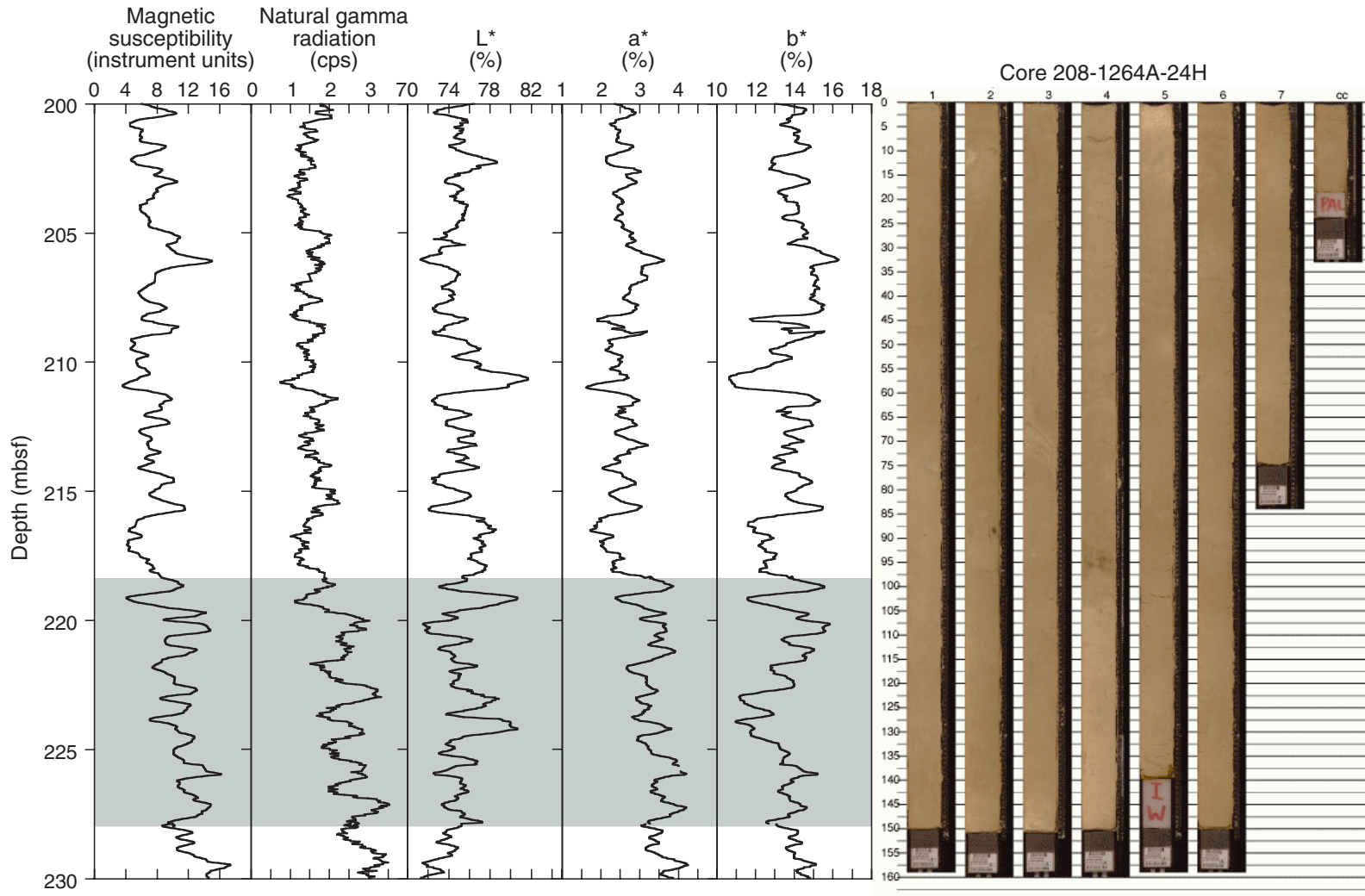


Figure F18. Summary of composite planktonic foraminiferal and calcareous nannofossil biozonation constructed for Site 1264. Shading indicates intervals of downslope transport and reworking. B = bottom.

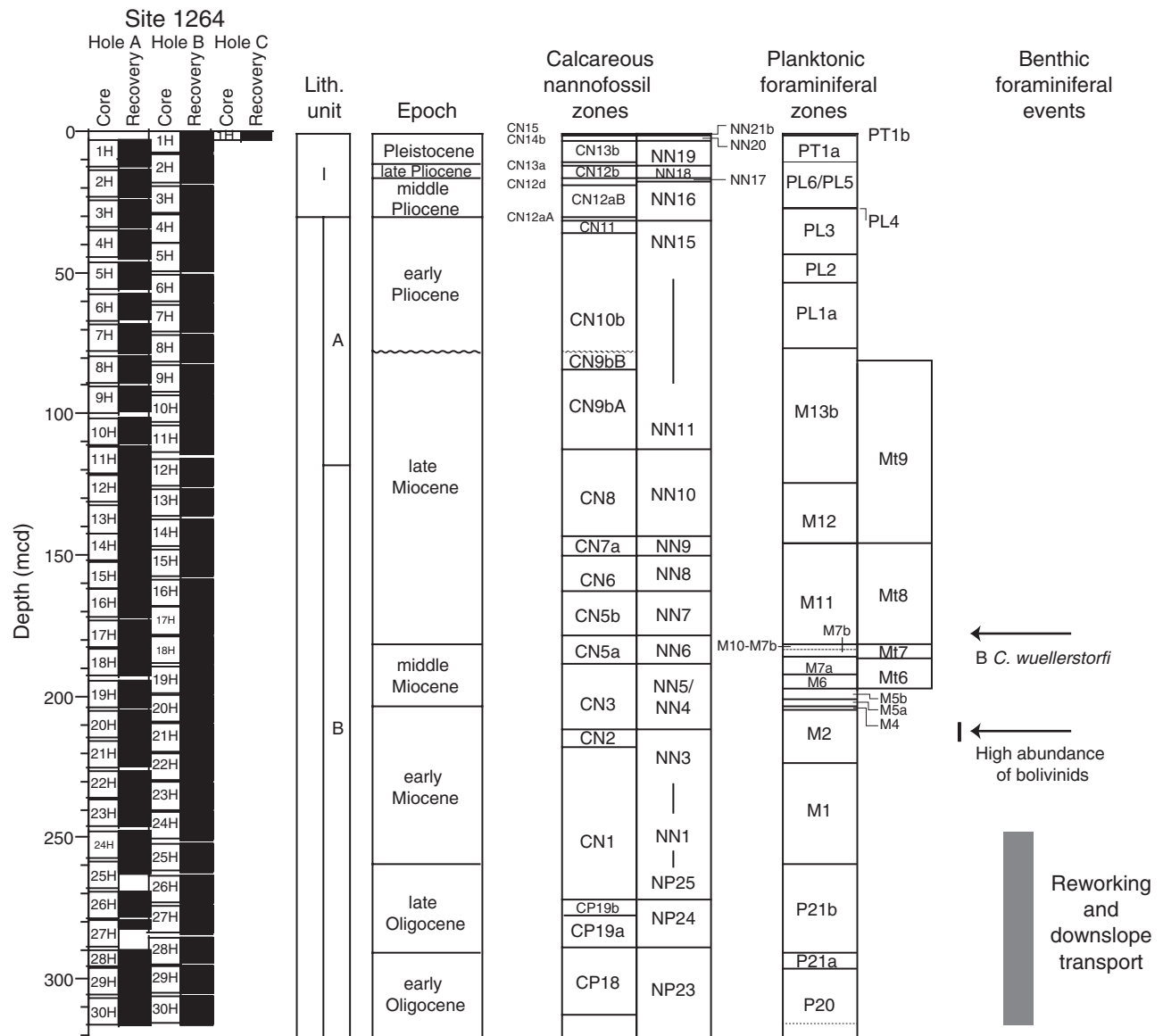


Figure F19. Summary of sedimentation rates at Site 1264 as delineated by a composite age/depth curve constructed using calcareous nannofossils and planktonic and benthic foraminifers.

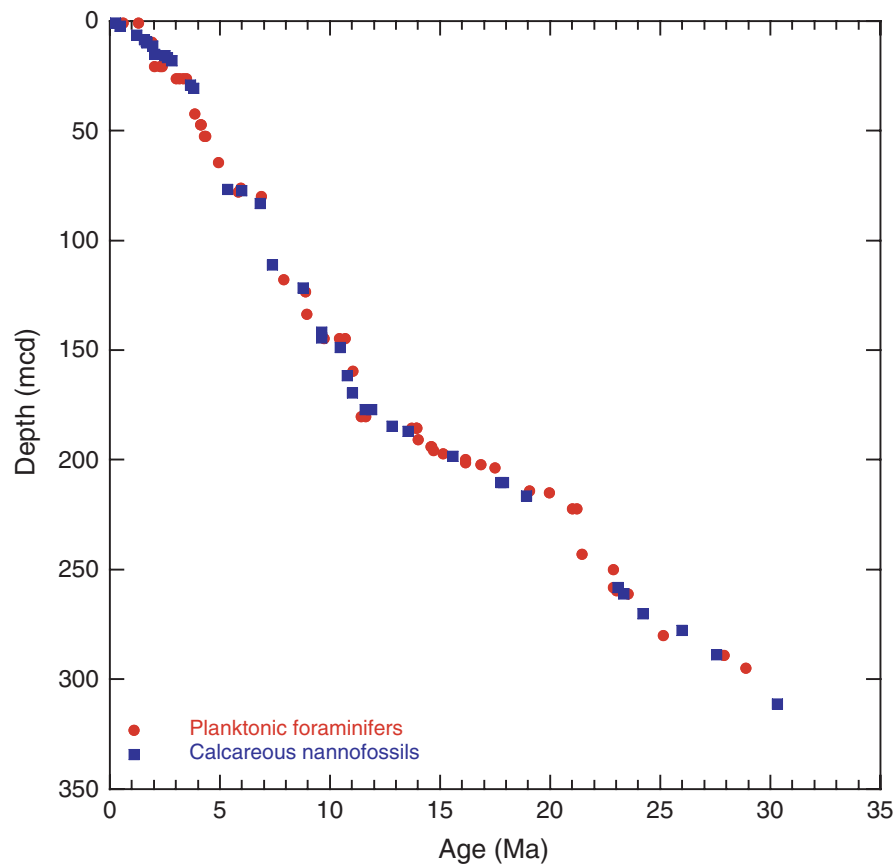


Figure F20. Downhole variation in intensities of remanent magnetization before (gray) and after (black) demagnetization at 15 mT of Holes 1264A and 1264B.

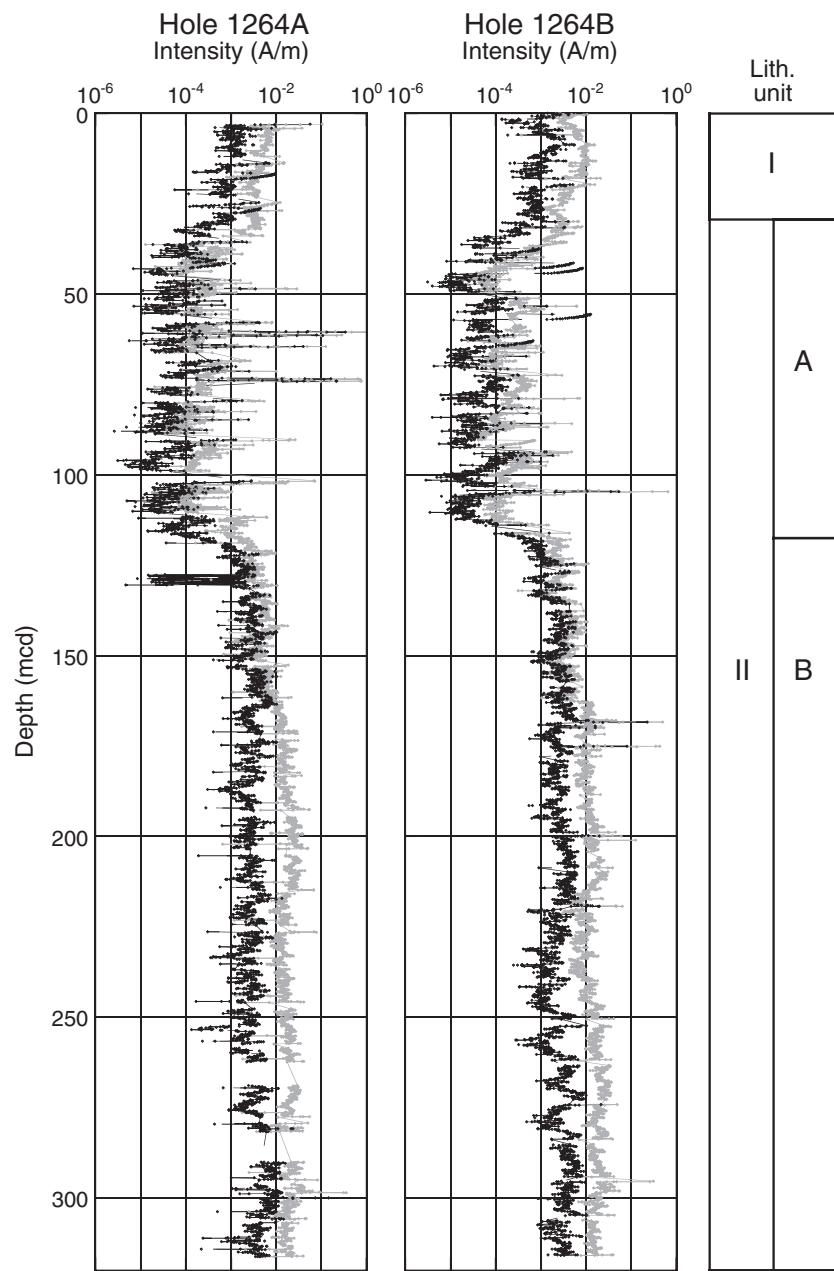


Figure F21. Downhole variation in initial magnetic susceptibility from Holes 1264A and 1264B.

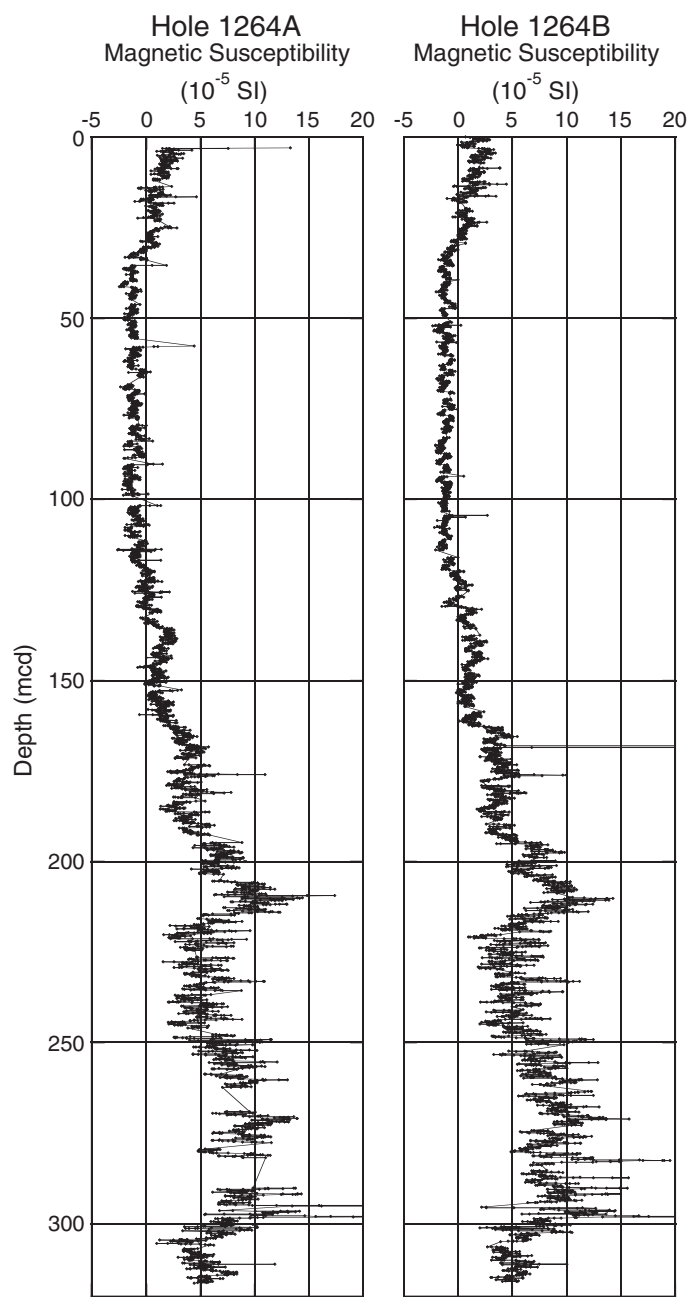


Figure F22. Downhole variation in depositional remanent magnetization after demagnetization to 15 mT and normalized by magnetic susceptibility ($nDRM_{15\text{ mT}}$) from Holes 1264A and 1264B.

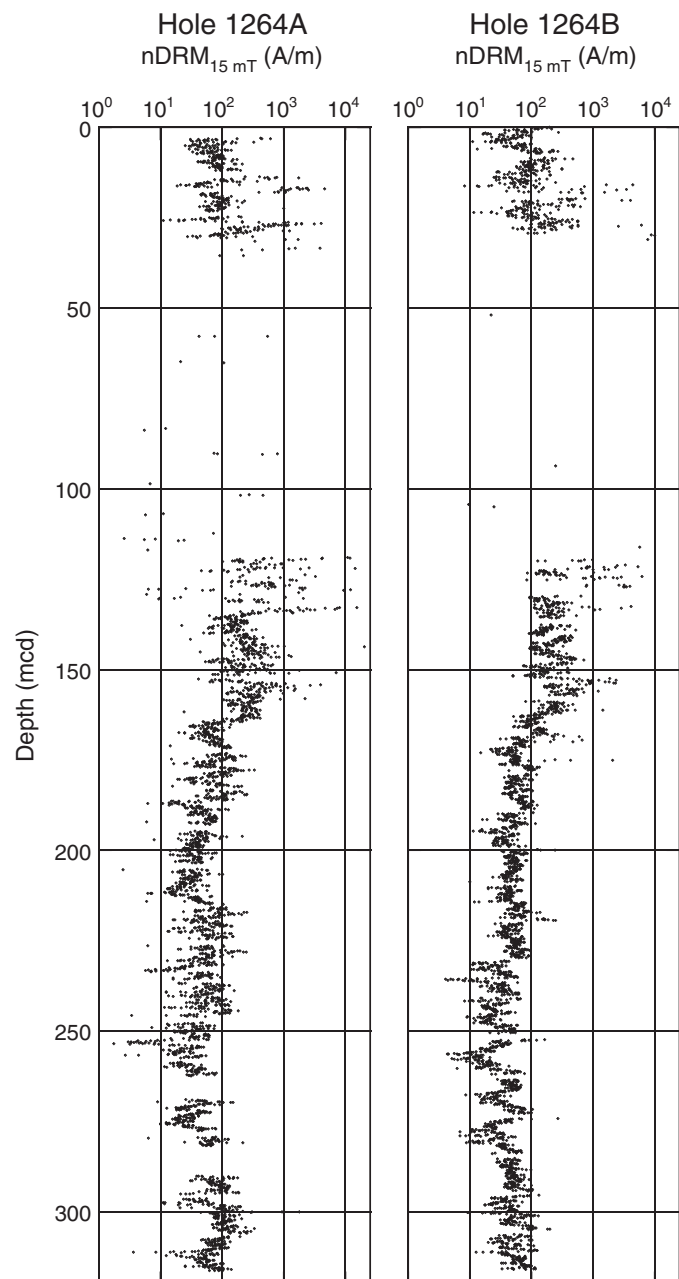


Figure F23. Preliminary magnetostratigraphic interpretation. Inclination data (at 15 mT) shown for Holes 1264A and 1264B. Data within 50 cm of a core top and 5 cm of section ends are not shown. Core breaks are denoted by green squares. Black rectangle = normal polarity, white = reversed polarity, shaded = uncertain polarity. X = intervals with no core recovery. A. 0–75 mcd. (Continued on next three pages.)

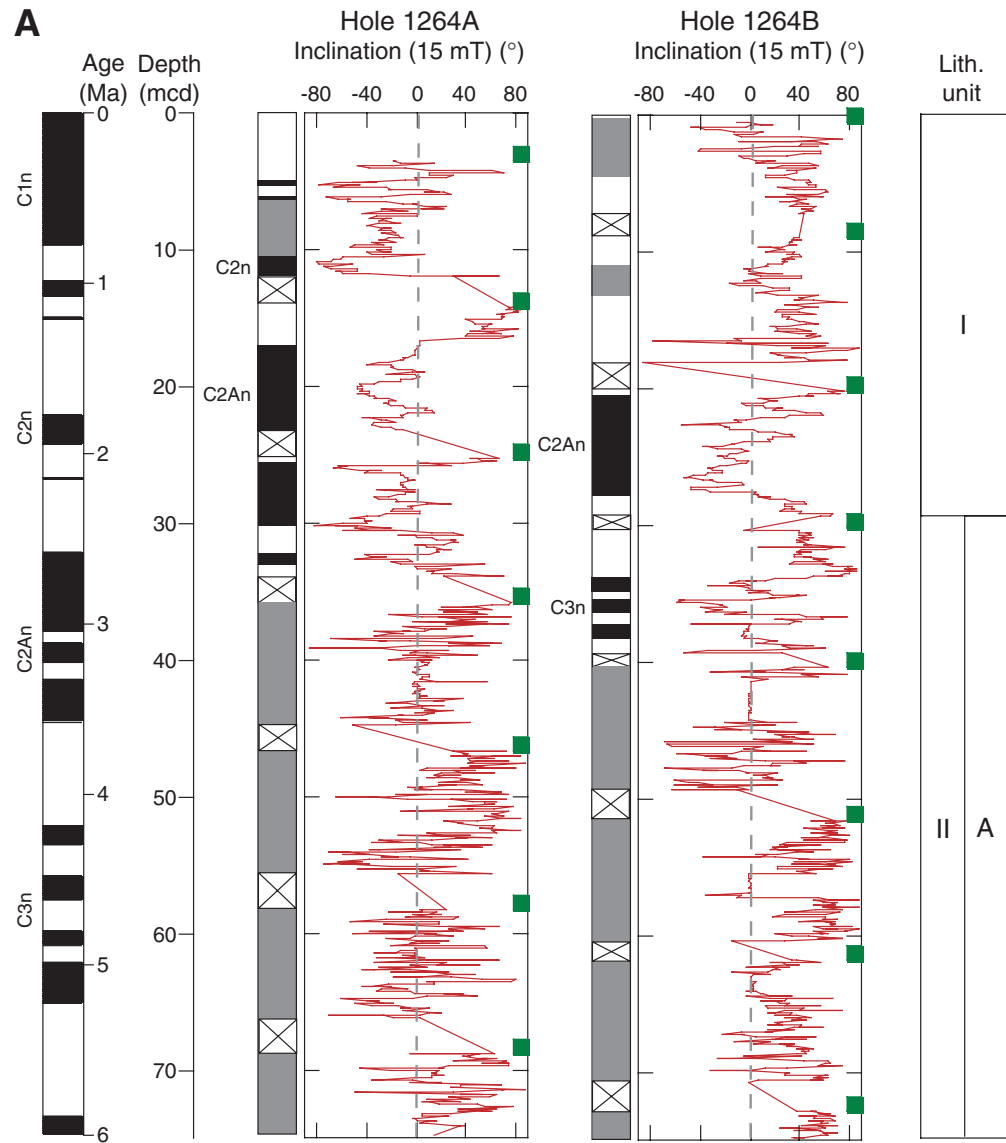


Figure F23 (continued). B. 65–150 mcd.

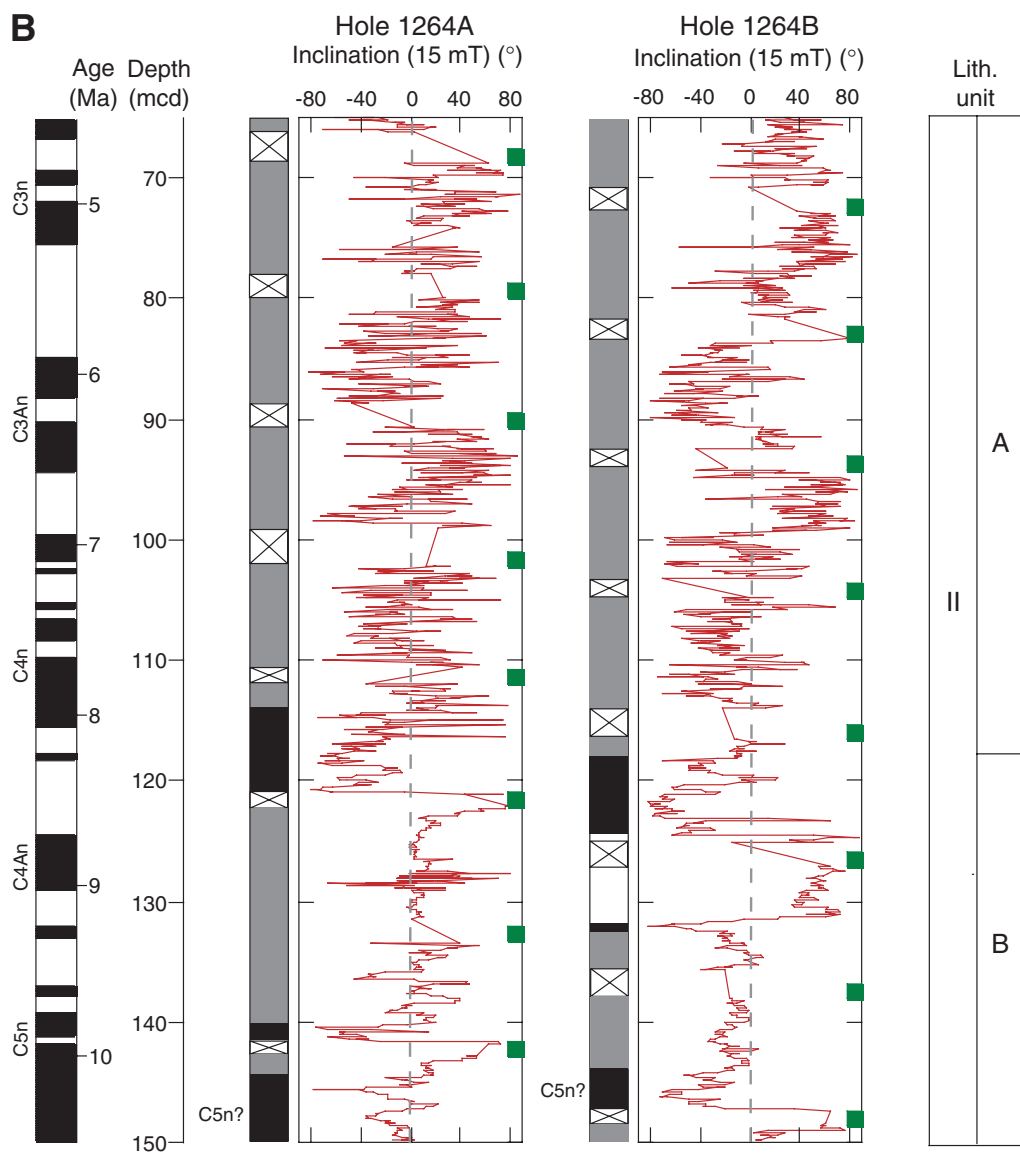


Figure F23 (continued). C. 140–225 mcd.

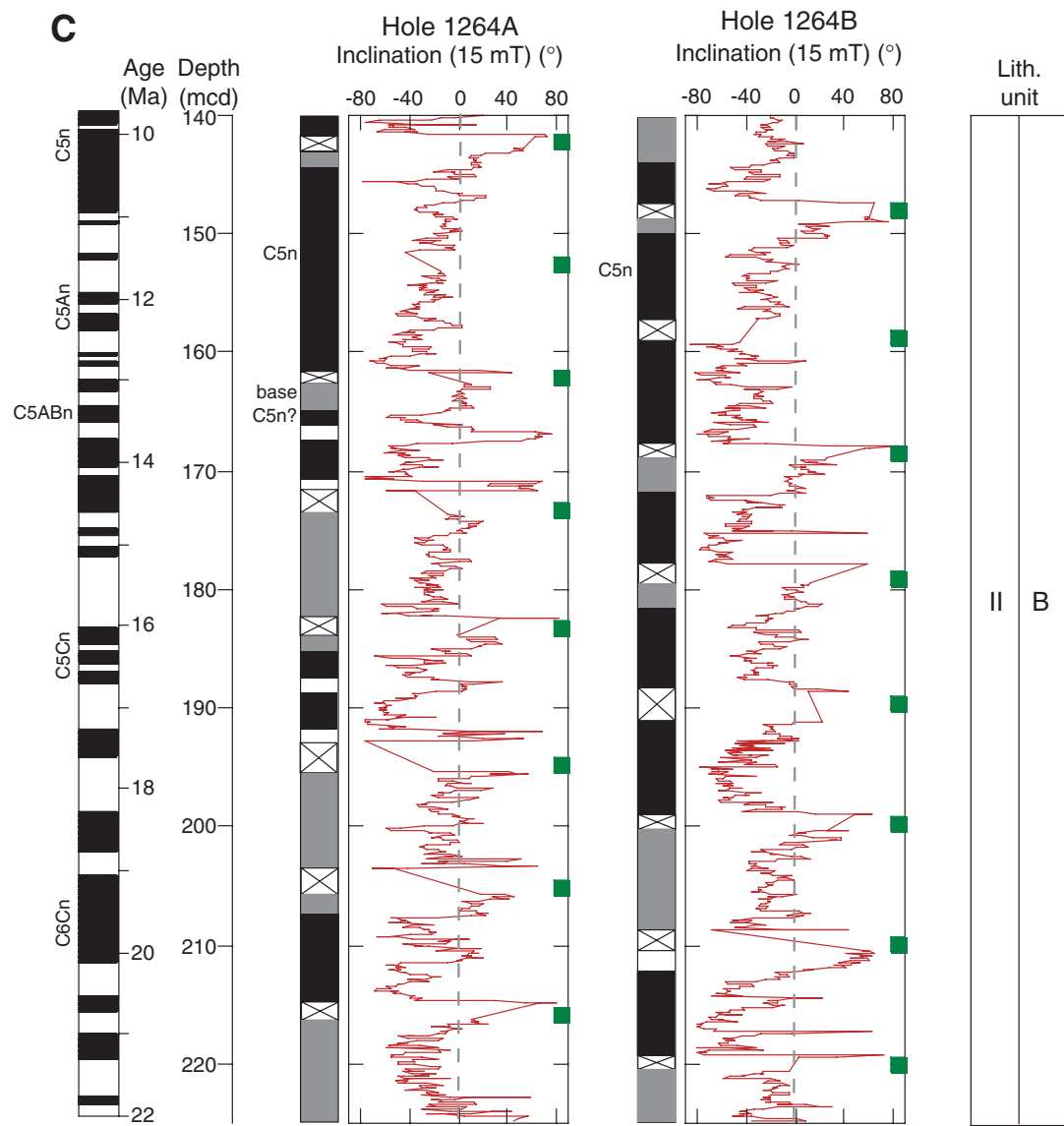


Figure F23 (continued). D. 115–320 mcd.

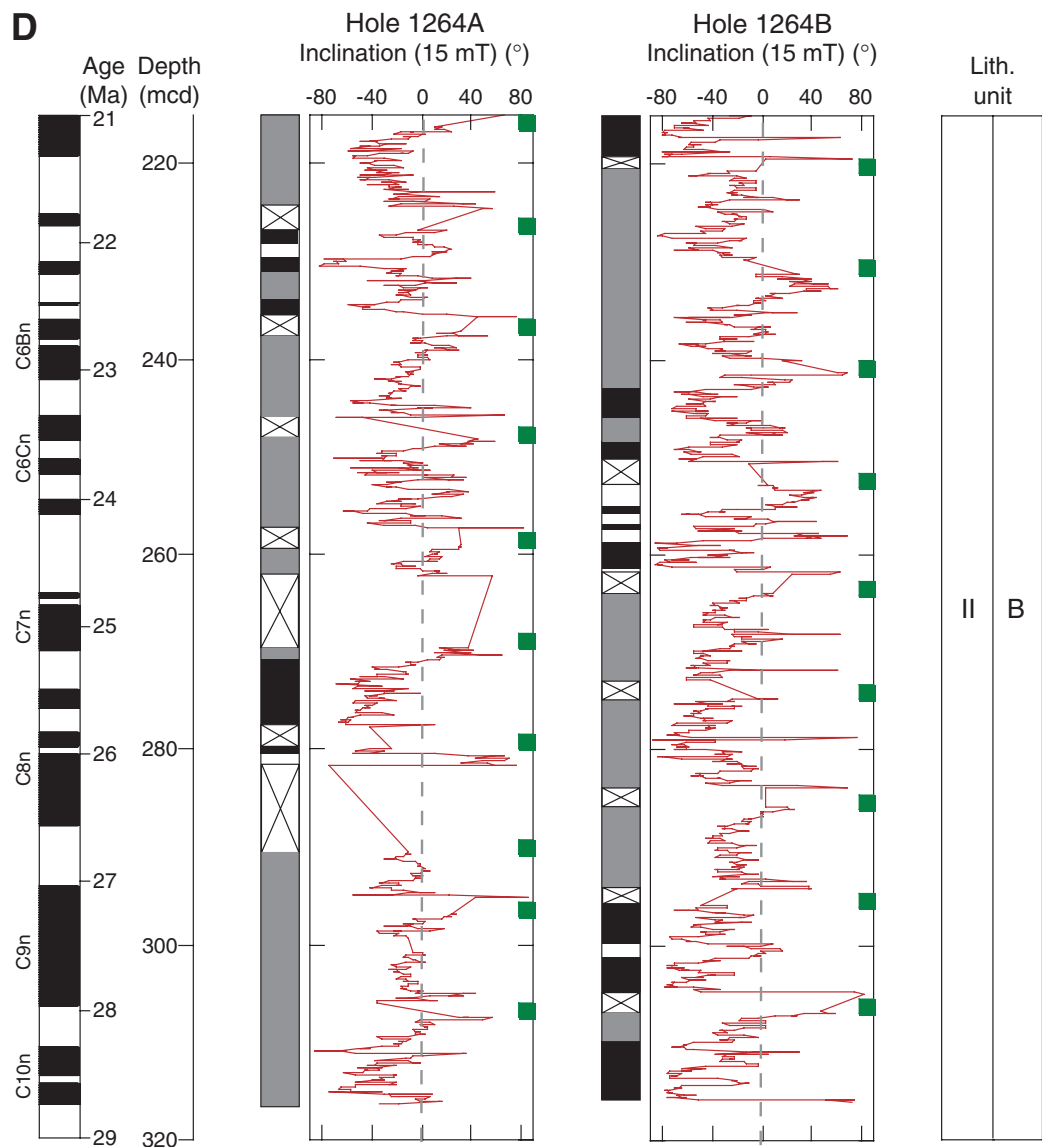


Figure F24. Profiles of chemical constituents in interstitial waters. A. Alkalinity. B. Chloride. C. Sodium. D. Potassium. E. Calcium. F. Magnesium. G. Strontium. H. Lithium. I. Boron. J. Barium. K. Sulfate. L. Manganese. M. Iron. N. Silicon. O. Zinc.

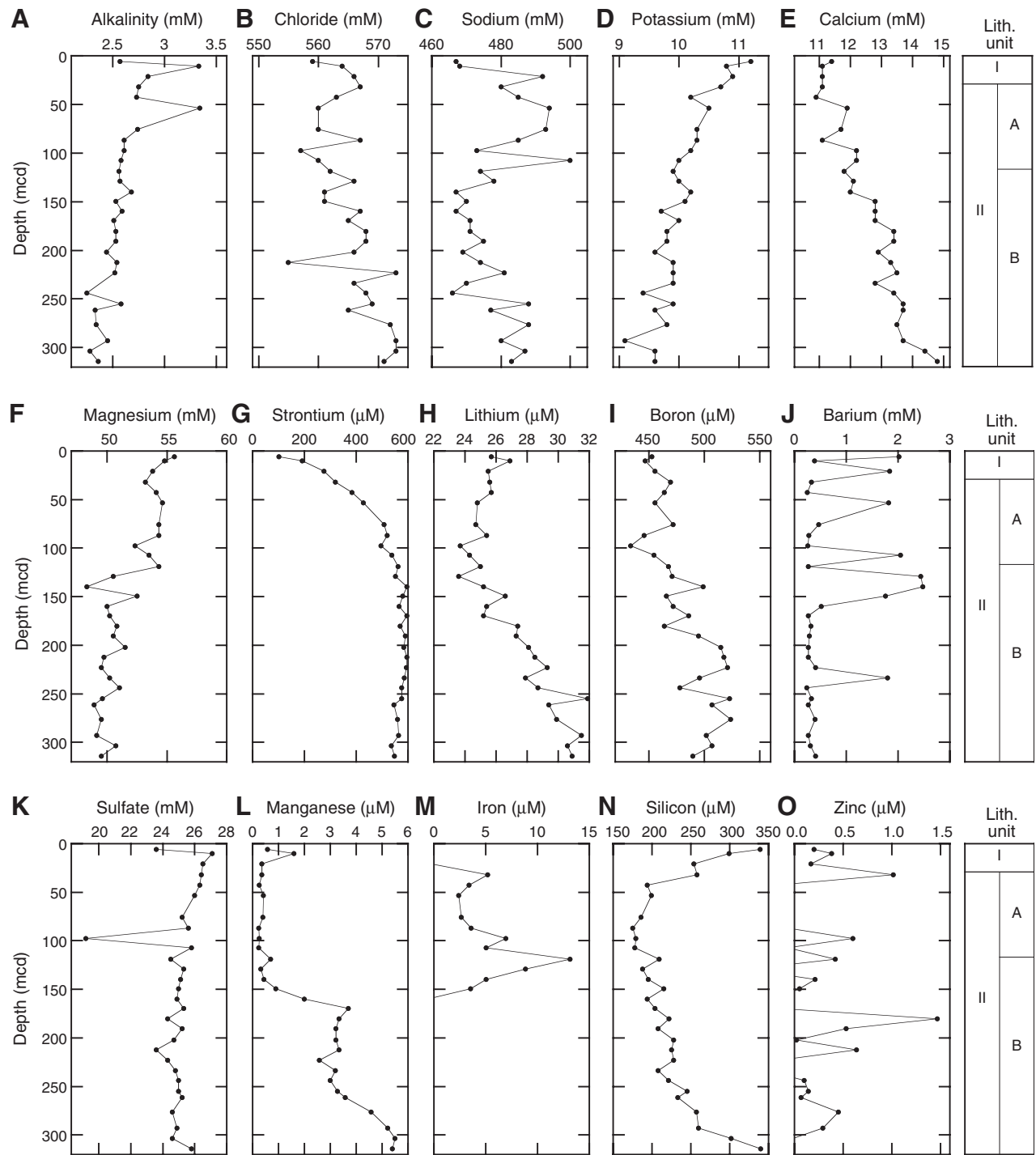


Figure F25. Sedimentary carbonate contents vs. composite depth.

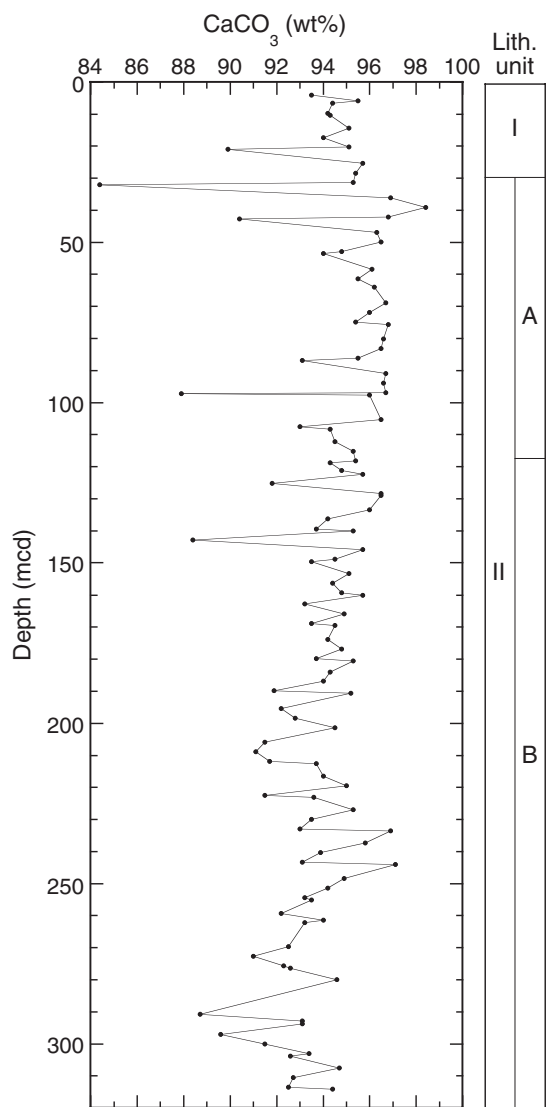


Figure F26. Selected ion chromatograms from Sites 1264 and 1263.

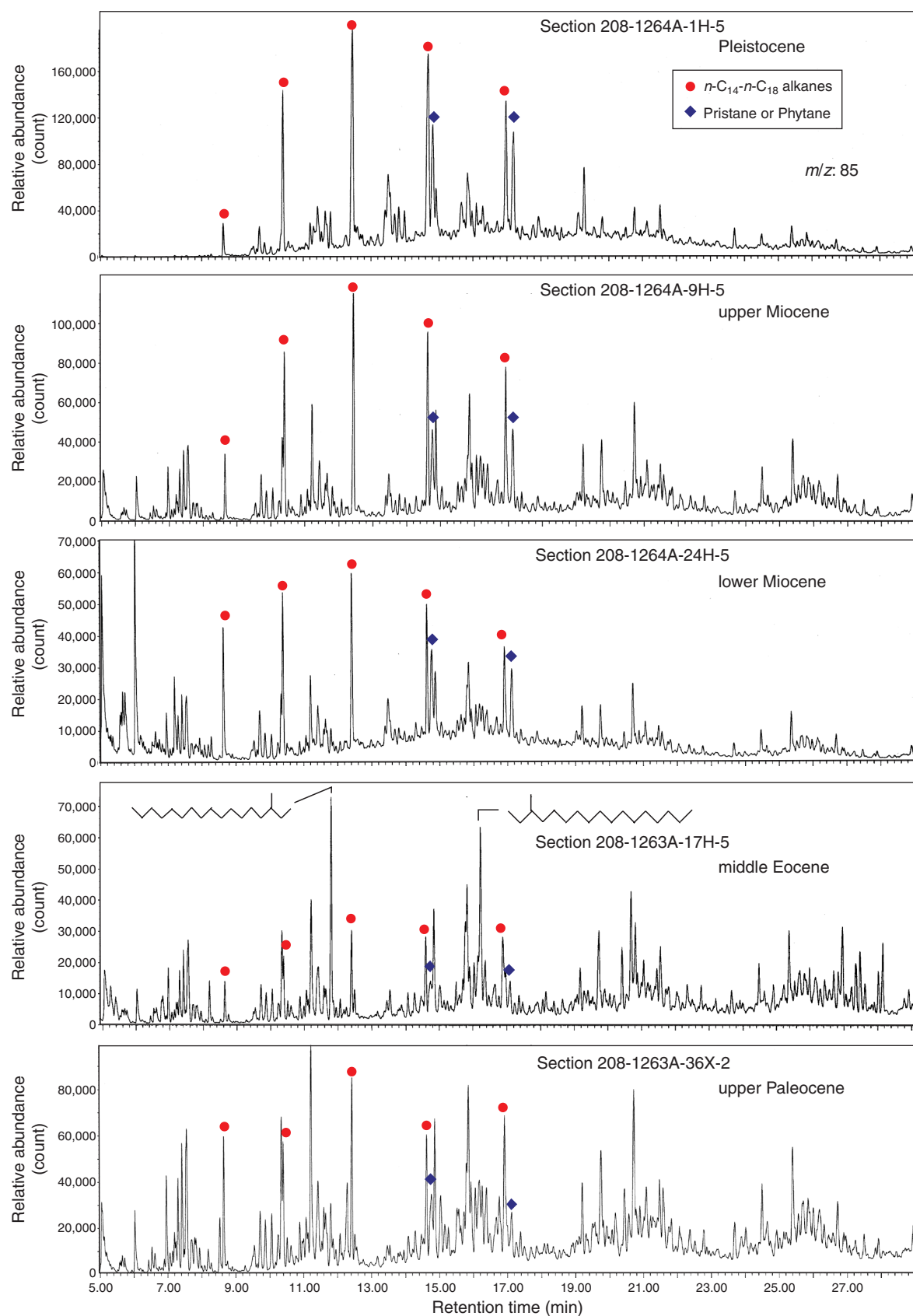


Figure F27. Boron concentration depth profiles of sediment dissolution and pore water samples for Sites 1263 and 1264. Error bars represent the precision of repeated analyses of one sediment dissolution sample.

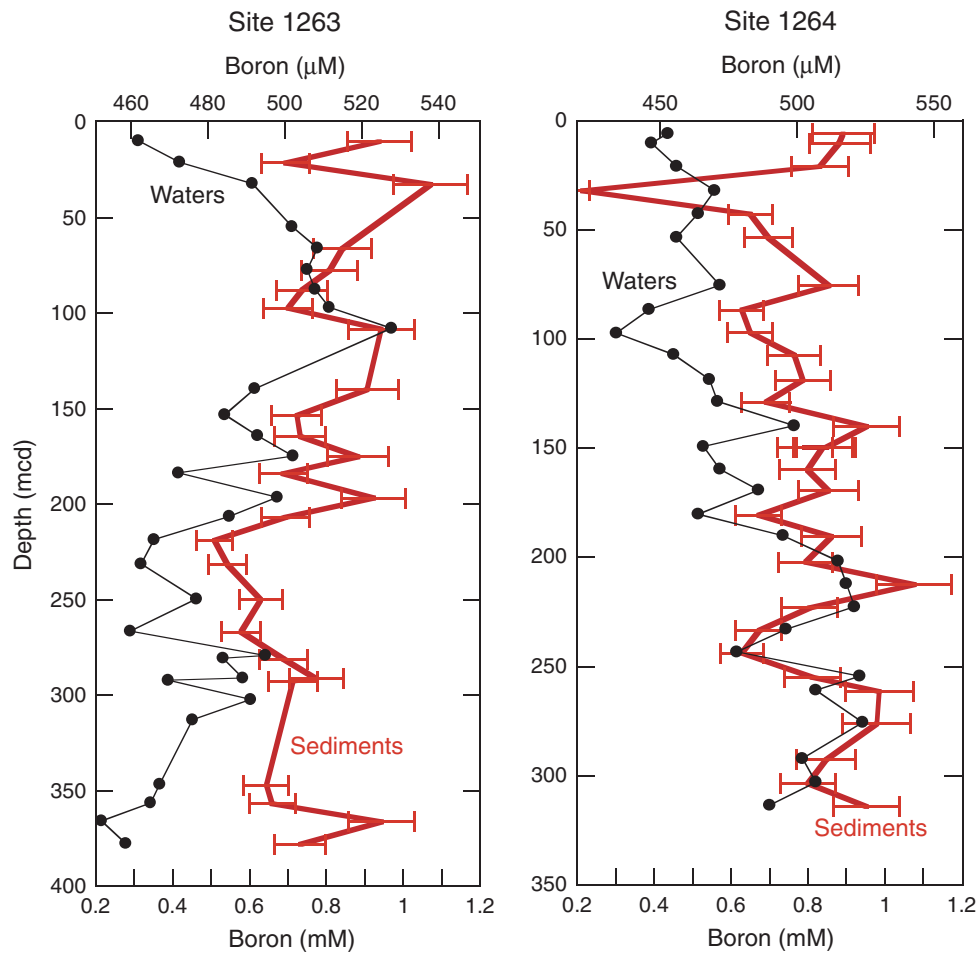


Figure F28. Strontium concentration depth profiles of sediment dissolution and pore water samples for Sites 1263 and 1264. Error bars represent the precision of repeated analyses of one sediment dissolution sample.

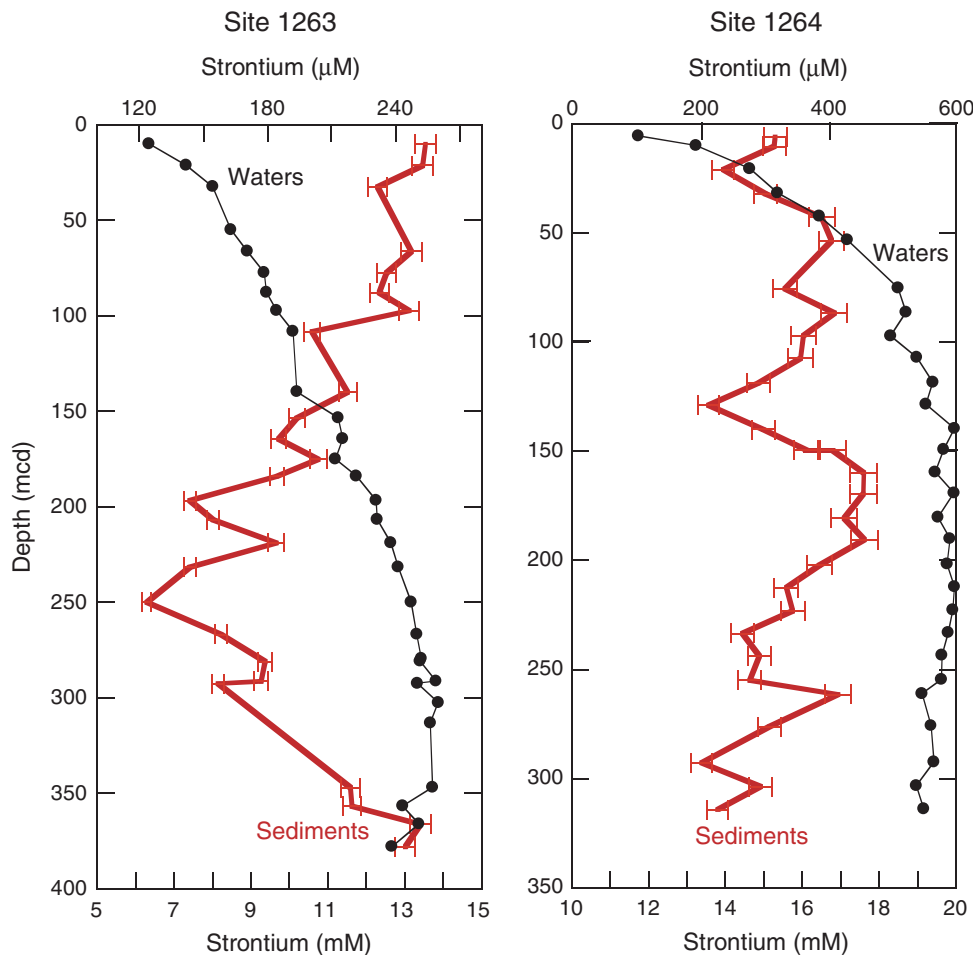
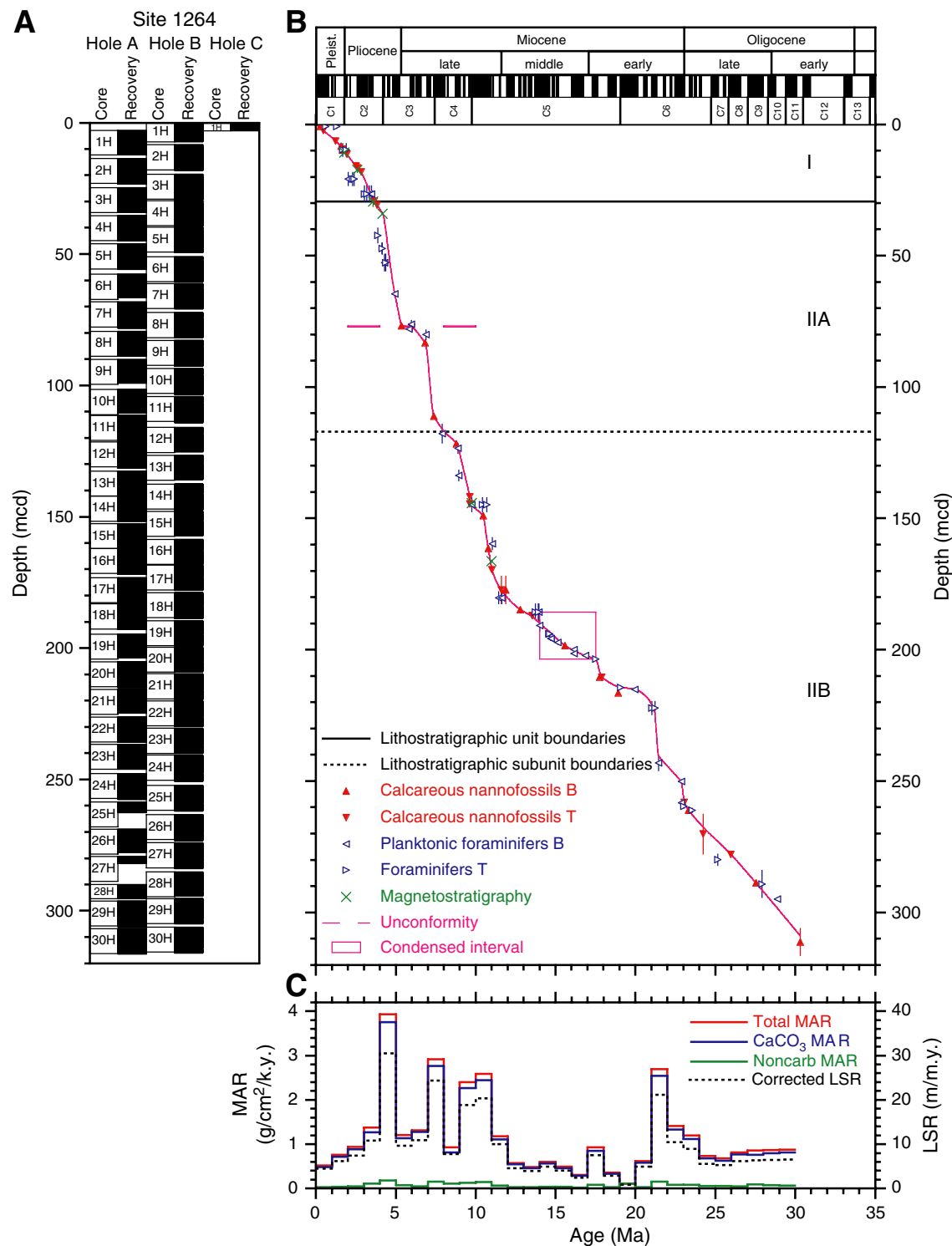


Figure F29. A. Core recovery plot. B. Shipboard biostratigraphic and magnetostratigraphic datums and the interpreted age-depth model. C. Corrected linear sedimentation rate (LSR), total, carbonate, and noncarbonate mass accumulation rates (MAR), calculated from the age model sampled at 1-m.y. intervals, and dry density and calcium carbonate concentrations averaged over the same 1-m.y. intervals. B = bottom, T = top.



SHIPBOARD SCIENTIFIC PARTY
CHAPTER 5, SITE 1264

54

Table T1. Coring summary, Site 1264. (See table notes. Continued on next page.)

Core	Date (Apr 2003)	Local time (hr)	Depth (mbsf)		Length (m)		Recovery (%)	Tool deployment
			Top	Bottom	Cored	Recovered		
208-1264A-								
1H	5	1520	0.0	9.3	9.3	9.35	100.5	
2H	5	1605	9.3	18.8	9.5	9.84	103.6	NMCB
3H	5	1650	18.8	28.3	9.5	9.54	100.4	Tensor
4H	5	1800	28.3	37.8	9.5	9.78	103.0	APCT, Tensor
5H	5	1845	37.8	47.3	9.5	9.80	103.2	Tensor
6H	5	1920	47.3	56.8	9.5	8.99	94.6	Tensor, NMCB
7H	5	2025	56.8	66.3	9.5	10.05	105.8	APCT, Tensor
8H	5	2110	66.3	75.8	9.5	9.52	100.2	Tensor, NMCB
9H	5	2155	75.8	85.3	9.5	9.05	95.3	Tensor
10H	5	2255	85.3	94.8	9.5	9.08	95.6	APCT, Tensor
11H	5	2355	94.8	104.3	9.5	10.0	105.3	Tensor
12H	6	50	104.3	113.8	9.5	10.03	105.6	Tensor, NMCB
13H	6	155	113.8	123.3	9.5	9.43	99.3	APCT, Tensor
14H	6	245	123.3	132.8	9.5	9.65	101.6	Tensor, NMCB
15H	6	420	132.8	142.3	9.5	9.37	98.6	DO, Tensor
16H	6	535	142.3	151.8	9.5	9.88	104.0	DO, Tensor
17H	6	640	151.8	161.3	9.5	9.50	100.0	DO, Tensor
18H	6	740	161.3	170.8	9.5	9.73	102.4	DO, Tensor
19H	6	845	170.8	180.3	9.5	9.01	94.8	DO, Tensor
20H	6	950	180.3	189.8	9.5	9.92	104.4	Tensor
21H	6	1040	189.8	199.3	9.5	9.07	95.5	Tensor
22H	6	1130	199.3	208.8	9.5	9.67	101.8	Tensor
23H	6	1220	208.8	218.3	9.5	9.57	100.7	DO, Tensor
24H	6	1315	218.3	227.8	9.5	10.00	105.3	DO, Tensor
25H	6	1400	227.8	237.3	9.5	4.11	43.3	Tensor
26H	6	1450	237.3	246.8	9.5	8.96	94.3	Tensor
27H	6	1545	246.8	256.3	9.5	2.86	30.1	Tensor
28H	6	1635	256.3	261.7	5.4	5.47	101.3	DO, Tensor
29H	6	1800	261.7	271.2	9.5	9.82	103.4	DO, Tensor
30H	6	1935	271.2	280.7	9.5	9.71	102.2	DO, Tensor
			Cored totals:		280.7	270.76	96.5	
208-1264B-								
1H	6	2335	0.0	7.3	7.3	7.38	101.1	APCT
2H	7	15	7.3	16.8	9.5	9.88	104.0	
3H	7	105	16.8	26.3	9.5	9.92	104.4	Tensor, NMCB
4H	7	145	26.3	35.8	9.5	9.81	103.3	Tensor
5H	7	230	35.8	45.3	9.5	9.74	102.5	Tensor, NMCB
6H	7	315	45.3	54.8	9.5	9.69	102.0	Tensor, NMCB
7H	7	350	54.8	64.3	9.5	9.66	101.7	Tensor, NMCB
8H	7	430	64.3	73.8	9.5	9.64	101.5	Tensor
9H	7	510	73.8	83.3	9.5	9.93	104.5	Tensor, NMCB
10H	7	550	83.3	92.8	9.5	9.98	105.1	Tensor
11H	7	645	92.8	102.3	9.5	10.05	105.8	APCT, Tensor
12H	7	725	102.3	111.8	9.5	9.40	99.0	Tensor
13H	7	810	111.8	121.3	9.5	9.36	98.5	Tensor, NMCB
14H	7	855	121.3	130.8	9.5	10.03	105.6	Tensor
15H	7	935	130.8	140.3	9.5	9.44	99.4	Tensor, NMCB
16H	7	1040	140.3	149.8	9.5	9.57	100.7	DO, Tensor, NMCB
17H	7	1210	149.8	159.3	9.5	9.67	101.8	DO, Tensor
18H	7	1255	159.3	168.8	9.5	9.88	104.0	Tensor
19H	7	1335	168.8	178.3	9.5	9.69	102.0	Tensor
20H	7	1425	178.3	187.8	9.5	9.31	98.0	Tensor
21H	7	1545	187.8	197.3	9.5	9.86	103.8	DO, APCT, Tensor
22H	7	1630	197.3	206.8	9.5	9.93	104.5	Tensor
23H	7	1720	206.8	216.3	9.5	9.63	101.4	Tensor
24H	7	1820	216.3	225.8	9.5	10.03	105.6	DO, Tensor
25H	7	1905	225.8	235.3	9.5	9.84	103.6	Tensor
26H	7	2005	235.3	244.8	9.5	10.01	105.4	DO, Tensor
27H	7	2125	244.8	254.3	9.5	9.90	104.2	DO, Tensor
28H	7	2245	254.3	263.8	9.5	9.25	97.4	DO, Tensor
29H	8	20	263.8	273.3	9.5	9.72	102.3	DO, Tensor
30H	8	145	273.3	282.8	9.5	9.89	104.1	DO, Tensor
			Cored totals:		282.8	290.09	102.6	
208-1264C-								
1H	8	500	0.0	3.0	3.0	3.00	100.0	
			Cored totals:		3.0	3.00	100.0	
			Total:		566.5	563.85	99.5	

Table T1 (continued).

Notes: NMCB = nonmagnetic core barrel, including cutting shoe (made from Monel). Tensor = brand name for core barrel orientation tool.
APCT = Advanced Piston Corer Temperature tool (stainless steel housing is cutting shoe). DO = drillover. See Table **T1**, p. 106, in the
"Leg 208 Summary" chapter.

Table T2. Composite depth scale, Site 1264.

Core	Offset (m)	Depth	
		(mbsf)	(mcd)
208-1264A-			
1H	2.96	0.00	2.96
2H	4.33	9.30	13.63
3H	5.89	18.80	24.69
4H	7.06	28.30	35.36
5H	8.35	37.80	46.15
6H	10.41	47.30	57.71
7H	11.44	56.80	68.24
8H	13.12	66.30	79.42
9H	14.37	75.80	90.17
10H	16.31	85.30	101.61
11H	16.61	94.80	111.41
12H	17.25	104.30	121.55
13H	18.84	113.80	132.64
14H	18.89	123.30	142.19
15H	19.84	132.80	152.64
16H	19.84	142.30	162.14
17H	21.39	151.80	173.19
18H	21.92	161.30	183.22
19H	23.91	170.80	194.71
20H	24.89	180.30	205.19
21H	25.95	189.80	215.75
22H	26.97	199.30	226.27
23H	27.84	208.80	236.64
24H	29.40	218.30	247.70
25H	30.78	227.80	258.58
26H	31.65	237.30	268.95
27H	32.50	246.80	279.30
28H	33.72	256.30	290.02
29H	34.61	261.70	296.31
30H	35.61	271.20	306.81
208-1264B-			
1H	0.00	0.00	0.00
2H	1.11	7.30	8.41
3H	2.81	16.80	19.61
4H	3.45	26.30	29.75
5H	4.02	35.80	39.82
6H	5.73	45.30	51.03
7H	6.49	54.80	61.29
8H	8.01	64.30	72.31
9H	9.06	73.80	82.86
10H	10.30	83.30	93.60
11H	11.41	92.80	104.21
12H	13.72	102.30	116.02
13H	14.77	111.80	126.57
14H	16.23	121.30	137.53
15H	17.14	130.80	147.94
16H	18.34	140.30	158.64
17H	18.59	149.80	168.39
18H	19.63	159.30	178.93
19H	20.79	168.80	189.59
20H	21.41	178.30	199.71
21H	22.02	187.80	209.82
22H	22.77	197.30	220.07
23H	23.77	206.80	230.57
24H	24.47	216.30	240.77
25H	26.48	225.80	252.28
26H	28.05	235.30	263.35
27H	29.33	244.80	274.13
28H	30.92	254.30	285.22
29H	31.55	263.80	295.35
30H	32.97	273.30	306.27
208-1264C-			
1H	0.10	0.00	0.10

Table T3. Splice tie points, Site 1264.

Hole, core, section, interval (cm)	Depth		Hole, core, section, interval (cm)	Depth	
	(mbsf)	(mcd)		(mbsf)	(mcd)
208-					
1264B-1H-3, 95	3.95	3.95	Tie to	1264A-1H-1, 98.5	0.99
1264A-1H-7, 10	8.60	11.56	Tie to	1264B-2H-3, 15	10.45
1264B-2H-6, 122.5	16.02	17.13	Tie to	1264A-2H-3, 50	12.80
1264A-2H-5, 75	16.05	20.38	Tie to	1264B-3H-1, 76	17.57
1264B-3H-5, 92.5	23.70	26.51	Tie to	1264A-3H-2, 32.5	20.62
1264A-3H-6, 97.5	27.27	33.16	Tie to	1264B-4H-3, 39.5	29.71
1264B-4H-5, 85	33.15	36.60	Tie to	1264A-4H-1, 123.5	29.54
1264A-4H-4, 90	33.70	40.76	Tie to	1264B-5H-1, 93.5	36.74
1264B-5H-7, 22.5	45.03	49.05	Tie to	1264A-5H-2, 140	40.70
1264A-5H-6, 25	45.55	53.90	Tie to	1264B-6H-2, 137.5	48.17
1264B-6H-6, 85	53.65	59.38	Tie to	1264A-6H-2, 17.5	48.97
1264A-6H-6, 102.5	54.71	65.12	Tie to	1264B-7H-3, 82	58.63
1264B-7H-6, 125	63.55	70.04	Tie to	1264A-7H-2, 30	58.60
1264A-7H-5, 35	63.15	74.59	Tie to	1264B-8H-2, 77	66.58
1264B-8H-7, 10	73.40	81.41	Tie to	1264A-8H-2, 48.5	68.29
1264A-8H-5, 95	73.25	86.37	Tie to	1264B-9H-3, 51	77.31
1264B-9H-7, 17.5	82.97	92.03	Tie to	1264A-9H-2, 34.5	77.66
1264A-9H-5, 82.5	82.62	96.99	Tie to	1264B-10H-3, 38.5	86.69
1264B-10H-7, 7.5	92.26	102.56	Tie to	1264A-10H-1, 95	86.25
1264A-10H-4, 135	91.15	107.46	Tie to	1264B-11H-3, 93.5	96.05
1264B-11H-8, 55	102.66	114.07	Tie to	1264A-11H-2, 116	97.46
1264A-11H-6, 125	103.55	120.16	Tie to	1264B-12H-4, 59.5	106.44
1264B-12H-6, 5	108.88	122.60	Tie to	1264A-12H-1, 105	105.35
1264A-12H-6, 17.5	111.97	129.22	Tie to	1264B-13H-2, 115	114.45
1264B-13H-6, 65	119.95	134.72	Tie to	1264A-13H-2, 57.5	115.88
1264A-13H-5, 137.5	121.18	140.02	Tie to	1264B-14H-2, 98.5	123.79
1264B-14H-6, 92.5	129.73	145.96	Tie to	1264A-14H-3, 77.5	127.07
1264A-14H-6, 97.5	131.77	150.66	Tie to	1264B-15H-2, 122.5	133.52
1264B-15H-5, 120	138.00	155.14	Tie to	1264A-15H-2, 100	135.30
1264A-15H-6, 77.5	141.07	160.91	Tie to	1264B-16H-2, 75.5	142.57
1264B-16H-5, 122.5	147.52	165.86	Tie to	1264A-16H-3, 72.5	146.02
1264A-16H-6, 105	150.85	170.69	Tie to	1264B-17H-2, 80	152.10
1264B-17H-5, 90	156.70	175.29	Tie to	1264A-17H-2, 58	153.90
1264A-17H-5, 27.5	158.07	179.46	Tie to	1264B-18H-1, 52	159.83
1264B-18H-6, 10	166.90	186.53	Tie to	1264A-18H-3, 31	164.61
1264A-18H-7, 42.5	170.73	192.65	Tie to	1264B-19H-3, 4.5	171.86
1264B-19H-6, 100	177.30	198.09	Tie to	1264A-19H-3, 37.5	174.18
1264A-19H-5, 105	177.85	201.76	Tie to	1264B-20H-2, 55	180.35
1264B-20H-5, 87.5	185.18	206.59	Tie to	1264A-20H-1, 140	181.70
1264A-20H-6, 95	188.75	213.64	Tie to	1264B-21H-3, 82.5	191.62
1264B-21H-5, 75	194.55	216.57	Tie to	1264A-21H-1, 82.5	190.62
1264A-21H-5, 92.5	196.72	222.67	Tie to	1264B-22H-2, 109.5	199.90
1264B-22H-6, 92.5	205.72	228.49	Tie to	1264A-22H-2, 72.5	201.52
1264A-22H-5, 95	206.25	233.22	Tie to	1264B-23H-2, 115	209.45
1264B-23H-6, 87.5	215.18	238.95	Tie to	1264A-23H-2, 81	211.11
1264A-23H-6, 32.5	216.62	244.46	Tie to	1264B-24H-3, 68.5	219.99
1264B-24H-6, 102.5	224.82	249.29	Tie to	1264A-24H-2, 8.5	219.89
1264A-24H-4, 90	223.70	253.10	Tie to	1264B-25H-1, 80.5	226.62
1264B-25H-5, 57.5	232.38	258.86	Tie to	1264A-25H-1, 27.5	228.08
1264A-25H-C, 20	231.82	262.60	Append to	1264B-26H-1, 0	235.30
1264B-26H-5, 5	241.35	269.40	Tie to	1264A-26H-1, 45	237.75
1264A-26H-5, 127.5	244.58	276.23	Tie to	1264B-27H-2, 60	246.90
1264B-27H-7, 75	254.55	283.88	Append to	1264B-28H-1, 0	254.30
1264B-28H-5, 35	260.65	291.57	Tie to	1264A-28H-2, 5	257.85
1264A-28H-C, 17.5	261.67	295.39	Append to	1264B-29H-1, 0	263.80
1264B-29H-2, 107.5	266.38	297.93	Tie to	1264A-29H-2, 12.5	263.32
1264A-29H-C, 5	271.44	306.05	Append to	1264B-30H-1, 0	273.30
1264B-30H-3, 85	277.15	310.12	Tie to	1264A-30H-3, 31	274.51
1264A-30H-C, 7.5	280.83	316.44			310.12

Note: This table is also available in [ASCII](#).

Table T4. Lithostratigraphic subdivisions, Site 1264.

Unit/ subunit	Unit boundary depth (mcd)	Hole 1264A						Hole 1264B						Hole 1264C					
		Core, section, interval (cm)		Depth (mbsf)		Depth (mcd)		Core, section, interval (cm)		Depth (mbsf)		Depth (mcd)		Core, section, interval (cm)		Depth (mbsf)		Depth (mcd)	
		Top	Base	Top	Base	Top	Base	Top	Base	Top	Base	Top	Base	Top	Base	Top	Base	Top	Base
I	29.4	1H-1, 0	3H-4, 21	0.0	23.5	3.0	29.4	1H-1, 0	4H-1, 29	0.0	26.6	0.0	30.0	1H-1, 0	1H-CC, 18	0.0	3.0	0.1	3.1
IIA	117.0	3H-4, 21	11H-4, 109	23.5	100.4	29.4	117.0	4H-1, 29	12H-2, 45	26.6	103.3	30.0	117.0	—	—	—	—	—	—
IIB	316.5	11H-4, 109	30H-CC, 15	100.4	280.9	117.0	316.5	12H-2, 45	30H-CC, 12	103.3	283.2	117.0	316.2	—	—	—	—	—	—

Notes: Bold intervals and depths define the unit boundaries; other intervals are recognized as part of units but do not contain the unit boundaries. — = lithostratigraphic unit not recovered.

Unit/ subunit	Unit boundary depth (mcd)	Description
I	29.4	Foraminifer-bearing nannofossil ooze, foraminifer nannofossil ooze, and nannofossil foraminifer ooze
IIA	117.0	Nannofossil ooze and foraminifer-bearing nannofossil ooze
IIB	316.5	Nannofossil ooze and foraminifer-bearing nannofossil ooze

Table T5. Stratigraphic positions of selected calcareous nannofossil datums, Site 1264.

Datum	Age (Ma)		Top of sample interval			Base of sample interval			
	Youngest	Oldest	Core, section, interval (cm)	Depth (mbsf)	(mcd)	Core, section, interval (cm)	Depth (mbsf)	(mcd)	
T	Large <i>Gephyrocapsa</i> spp.	1.24	1.24	1H-3, 20	3.20	6.16	1H-3, 70	3.70	6.66
B	Large <i>Gephyrocapsa</i> spp.	1.58	1.58	1H-4, 70	5.20	8.16	1H-4, 120	5.70	8.66
T	<i>Calcidiscus macintyrei</i>	1.67	1.67	1H-5, 20	6.20	9.16	1H-5, 70	6.70	9.66
B	Medium <i>Gephyrocapsa</i> spp.	1.69	1.69	1H-5, 70	6.70	9.66	1H-5, 120	7.20	10.16
T	<i>Discoaster brouweri</i> and <i>D. triradiatus</i>	1.95	1.97	1H-6, 70	8.20	11.16	1H-7, 20	8.70	11.66
T	<i>Discoaster pentaradiatus</i>	2.52	2.52	2H-2, 40	11.20	15.53	2H-2, 110	11.90	16.23
T	<i>Discoaster surculus</i>	2.63	2.63	2H-2, 110	11.90	16.23	2H-3, 40	12.70	17.03
T	<i>Discoaster tamalis</i>	2.83	2.83	2H-3, 110	13.40	17.73	2H-4, 40	14.20	18.53
T	<i>Sphenolithus</i> spp.	3.66	3.66	3H-3, 120	23.00	28.89	3H-4, 40	23.70	29.59
T	<i>Reticulofenestra pseudoumbilicus</i>	3.82	3.82	3H-4, 120	24.50	30.39	3H-5, 40	25.20	31.09
T	<i>Amaurolithus</i> spp.	4.56	4.56	3H-CC	28.29	34.18	4H-1, 40	28.70	35.76
B	<i>Ceratolithus acutus</i>	5.37	5.37	7H-6, 80	65.10	76.54	7H-6, 130	65.60	77.04
T	<i>Nicklithus amplificus</i>	6.00	6.00	7H-6, 130	65.60	77.04	7H-7, 20	66.00	77.44
B	<i>Nicklithus amplificus</i>	6.84	6.84	8H-3, 40	69.70	82.82	8H-3, 120	70.50	83.62
B	<i>Amaurolithus primus</i>	7.39	7.39	10H-CC	94.33	110.64	11H-1, 40	95.20	111.81
B	<i>Paracme Reticulofenestra pseudoumbilicus</i>	8.79	8.79	11H-CC	104.75	121.36	12H-1, 40	104.70	121.95
T	<i>Discoaster hamatus</i>	9.63	9.63	13H-7, 55	122.85	141.69	13H-CC	123.18	142.02
T	<i>Catinaster calyculus</i>	9.64	9.64	14H-2, 40	125.20	144.09	14H-2, 120	126.00	144.89
B	<i>Discoaster neohamatus</i>	8.45	8.45	14H-3, 120	127.50	146.39	14H-5, 40	129.70	148.59
B	<i>Discoaster bellus</i> gr. (= <i>B D. hamatus</i>)	10.48	10.48	14H-5, 40	129.70	148.59	14H-5, 120	130.50	149.39
B	<i>Catinaster coalitus</i>	10.79	10.79	15H-7, 20	141.50	161.34	15H-7, 60	141.90	161.74
T	<i>Coccoolithus miopelagicus</i>	11.02	11.02	16H-5, 120	149.50	169.34	16H-6, 40	150.20	170.04
TC	<i>Discoaster kugleri</i>	11.60	11.60	16H-CC	152.13	171.97	17H-CC	161.15	182.54
BC	<i>Discoaster kugleri</i>	11.88	11.88	16H-CC	152.13	171.97	17H-CC	161.15	182.54
B	<i>Triquetrorhabdulus rugosus</i>	12.81	12.81	18H-1, 120	162.50	184.42	18H-2, 40	163.20	185.12
T	<i>Sphenolithus heteromorphus</i>	13.55	13.55	18H-3, 40	164.70	186.62	18H-3, 120	165.50	187.42
B	<i>Discoaster signus</i> gr.	15.60	15.60	19H-3, 40	174.20	198.11	19H-3, 120	175.00	198.91
T	Acme <i>Discoaster deflandrei</i>	15.60	15.60	19H-3, 40	174.20	198.11	19H-3, 120	175.00	198.91
B	<i>Sphenolithus heteromorphus</i>	17.76	17.76	20H-4, 40	185.20	210.09	20H-4, 120	186.00	210.89
T	<i>Sphenolithus belemnos</i>	17.89	17.89	20H-4, 40	185.20	210.09	20H-4, 120	186.00	210.89
B	<i>Sphenolithus belemnos</i>	18.92	18.92	21H-1, 40	190.2	216.15	21H-1, 120	191.00	216.95
T	<i>Sphenolithus delphix</i>	23.07	23.07	24H-CC	228.25	257.65	25H-1, 10	227.90	258.68
B	<i>Sphenolithus delphix</i>	23.33	23.33	25H-2, 90	230.2	260.98	25H-2, 110	230.40	261.18
T	<i>Sphenolithus ciperoensis</i>	24.23	24.23	25H-CC	231.89	262.64	26H-CC	246.21	277.86
B	<i>Sphenolithus ciperoensis</i>	27.55	27.55	27H-CC	249.61	282.11	28H-1, 40	256.70	290.42
B	<i>Sphenolithus distentus</i>	30.32	30.32	29H-CC	271.47	306.08	30H-CC	280.86	316.47
			208-1264B-			208-1264B-			
B	Large <i>Gephyrocapsa</i> spp.	1.58	1.58	1H-CC	7.33	7.33	2H-CC	17.08	18.19
T	<i>Calcidiscus macintyrei</i>	1.67	1.67	1H-CC	7.33	7.33	2H-CC	17.08	18.19
B	Medium <i>Gephyrocapsa</i> spp.	1.69	1.69	1H-CC	7.33	7.33	2H-CC	17.08	18.19
T	<i>Discoaster brouweri</i> and <i>D. triradiatus</i>	1.95	1.97	1H-CC	7.33	7.33	2H-CC	17.08	18.19
T	<i>Discoaster pentaradiatus</i>	2.52	2.52	1H-CC	7.33	7.33	2H-CC	17.08	18.19
T	<i>Discoaster surculus</i>	2.63	2.63	1H-CC	7.33	7.33	2H-CC	17.08	18.19
T	<i>Discoaster tamalis</i>	2.83	2.83	2H-CC	17.08	18.19	3H-CC	26.67	29.48
T	<i>Sphenolithus</i> spp.	3.66	3.66	3H-CC	26.67	29.48	4H-CC	36.06	39.51
T	<i>Reticulofenestra pseudoumbilicus</i>	3.82	3.82	3H-CC	26.67	29.48	4H-CC	36.06	39.51
T	<i>Amaurolithus</i> spp.	4.56	4.56	4H-CC	36.06	39.51	5H-CC	45.44	49.46
B	<i>Amaurolithus primus</i>	7.39	7.39	10H-CC	93.23	103.53	11H-CC	102.8	114.21
T	<i>Discoaster hamatus</i>	9.63	9.63	13H-CC	121.11	135.88	14H-CC	131.28	147.51
B	<i>Discoaster bellus</i> gr. (= <i>B D. hamatus</i>)	10.48	10.48	14H-CC	131.28	147.51	15H-CC	140.14	157.28
B	<i>Catinaster coalitus</i>	10.79	10.79	15H-CC	140.14	157.28	16H-CC	149.82	168.16
T	<i>Coccoolithus miopelagicus</i>	11.02	11.02	15H-CC	140.14	157.28	16H-CC	149.82	168.16
B	<i>Triquetrorhabdulus rugosus</i>	12.81	12.81	17H-CC	159.37	177.96	18H-CC	169.13	188.76
T	<i>Sphenolithus heteromorphus</i>	13.55	13.55	17H-CC	159.37	177.96	18H-CC	169.13	188.76
B	<i>Sphenolithus heteromorphus</i>	17.76	17.76	20H-CC	187.56	208.97	21H-CC	197.61	219.63
T	<i>Sphenolithus belemnos</i>	17.89	17.89	21H-CC	197.61	219.63	22H-CC	207.18	229.95
T	<i>Sphenolithus delphix</i>	23.07	23.07	24H-CC	226.28	250.75	25H-CC	235.59	262.07
B	<i>Sphenolithus delphix</i>	23.33	23.33	24H-CC	226.28	250.75	25H-CC	235.59	262.07
T	<i>Sphenolithus ciperoensis</i>	24.23	24.23	26H-3, 10	238.40	266.45	26H-3, 40	238.70	266.75
T	<i>Sphenolithus distentus</i>	25.98	25.98	27H-3, 60	248.40	277.73	27H-3, 100	248.80	278.13
B	<i>Sphenolithus ciperoensis</i>	27.55	27.55	28H-3, 30	257.60	288.52	28H-3, 100	258.30	289.22
			208-1264C-			208-1264C-			
B	<i>Emiliania huxleyi</i>	0.26	0.26	1H-1, 1	0	0.1	1H-2, 1	1.46	1.56
T	<i>Pseudoemiliania lacunosa</i>	0.46	0.46	1H-2, 1	1.46	1.56	1H-CC	2.95	3.05

Note: T = top, B = bottom.

Table T6. Stratigraphic positions of selected planktonic foraminiferal datums, Site 1264.

Datum	Age (Ma)		Hole, core, section, interval (cm)	Depth		Hole, core, section, interval (cm)	Depth	
	Youngest	Oldest		(mbsf)	(mcd)		(mbsf)	(mcd)
208-								
T <i>Globorotalia tosaensis</i>	0.61	0.61	1264C-1H-1, 0–1	0.00	0.10	1264C-2H-2, 0–2	1.45	1.55
T <i>Globigerinoides obliquus</i>	1.30	1.30	1264C-1H-1, 0–1	0.00	0.10	1264C-2H-2, 0–2	1.45	1.55
T <i>Globigerina apertura</i>	1.68	1.68	1264B-1H-CC	7.33	7.33	1264A-1H-CC	9.30	12.26
T <i>Globigerinoides extremus</i>	1.91	1.91	1264B-1H-CC	7.33	7.33	1264A-1H-CC	9.30	12.26
B <i>Globorotalia truncatulinoides</i>	2.03	2.03	1264B-2H-CC	17.08	18.19	1264A-2H-CC	19.09	23.42
T <i>Globoturborotalita woodi</i>	2.30	2.30	1264B-2H-CC	17.08	18.19	1264A-2H-CC	19.09	23.42
T <i>Menardella miocenica</i>	2.38	2.38	1264B-2H-CC	17.08	18.19	1264A-2H-CC	19.09	23.42
T <i>Dentoglobigerina altispira</i>	3.02	3.02	1264A-2H-CC	19.09	23.42	1264B-3H-CC	26.67	29.48
T <i>Sphaeroidinellopsis seminulina</i>	3.18	3.18	1264A-2H-CC	19.09	23.42	1264B-3H-CC	26.67	29.48
B <i>Globorotalia tosaensis</i>	3.35	3.35	1264A-2H-CC	19.09	23.42	1264B-3H-CC	26.67	29.48
B <i>Menardella miocenica</i>	3.48	3.48	1264A-2H-CC	19.09	23.42	1264B-3H-CC	26.67	29.48
T <i>Hirsutella margaritae</i>	3.88	3.88	1264B-4H-CC	36.06	39.51	1264A-4H-CC	38.03	45.09
T <i>Globorotalia plesiotumida</i>	4.15	4.15	1264A-4H-CC	38.03	45.09	1264B-5H-CC	45.44	49.46
T <i>Hirsutella cibaoensis</i>	4.16	4.16	1264A-4H-CC	38.03	45.09	1264B-5H-CC	45.44	49.46
B <i>Globorotalia crassaformis</i> s.l.	4.31	4.31	1264B-5H-CC	45.44	49.46	1264A-5H-CC	47.55	55.90
T <i>Globoturborotalita nepenthes</i>	4.37	4.37	1264B-5H-CC	45.44	49.46	1264A-5H-CC	47.55	55.90
B <i>Sphaeroidinella dehiscens</i> s.l.	4.94	4.94	1264A-6H-5, 32–34	53.12	63.53	1264A-6H-7, 32–34	55.30	65.71
B <i>Globigerinoides conglobatus</i>	5.84	5.84	1264A-7H-7, 32–34	66.12	77.56	1264A-7H-CC	66.80	78.24
B <i>Globorotalia tumida</i>	5.96	5.96	1264A-7H-5, 32–34	63.11	74.55	1264A-7H-7, 32–34	66.12	77.56
B <i>Globoconella conomiozea</i>	6.90	6.90	1264A-7H-CC	66.80	78.24	1264B-8H-CC	73.89	81.90
B <i>Hirsutella cibaoensis</i>	7.91	7.91	1264B-11H-CC	102.80	114.21	1264A-11H-CC	104.75	121.36
B <i>Globorotalia plesiotumida</i>	8.91	8.91	1264A-11H-CC	104.75	121.36	1264B-12H-CC	111.65	125.37
B <i>Globigerinoides extremus</i>	8.94	8.94	1264A-12H-CC	114.28	131.53	1264B-13H-CC	121.11	135.88
B <i>Hirsutella juanai</i>	9.75	9.75	1264A-13H-CC	123.18	142.02	1264B-14H-CC	131.28	147.51
T <i>Paragloborotalia siakensis</i>	10.43	10.43	1264A-13H-CC	123.18	142.02	1264B-14H-CC	131.28	147.51
T <i>Paragloborotalia mayeri</i>	10.70	10.70	1264A-13H-CC	123.18	142.02	1264B-14H-CC	131.28	147.51
B <i>Globigerina apertura</i>	11.06	11.06	1264B-15H-CC	140.14	157.28	1264A-15H-CC	142.12	161.96
B <i>Globigerina decoraperta</i>	11.43	11.43	1264B-17H-CC	159.37	177.96	1264A-17H-CC	161.15	182.54
B <i>Globoturborotalita nepenthes</i>	11.64	11.64	1264B-17H-CC	159.37	177.96	1264A-17H-CC	161.15	182.54
T <i>Hirsutella praescitula</i>	13.73	13.73	1264A-17H-CC	161.15	182.54	1264B-18H-CC	169.13	188.76
T <i>Menardella archeomenardii</i>	13.92	13.92	1264A-17H-CC	161.15	182.54	1264B-18H-CC	169.13	188.76
T <i>Fohsella peripheronoda</i>	13.92	13.92	1264A-17H-CC	161.15	182.54	1264B-18H-CC	169.13	188.76
B <i>Menardella praemenardii</i>	13.95	13.95	1264A-17H-CC	161.15	182.54	1264B-18H-CC	169.13	188.76
B <i>Fohsella peripheroacuta</i>	14.02	14.02	1264B-18H-CC	169.13	188.76	1264A-18H-CC	170.93	192.85
T <i>Praeorbulina circularis</i>	14.58	14.58	1264A-18H-CC	170.93	192.85	1264A-19H-1, 32–34	171.12	195.03
T <i>Praeorbulina sicana</i>	14.63	14.63	1264A-18H-CC	170.93	192.85	1264A-19H-1, 32–34	171.12	195.03
B <i>Orbulina suturalis</i>	14.70	14.70	1264A-19H-1, 32–34	171.12	195.03	1264A-19H-2, 32–34	172.62	196.53
B <i>Orbulina</i> spp.	14.71	14.71	1264A-19H-1, 32–34	171.12	195.03	1264A-19H-2, 32–34	172.62	196.53
B <i>Praeorbulina circularis</i>	15.15	15.15	1264A-19H-2, 32–34	172.62	196.53	1264A-19H-3, 32–34	174.12	198.03
B <i>Menardella archeomenardii</i>	16.16	16.16	1264A-19H-5, 32–34	177.12	201.03	1264B-20H-2, 78–80	180.58	201.99
B <i>Praeorbulina glomerosa</i>	16.16	16.16	1264A-19H-4, 32–34	175.62	199.53	1264B-20H-1, 78–80	179.08	200.49
B <i>Praeorbulina sicana</i>	16.86	16.86	1264B-20H-2, 78–80	180.58	201.99	1264A-19H-6, 32–34	178.62	202.53
T <i>Catapsydrax dissimilis</i>	17.51	17.51	1264B-20H-3, 78–80	182.08	203.49	1264A-19H-CC	179.76	203.67
T <i>Globoquadrina binaiensis</i>	19.08	19.08	1264B-21H-3, 78–80	191.58	213.60	1264A-20H-CC	190.17	215.06
B <i>Globoquadrina binaiensis</i>	19.98	19.98	1264A-20H-CC	190.17	215.06	1264B-21H-4, 78–80	193.08	215.10
T <i>Paragloborotalia kugleri</i>	21.03	21.03	1264B-21H-CC	197.61	219.63	1264A-21H-CC	198.82	224.77
T <i>Paragloborotalia pseudokugleri</i>	21.22	21.22	1264B-21H-CC	197.61	219.63	1264A-21H-CC	198.82	224.77
B <i>Globoquadrina dehiscens</i>	21.44	21.44	1264B-23H-CC	216.33	240.10	1264A-23H-CC	218.32	246.16
B <i>Globigerinoides trilobus</i> s.l.	22.87	22.87	1264A-24H-2, 32–34	220.12	249.52	1264B-24H-CC	226.28	250.75
B <i>Paragloborotalia kugleri</i>	22.87	22.87	1264A-24H-CC	228.25	257.65	1264A-25H-1, 32–34	228.12	258.90
T <i>Globigerina euapertura</i>	23.03	23.03	1264A-25H-1, 32–34	228.12	258.90	1264A-25H-2, 32–34	229.62	260.40
T <i>Tenuitella gemma</i>	23.54	23.54	1264A-25H-2, 32–34	229.62	260.40	1264A-25H-3, 32–34	231.12	261.90
B <i>Globigerinoides primordius</i> (common)	23.54	23.54	1264A-25H-2, 32–34	229.62	260.40	1264A-25H-3, 32–34	231.12	261.90
B <i>Paragloborotalia pseudokugleri</i>	25.15	25.15	1264A-26H-CC	246.21	277.86	1264A-27H-CC	249.61	282.11
T <i>Chilogumbelina cubensis</i> (common)	27.92	27.92	1264B-27H-CC	254.65	283.98	1264B-28H-CC	263.50	294.42
B "Globigerina" angulisuturalis	28.89	28.89	1264B-28H-CC	263.50	294.42	1264A-28H-CC	261.72	295.44

Note: T = top, B = bottom.

Table T7. Stratigraphic ranges and relative abundances for selected calcareous nannofossil taxa, Site 1264.
(This table is available in an [oversized format](#).)

Table T8. Stratigraphic ranges and relative abundances for selected planktonic foraminifer taxa, Site 1264.
(This table is available in an [oversized format](#).)

Table T9. Occurrence of selected benthic foraminifer taxa, Site 1264. (Continued on next page.)

Hole, core, section, interval (cm)	Depth (mbsf)	Depth (mcd)	Abundance	Preservation	Paleodepth	<i>Astronion pusillum</i>	<i>Biganterina nodosaria</i>	<i>Bolivina</i> sp. small	<i>Bolivinella pseudothalimanni</i>	<i>Bolivinoides haneri</i>	" <i>Bulava indica</i> "	<i>Buliminella elongata</i>	<i>Buliminella exilis</i>	<i>Buliminella rostrata</i>	<i>Buliminella semicostata</i>	<i>Buliminella grata</i>	<i>Casidulinina laevigata</i>	<i>Cibicidoides grimsdalei</i>	<i>Cibicidoides mundulus</i>	<i>Cibicidoides praemundulus</i>	<i>Cibicidoides wuellestorffii</i>	<i>Eggerella bradyi</i>	<i>Epistominella exigua</i>	<i>Globocassidulina subglobosa</i>	<i>Gyroidinoides</i> spp.
208-																									
1264C-1H-1, 0–2	0.00	0.10	R	E	UA	x					x	x							x	x	x	x	x	x	x
1264A-1H-1, 0–2	0.00	2.96	R	G	UA		x				x	x	x	x	x	x	x	x	x	x	x	x	x	x	x
1264C-1H-CC, 13–18	2.95	3.05	R	E	UA		x				x	x	x	x	x	x	x	x	x	x	x	x	x	x	x
1264B-1H-CC, 7–12	7.33	7.33	R	E	UA			x			x	x	x	x	x	x	x	x	x	x	x	x	x	x	x
1264A-1H-CC, 23–28	9.30	12.26	R	G	UA			x			x	x	x	x	x	x	x	x	x	x	x	x	x	x	x
1264A-2H-CC, 15–20	19.09	23.42	R	G	UA	x		x			x	x	x	x	x	x	x	x	x	x	x	x	x	x	x
1264A-3H-CC, 19–24	28.29	34.18	R	G	UA		x				x	x	x	x	x	x	x	x	x	x	x	x	x	x	x
1264A-4H-CC, 23–28	38.03	45.09	R	G	UA		x				x	x	x	x	x	x	x	x	x	x	x	x	x	x	x
1264A-5H-CC, 13–18	47.55	55.90	R	G	UA		x				x	x	x	x	x	x	x	x	x	x	x	x	x	x	x
1264A-6H-CC, 34–39	56.24	66.65	R	G	UA		x				x	x	x	x	x	x	x	x	x	x	x	x	x	x	x
1264A-7H-CC, 21–26	66.80	78.24	R	G	UA		x				x	x	x	x	x	x	x	x	x	x	x	x	x	x	x
1264A-8H-CC, 13–18	75.77	88.89	R	G	UA		x				x	x	x	x	x	x	x	x	x	x	x	x	x	x	x
1264A-9H-CC, 12–17	84.80	99.17	R	G	UA		x				x	x	x	x	x	x	x	x	x	x	x	x	x	x	x
1264A-10H-CC, 6–11	94.33	110.64	R	G	UA		x				x	x	x	x	x	x	x	x	x	x	x	x	x	x	x
1264A-11H-CC, 12–17	104.75	121.36	R	G	UA		x				x	x	x	x	x	x	x	x	x	x	x	x	x	x	x
1264A-12H-CC, 7–12	114.28	131.53	R	G	UA		x				x	x	x	x	x	x	x	x	x	x	x	x	x	x	x
1264A-13H-CC, 16–21	123.18	142.02	R	G	UA		x				x	x	x	x	x	x	x	x	x	x	x	x	x	x	x
1264A-14H-CC, 19–24	132.90	151.79	R	G	UA		x				x	x	x	x	x	x	x	x	x	x	x	x	x	x	x
1264A-15H-CC, 14–19	142.12	161.96	R	G	UA		x				x	x	x	x	x	x	x	x	x	x	x	x	x	x	x
1264A-16H-CC, 23–28	152.13	171.97	R	G	UA		x				x	x	x	x	x	x	x	x	x	x	x	x	x	x	x
1264A-17H-CC, 0–10	161.15	182.54	R	G	UA		x				x	x	x	x	x	x	x	x	x	x	x	x	x	x	x
1264A-18H-CC, 0–10	170.93	192.85	R	G	UA		x				x	x	x	x	x	x	x	x	x	x	x	x	x	x	x
1264A-19H-CC, 11–16	179.76	203.67	R	G	UA		xx	x			x	x	x	x	x*	x	x	x	x	x	x	x	x	x	x
1264B-21H-1, 78–80	188.58	210.60	R	G	UA		xx	x			x	x	x	x	x*	x	x	x	x	x	x	x	x	x	x
1264B-21H-2, 78–80	190.08	212.10	R	G	UA		xx	x			x	x	x	x	x*	x	x	x	x	x	x	x	x	x	x
1264A-20H-CC, 8–13	190.17	215.06	R	G	UA		x				x	x	x	x	x	x	x	xx	x	x	x	x	x	x	x
1264A-21H-CC, 13–18	198.82	224.77	R	G	UA		x				x	x	x	x	x	x	x	x	x	x	x	x	x	x	x
1264A-22H-CC, 14–19	208.92	235.89	R	G	UA		x				x	x	x	x	x*	x	x	x	x	x	x	x	x	x	x
1264A-23H-CC, 10–15	218.32	246.16	R	G	UA		x				x	x	x	x	x*	x	x	x	x	x	x	x	x	x	x
1264A-24H-CC, 20–25	228.25	257.65	R	G/M	DT/UA		x				x	x	x	x	x	x	x	x	x	x	x	x	x	x	x
1264A-25H-CC, 24–29	231.86	262.64	R	G/M	DT/UA	x				x	x	x	x	x	x	x	x	x	x	x	x	x	x	x	x
1264A-26H-CC, 14–19	246.21	277.86	R	G/M	DT/UA	x		x		x	x	x	x	x	x	x	x	x	x	x	x	x	x	x	x
1264A-27H-CC, 30–35	249.61	282.11	R	G/M	DT/UA	x		x		x	x	x	x	x*	x	x	x	x	x	x	x	x	x	x	x
1264A-28H-CC, 23–28	261.72	295.44	R	G/M	DT/UA/LB		x			x	x	x	x	x	x	x	x	x	x	x	x	x	x	x	x
1264A-29H-CC, 8–13	271.47	306.08	R	G/M	DT/UA/LB		x			x	x	x	x	x	x	x	x	x	x	x	x	x	x	x	x
1264A-30H-CC, 11–16	280.86	316.47	R	G/M	DT/UA/LB		x			x	x	x	x	x	x	x	x	x	x	x	x	x	x	x	x

Notes: Abundance: R = rare. Preservation: E = excellent, G = good, M = moderate. Paleodepth: UA = upper abyssal, DT = downslope transport, LB = lower bathyal. x = present, xx = dominant species, * = reworked.

Table T9 (continued).

Table T10. Magnetostratigraphic age-depth tie points, Site 1264.

Chron	Age (Ma)		Top			Bottom		
	1	2	Hole, core, section, interval (cm)	Depth (mbsf)	Depth (mcd)	Hole, core, section, interval (cm)	Depth (mbsf)	Depth (mcd)
C2n (y)	1.785	1.770	208-			208-		
C2An (y)	2.582	2.581	1264A-1H-5, 140	7.40	10.36	1264B-2H-2, 135	10.15	11.26
C2An (o)	3.596	3.580	1264A-2H-2, 125	12.05	16.38	1264A-2H-4, 25	14.05	18.38
C3n (y)	4.188	4.180	1264B-3H-6, 140	24.68	27.49	1264A-3H-5, 60	25.40	31.29
			1264B-4H-3, 100	30.30	33.75	1264B-4H-3, 145	30.75	34.20

Notes: o = old end of chron, y = young end of chron. 1 = ages as in Lourens et al. (in press), 2 = ages as in Cande and Kent (1995).

Table T11. Interstitial water analyses, Site 1264.

Hole, core, section, interval (cm)	Depth (mcd)	pH	Alkalinity (mM)	Salinity	Cl (mM)	SO ₄ (mM)	Na (mM)	Mg (mM)	Ca (mM)	K (mM)	B (μM)	Fe (μM)	Mn (μM)	Li (μM)	Ba (μM)	Sr (μM)	Si (μM)	Zn (μM)
208-																		
1264B-1H-4, 140–150	5.9	7.53	2.57	35.0	559	23.6	467	55.6	11.4	11.2	453	0.00	0.58	25.7	2.02	101	339	0.20
1264A-1H-5, 140–150	10.4	7.64	3.33	35.0	564	27.1	468	54.8	11.1	10.8	447	0.00	1.60	26.9	0.39	191	299	0.38
1264A-2H-5, 140–150	21.0	7.47	2.84	35.0	566	26.5	492	53.8	11.1	10.9	456	0.00	0.35	25.5	1.84	275	254	0.17
1264A-3H-5, 140–150	32.1	7.40	2.75	35.0	567	26.4	480	53.2	11.1	10.7	470	5.17	0.35	25.6	0.33	319	258	1.02
1264A-4H-5, 140–150	42.8	7.42	2.73	3.5	563	26.3	485	54.1	10.9	10.2	464	3.37	0.26	25.7	0.25	384	194	0.00
1264A-5H-5, 140–150	53.6	7.36	3.34	35.0	560	26.0	494	54.6	11.9	10.5	456	2.39	0.41	24.8	1.82	428	199	0.00
1264A-7H-5, 140–150	75.6	7.51	2.74	35.0	560	25.2	493	54.3	11.7	10.3	472	2.62	0.40	24.7	0.47	507	186	0.00
1264A-8H-5, 140–150	86.8	7.34	2.61	35.0	567	25.6	485	54.3	11.1	10.3	446	3.59	0.24	25.4	0.28	520	175	0.00
1264A-9H-5, 140–150	97.6	7.41	2.61	35.0	557	19.2	473	52.3	12.2	10.2	434	6.94	0.25	23.7	0.26	496	179	0.60
1264A-10H-4, 140–150	107.5	7.47	2.58	35.0	560	25.8	500	53.5	12.2	10.0	455	5.02	0.23	24.3	2.05	537	178	0.00
1264A-11H-5, 140–150	118.8	7.38	2.56	35.0	562	24.5	474	54.3	11.8	9.9	468	13.14	0.69	25.0	0.27	562	209	0.42
1264A-12H-5, 140–150	129.0	7.40	2.57	35.5	566	25.3	478	50.5	12.1	10.0	471	8.84	0.32	23.6	2.44	551	188	0.00
1264A-13H-5, 140–150	140.0	7.44	2.68	35.5	561	25.1	467	48.3	12.0	10.2	499	5.05	0.44	25.2	2.48	596	195	0.21
1264A-14H-5, 140–150	149.6	7.49	2.53	35.5	561	25.0	470	52.5	12.8	10.1	466	3.56	0.89	26.6	1.76	579	215	0.05
1264A-15H-5, 140–150	160.0	7.34	2.59	35.5	567	24.9	467	50.0	12.8	9.7	472	0.00	2.00	25.4	0.52	565	194	0.00
1264A-16H-5, 140–150	169.5	7.52	2.51	35.5	565	25.3	471	50.2	12.8	10.0	486	0.00	3.70	25.2	0.27	595	204	0.00
1264A-17H-5, 140–150	180.6	7.44	2.53	35.5	568	24.3	471	50.8	13.4	9.8	464	0.00	3.33	27.4	0.32	570	222	1.47
1264A-18H-5, 140–150	190.6	7.44	2.53	35.5	568	25.2	475	50.5	13.4	9.8	495	0.00	3.21	27.3	0.29	589	208	0.53
1264A-19H-5, 140–150	202.1	7.49	2.44	35.5	566	24.7	469	51.5	12.9	9.6	515	0.00	3.21	28.1	0.27	584	228	0.02
1264A-20H-5, 140–150	212.6	7.45	2.54	35.5	555	23.6	474	49.7	13.3	9.9	518	0.00	3.34	28.5	0.27	596	225	0.64
1264A-21H-5, 140–150	223.2	7.39	2.52	35.5	573	24.3	481	49.5	13.5	9.9	521	0.00	2.57	29.3	0.41	593	228	0.00
1264A-22H-5, 140–150	233.7	ND	ND	35.0	566	24.8	470	50.2	12.8	9.9	496	0.00	3.19	27.9	1.80	586	208	0.00
1264A-23H-5, 140–150	244.0	7.39	2.25	35.0	568	25.0	466	51.0	13.4	9.4	478	0.00	2.99	28.7	0.24	576	221	0.10
1264A-24H-5, 140–150	255.1	7.49	2.58	35.0	569	25.0	488	49.6	13.7	9.9	523	0.00	3.28	31.9	0.33	575	245	0.14
1264A-25H-2, 140–150	261.5	7.36	2.33	35.0	565	25.2	477	48.9	13.7	9.6	507	0.00	3.58	29.4	0.27	545	233	0.07
1264A-26H-5, 140–150	276.4	7.45	2.34	34.5	572	24.6	488	49.5	13.5	9.8	524	0.00	4.57	29.9	0.40	559	257	0.45
1264A-28H-2, 140–150	292.9	7.46	2.45	34.5	573	24.9	480	49.1	13.7	9.1	502	0.00	5.22	31.5	0.27	564	260	0.29
1264A-29H-5, 140–150	303.7	7.44	2.28	35.0	573	24.6	487	50.7	14.4	9.6	507	0.00	5.50	30.6	0.31	536	302	0.00
1264A-30H-5, 140–150	314.2	7.43	2.36	35.0	571	25.8	483	49.5	14.8	9.6	490	0.00	5.40	30.9	0.41	547	340	0.00

Note: ND = not determined.

SHIPBOARD SCIENTIFIC PARTY
CHAPTER 5, SITE 1264

67

Table T12. Sedimentary calcium carbonate, total carbon, and organic carbon concentrations, Site 1264.
 (Continued on next page.)

Hole, core, section, interval (cm)	Depth (mcd)	Inorganic carbon (wt%)	CaCO ₃ (wt%)	Total carbon (wt%)	Organic carbon (wt%)
208-					
1264A-1H-1, 113–114	4.09	11.2	93.5		
1264B-1H-5, 140–150	5.90	11.5	95.5	11.4	0.3
1264A-1H-3, 72–73	6.68	11.3	94.4		
1264A-1H-5, 72–73	9.68	11.3	94.2		
1264A-1H-5, 145–150	10.36	11.3	94.3	11.4	0.1
1264A-2H-1, 72–73	14.35	11.4	95.1		
1264A-2H-3, 72–73	17.35	11.3	94.0		
1264A-2H-5, 72–73	20.35	11.4	95.1		
1264A-2H-5, 140–150	21.03	10.8	89.9	10.1	0.0
1264A-3H-1, 72–73	25.41	11.5	95.7		
1264A-3H-3, 72–73	28.41	11.5	95.4		
1264A-3H-5, 72–73	31.41	11.4	95.3		
1264A-3H-5, 140–150	32.09	10.1	84.4	10.1	0.0
1264A-4H-1, 72–73	36.08	11.6	96.9		
1264A-4H-3, 72–73	39.08	11.8	98.4		
1264A-4H-5, 72–73	42.08	11.6	96.8		
1264A-4H-5, 140–150	42.76	10.9	90.4	10.5	0.1
1264A-5H-1, 72–73	46.87	11.6	96.3		
1264A-5H-3, 72–73	49.87	11.6	96.5		
1264A-5H-5, 72–73	52.87	11.4	94.8		
1264A-5H-5, 140–150	53.55	11.3	94.0	11.2	0.0
1264A-6H-1, 72–73	58.43	11.5	96.1		
1264A-6H-3, 72–73	61.43	11.5	95.5		
1264A-6H-5, 72–73	63.93	11.6	96.2		
1264A-7H-1, 72–73	68.96	11.6	96.7		
1264A-7H-3, 72–73	71.96	11.5	96.0		
1264A-7H-5, 71–72	74.95	11.5	95.4		
1264A-7H-5, 140–150	75.64	11.6	96.8	10.4	0.0
1264A-8H-1, 72–73	80.14	11.6	96.6		
1264A-8H-3, 72–73	83.14	11.6	96.5		
1264A-8H-5, 72–73	86.14	11.5	95.5		
1264A-8H-5, 140–150	86.82	11.2	93.1	11.1	0.0
1264A-9H-1, 72–73	90.89	11.6	96.7		
1264A-9H-3, 72–73	93.89	11.6	96.6		
1264A-9H-5, 72–73	96.89	11.6	96.7		
1264A-9H-5, 140–150	97.20	10.6	87.9	10.4	0.0
1264A-10H-1, 72–73	97.57	11.5	96.0		
1264A-10H-3, 72–73	105.33	11.6	96.5		
1264A-10H-4, 140–150	107.51	11.2	93.0	11.4	0.2
1264A-10H-5, 72–73	108.33	11.3	94.3		
1264A-11H-1, 72–73	112.13	11.4	94.5		
1264A-11H-3, 72–73	115.13	11.4	95.3		
1264A-11H-5, 72–73	118.13	11.5	95.4		
1264A-11H-5, 140–150	118.81	11.3	94.3	10.9	3.4
1264A-11H-7, 72–73	121.13	11.4	94.8		
1264A-12H-1, 72–73	122.27	11.5	95.7		
1264A-12H-3, 72–73	125.27	11.0	91.8		
1264A-12H-5, 72–73	128.27	11.6	96.5		
1264A-12H-5, 140–150	128.95	11.6	96.5	11.5	0.0
1264A-13H-1, 72–73	133.36	11.5	96.0		
1264A-13H-3, 72–73	136.36	11.3	94.2		
1264A-13H-5, 72–73	139.36	11.3	93.7		
1264A-13H-5, 140–150	140.04	11.4	95.3	11.4	0.0
1264A-14H-1, 72–73	142.91	10.6	88.4		
1264A-14H-3, 72–73	145.91	11.5	95.7		
1264A-14H-5, 72–73	148.91	11.4	94.5		
1264A-14H-5, 140–150	149.59	11.2	93.5	11.2	0.0
1264A-15H-1, 72–73	153.36	11.4	95.1		
1264A-15H-3, 72–73	156.36	11.3	94.4		
1264A-15H-5, 72–73	159.36	11.4	94.8		
1264A-15H-5, 140–150	160.04	11.5	95.7	11.5	0.0
1264A-16H-1, 72–73	162.86	11.2	93.2		
1264A-16H-3, 72–73	165.86	11.4	94.9		
1264A-16H-5, 72–73	168.86	11.2	93.5		
1264A-16H-5, 140–150	169.54	11.4	94.5	11.3	0.0

Table T12 (continued).

Hole, core, section, interval (cm)	Depth (mcd)	Inorganic carbon (wt%)	CaCO ₃ (wt%)	Total carbon (wt%)	Organic carbon (wt%)
1264A-17H-1, 72-73	173.91	11.3	94.2		
1264A-17H-3, 72-73	176.91	11.4	94.8		
1264A-17H-5, 72-73	179.91	11.3	93.7		
1264A-17H-5, 140-150	180.59	11.4	95.3	11.3	0.0
1264A-18H-1, 72-73	183.94	11.3	94.3		
1264A-18H-3, 72-73	186.94	11.3	94.0		
1264A-18H-5, 72-73	189.94	11.0	91.9		
1264A-18H-5, 140-150	190.62	11.4	95.2	10.9	0.0
1264A-19H-1, 72-73	195.43	11.1	92.2		
1264A-19H-3, 72-73	198.43	11.1	92.8		
1264A-19H-5, 72-73	201.43	11.4	94.5		
1264A-20H-1, 72-73	205.91	11.0	91.5		
1264A-20H-3, 72-73	208.91	10.9	91.1		
1264A-20H-5, 72-73	211.91	11.0	91.7		
1264A-20H-5, 140-150	212.59	11.3	93.7	11.0	0.0
1264A-21H-1, 72-73	216.47	11.3	94.0		
1264A-21H-3, 72-73	219.47	11.4	95.0		
1264A-21H-5, 72-73	222.47	11.0	91.5		
1264A-21H-5, 140-150	223.15	11.2	93.6	10.8	0.0
1264A-22H-1, 72-73	226.99	11.4	95.3		
1264A-22H-3, 72-73	229.99	11.2	93.5		
1264A-22H-5, 72-73	232.99	11.2	93.0		
1264A-22H-5, 140-150	233.67	11.6	96.9	11.5	0.3
1264A-23H-1, 72-73	237.36	11.5	95.8		
1264A-23H-3, 72-73	240.36	11.3	93.9		
1264A-23H-5, 72-73	243.36	11.2	93.1		
1264A-23H-5, 140-150	244.04	11.7	97.1	11.5	0.0
1264A-24H-1, 72-73	248.42	11.4	94.9		
1264A-24H-3, 72-73	251.42	11.3	94.2		
1264A-24H-5, 72-73	254.42	11.2	93.2		
1264A-24H-5, 140-150	255.10	11.2	93.5	11.3	0.0
1264A-25H-1, 72-73	259.30	11.1	92.2		
1264A-25H-2, 140-150	261.48	11.3	94.0	11.1	0.0
1264A-25H-3, 72-73	262.30	11.2	93.2		
1264A-26H-1, 72-73	269.67	11.1	92.5		
1264A-26H-3, 72-73	272.67	10.9	91.0		
1264A-26H-5, 72-73	275.67	11.1	92.3		
1264A-26H-5, 140-150	276.35	11.1	92.6	11.0	0.0
1264A-27H-1, 72-73	280.02	11.4	94.6		
1264A-28H-1, 72-73	290.74	10.7	88.7		
1264A-28H-2, 140-150	292.92	11.2	93.1	11.1	0.0
1264A-28H-3, 72-73	293.74	11.2	93.1		
1264A-29H-1, 72-73	297.03	10.8	89.6		
1264A-29H-3, 72-73	300.03	11.0	91.5		
1264A-29H-5, 72-73	303.03	11.2	93.4		
1264A-29H-5, 140-150	303.71	11.1	92.6	11.0	0.0
1264A-30H-1, 72-73	307.53	11.4	94.7		
1264A-30H-3, 72-73	310.53	11.1	92.7		
1264A-30H-5, 72-73	313.53	11.1	92.5		
1264A-30H-5, 140-150	314.21	11.3	94.4	11.2	0.0

SHIPBOARD SCIENTIFIC PARTY
CHAPTER 5, SITE 1264

69

Table T13. Concentrations in dry samples of sediment dissolution inductively coupled plasma–atomic emission spectroscopy analyses, Site 1263.

Hole, core, section, interval (cm)	Depth (mcd)	B (mM)	Ba (mM)	Fe (mM)	Mn (mM)	Sr (mM)	Na (mM)	Mg (mM)	K (mM)	Ca (wt%)
208-										
1263A-2H-5, 145–150	10.2	0.94	0.92	27.8	2.03	13.5	161	47.0	16.2	50.2
1263A-3H-5, 145–150	21.4	0.69	0.98	20.2	1.16	13.5	151	53.1	13.4	52.2
1263A-4H-5, 140–150	32.5	1.07	1.57	40.6	3.08	12.3	161	61.3	28.4	51.2
1263A-7H-5, 140–150	66.3	0.84	1.66	32.6	2.95	13.2	193	56.3	21.4	50.7
1263A-8H-5, 140–150	77.4	0.81	3.04	19.6	2.91	12.5	117	53.8	18.8	49.3
1263A-9H-5, 140–150	88.0	0.74	2.08	32.5	3.02	12.3	107	54.6	24.2	52.0
1263A-10H-5, 140–150	97.5	0.70	0.77	29.6	3.19	13.1	119	51.9	21.3	51.6
1263A-11H-5, 140–150	108.4	0.94	0.80	44.7	3.82	10.6	87	62.8	30.9	50.5
1263A-14H-5, 140–150	140.0	0.91	2.23	55.4	4.80	11.5	161	67.5	36.3	50.8
1263A-15H-5, 140–150	153.7	0.72	2.52	34.7	4.73	10.2	120	57.2	25.9	50.4
1263A-16H-5, 140–150	164.6	0.73	2.33	36.8	4.66	9.7	155	71.5	27.5	49.3
1263A-17H-5, 140–150	175.2	0.88	3.39	43.9	5.73	10.8	179	60.4	35.6	49.7
1263A-18H-4, 140–150	184.1	0.69	1.45	39.9	2.37	9.7	162	61.5	28.1	52.0
1263A-19H-5, 140–150	196.7	0.92	3.35	41.5	3.59	7.4	82	77.7	30.9	50.8
1263A-20H-4, 140–150	207.0	0.69	4.32	33.9	5.17	8.0	158	76.8	22.4	54.4
1263A-21H-4, 140–150	219.0	0.51	4.76	24.7	4.70	9.7	144	55.9	17.3	52.1
1263A-22H-5, 140–150	231.8	0.54	6.64	28.6	5.25	7.4	74	66.6	19.1	51.4
1263A-24H-5, 140–150	250.2	0.63	9.44	38.4	6.46	6.3	125	72.3	22.3	49.9
1263A-26H-5, 140–150	266.9	0.58	4.70	18.0	1.87	8.2	165	56.3	21.3	51.0
1263B-23H-5, 140–150	281.3	0.69	4.34	31.8	3.25	9.4	66	55.0	24.1	51.8
1263A-28H-5, 140–150	291.5	0.77	5.30	38.3	1.94	9.3	130	62.2	31.7	52.8
1263B-24H-5, 140–150	292.6	0.71	6.82	35.4	2.99	8.2	96	57.3	23.9	49.6
1263A-35X-3, 140–150	347.1	0.64	5.73	15.8	3.70	11.6	193	48.6	20.8	51.8
1263A-36X-2, 140–150	357.0	0.66	5.38	15.3	3.49	11.6	122	43.9	18.2	52.3
1263A-37X-3, 90–100	366.4	0.94	5.51	40.6	3.25	13.4	156	54.2	36.3	50.9
1263A-38X-3, 140–150	378.2	0.73	3.39	34.2	3.91	13.0	93	44.4	30.5	50.7

Table T14. Concentrations in dry samples of sediment dissolution inductively coupled plasma–atomic emission spectroscopy analyses, Site 1264.

Hole, core, section, interval (cm)	Depth (mcd)	B (mM)	Ba (mM)	Fe (mM)	Mn (mM)	Sr (mM)	Na (mM)	Mg (mM)	K (mM)	Ca (wt%)
208-										
1264B-1H-4, 140–150	5.9	0.89	2.38	28.3	2.56	15.3	225	52.4	15.4	49.5
1264A-1H-5, 140–150	10.4	0.88	2.93	30.5	2.62	15.3	194	50.4	14.1	51.0
1264A-2H-5, 140–150	21.0	0.83	1.62	21.7	2.01	13.9	198	49.9	13.2	48.0
1264A-3H-5, 140–150	32.1	0.21	1.07	20.1	2.82	15.0	152	43.3	13.0	48.6
1264A-4H-5, 140–150	42.8	0.65	1.06	19.4	1.71	16.5	158	43.8	14.4	47.1
1264A-5H-5, 140–150	53.6	0.70	1.19	20.4	2.16	16.8	172	45.6	12.4	49.6
1264A-7H-5, 140–150	75.6	0.85	1.54	22.2	1.97	15.6	200	46.1	13.6	48.9
1264A-8H-5, 140–150	86.8	0.63	1.06	22.1	2.47	16.8	185	46.8	11.3	50.6
1264A-9H-5, 140–150	97.2	0.65	1.33	19.7	1.97	16.0	171	40.4	9.3	46.3
1264A-10H-4, 140–150	107.5	0.77	1.03	24.0	2.41	16.0	161	43.8	13.4	50.4
1264A-11H-5, 140–150	118.8	0.79	1.26	21.5	3.24	14.9	150	44.2	12.5	48.3
1264A-12H-5, 140–150	129.0	0.69	1.00	22.8	3.43	13.6	160	49.2	14.5	50.7
1264A-13H-5, 140–150	140.0	0.95	1.22	40.8	3.86	15.0	161	50.9	21.8	49.4
1264A-14H-5, 140–150	149.6	0.85	1.37	36.2	3.31	16.1	172	47.1	21.2	49.3
1264A-14H-5, 140–150	149.6	0.79	1.36	32.9	3.33	16.1	169	46.4	16.9	50.6
1264A-14H-5, 140–150	149.6	0.84	1.31	25.4	3.19	16.8	206	44.4	14.0	50.8
1264A-15H-5, 140–150	160.0	0.80	0.75	33.0	3.76	17.6	163	45.0	17.8	50.2
1264A-16H-5, 140–150	169.5	0.85	0.27	32.6	4.80	17.6	163	43.3	13.2	50.0
1264A-17H-5, 140–150	180.6	0.67	0.23	32.4	4.22	17.1	164	47.0	15.7	50.1
1264A-18H-5, 140–150	190.6	0.86	0.33	36.4	4.45	17.6	174	52.1	18.0	48.3
1264A-19H-5, 140–150	202.1	0.79	0.60	30.1	3.69	16.5	157	51.1	13.3	49.6
1264A-20H-5, 140–150	212.6	1.08	0.50	50.3	4.33	15.6	142	56.5	18.6	52.5
1264A-21H-5, 140–150	223.2	0.80	1.42	21.0	3.21	15.8	131	46.1	13.4	48.2
1264A-22H-5, 140–150	233.7	0.67	1.14	22.6	3.02	14.4	160	46.8	16.1	50.5
1264A-23H-5, 140–150	244.0	0.63	1.86	17.9	2.29	14.9	158	45.7	13.3	50.6
1264A-24H-5, 140–150	255.1	0.81	1.66	25.7	2.39	14.6	143	49.1	23.9	51.5
1264A-25H-2, 140–150	261.5	0.99	1.17	33.7	3.10	16.9	149	49.3	25.5	50.7
1264A-26H-5, 140–150	276.4	0.98	1.61	28.4	3.65	15.2	155	50.5	21.9	48.7
1264A-28H-2, 140–150	292.9	0.85	1.43	29.8	3.81	13.4	138	53.6	16.5	49.8
1264A-29H-5, 140–150	303.7	0.80	1.20	27.2	4.03	14.9	150	47.8	19.7	49.1
1264A-30H-5, 140–150	314.2	0.95	1.36	41.3	3.02	13.8	129	59.6	23.2	50.6

Table T15. Age-depth control points, Site 1264. (See table notes. Continued on next page.)

	Datum	Type	Upper depth (mcd)	Lower depth (mcd)	Minimum age (Ma)	Maximum age (Ma)
T	<i>Globorotalia tosaensis</i>	PF	0.10	1.55	0.61	0.61
T	<i>Globigerinoides obliquus</i>	PF	0.10	1.55	1.30	1.30
B	<i>Emiliana huxleyi</i>	CN	0.10	1.56	0.26	0.26
T	<i>Pseudoemiliana lacunosa</i>	CN	1.56	3.05	0.46	0.46
T	Large <i>Gephyrocapsa</i> spp.	CN	6.16	6.66	1.24	1.24
T	<i>Globigerina apertura</i>	PF	7.33	12.26	1.68	1.68
T	<i>Globigerinoides extremus</i>	PF	7.33	12.26	1.91	1.91
B	Large <i>Gephyrocapsa</i> spp.	CN	8.16	8.66	1.58	1.58
T	<i>Calcidiscus macintyrei</i>	CN	9.16	9.66	1.67	1.67
B	Medium <i>Gephyrocapsa</i> spp.	CN	9.66	10.16	1.69	1.69
	C2n (y)	PMAG	10.36	11.26	1.785	1.785
T	<i>Discoaster brouweri</i> and <i>D. triradiatus</i>	CN	11.16	11.66	1.95	1.95
T	<i>Discoaster pentaradiatus</i>	CN	15.53	16.23	2.52	2.52
T	<i>Discoaster surculus</i>	CN	16.23	17.03	2.63	2.63
	C2An (y)	PMAG	16.38	18.38	2.582	2.582
T	<i>Discoaster tamalis</i>	CN	17.73	18.53	2.83	2.83
B	<i>Globorotalia truncatulinoides</i>	PF	18.19	23.42	2.03	2.03
T	<i>Globoturborotalita woodi</i>	PF	18.19	23.42	2.30	2.30
T	<i>Menardella miocenica</i>	PF	18.19	23.42	2.38	2.38
T	<i>Dentoglobigerina altispira</i>	PF	23.42	29.48	3.02	3.02
T	<i>Sphaeroidinellopsis seminulina</i>	PF	23.42	29.48	3.18	3.18
B	<i>Globorotalia tosaensis</i>	PF	23.42	29.48	3.35	3.35
B	<i>Menardella miocenica</i>	PF	23.42	29.48	3.48	3.48
	C2An (o)	PMAG	27.49	31.29	3.596	3.596
T	<i>Sphenolithus</i> spp.	CN	28.89	29.59	3.66	3.66
T	<i>Reticulofenestra pseudoumbilicus</i>	CN	30.39	31.09	3.82	3.82
	C3n (y)	PMAG	33.75	34.20	4.188	4.188
T	<i>Hirsutella margaritae</i>	PF	39.51	45.09	3.88	3.88
T	<i>Globorotalia plesiotumida</i>	PF	45.09	49.46	4.15	4.15
T	<i>Hirsutella cibaoensis</i>	PF	45.09	49.46	4.16	4.16
B	<i>Globorotalia crassaformis</i> s.l.	PF	49.46	55.90	4.31	4.31
T	<i>Globoturborotalita nepenthes</i>	PF	49.46	55.90	4.37	4.37
B	<i>Sphaeroidinella dehiscens</i> s.l.	PF	63.53	65.71	4.94	4.94
B	<i>Globorotalia tumida</i>	PF	74.55	77.56	5.96	5.96
B	<i>Ceratolithus acutus</i>	CN	76.54	77.04	5.37	5.37
T	<i>Nicklithus amplificus</i>	CN	77.04	77.44	6.00	6.00
B	<i>Globigerinoides conglobatus</i>	PF	77.56	78.24	5.84	5.84
B	<i>Globoconella conomiozea</i>	PF	78.24	81.90	6.90	6.90
B	<i>Nicklithus amplificus</i>	CN	82.82	83.62	6.84	6.84
B	<i>Amaurolithus primus</i>	CN	110.64	111.81	7.39	7.39
B	<i>Hirsutella cibaoensis</i>	PF	114.21	121.36	7.91	7.91
B	<i>Globorotalia plesiotumida</i>	PF	121.36	125.37	8.91	8.91
B	<i>Paracme Reticulofenestra pseudoumbilicus</i>	CN	121.36	121.95	8.79	8.79
B	<i>Globigerinoides extremus</i>	PF	131.53	135.88	8.94	8.94
T	<i>Discoaster hamatus</i>	CN	141.69	142.02	9.63	9.63
B	<i>Hirsutella juanai</i>	PF	142.02	147.51	9.75	9.75
T	<i>Paragloborotalia siakensis</i>	PF	142.02	147.51	10.43	10.43
T	<i>Paragloborotalia mayeri</i>	PF	142.02	147.51	10.70	10.70
T	<i>Catinaster calyculus</i>	CN	144.09	144.89	9.64	9.64
B	<i>Discoaster bellus</i> gr. (<i>D. hamatus</i>)	CN	148.59	149.39	10.48	10.48
B	<i>Globigerina apertura</i>	PF	157.28	161.96	11.06	11.06
B	<i>Catinaster coolidus</i>	CN	161.34	161.74	10.79	10.79
T	<i>Coccolithus miopelagicus</i>	CN	169.34	170.04	11.02	11.02
TC	<i>Discoaster kugleri</i>	CN	171.97	182.54	11.60	11.60
BC	<i>Discoaster kugleri</i>	CN	171.97	182.54	11.88	11.88
B	<i>Globigerina decoraperta</i>	PF	177.96	182.54	11.43	11.43
B	<i>Globoturborotalita nepenthes</i>	PF	177.96	182.54	11.64	11.64
T	<i>Hirsutella praescitula</i>	PF	182.54	188.76	13.73	13.73
T	<i>Menardella archeomenardii</i>	PF	182.54	188.76	13.92	13.92
T	<i>Fohsella peripheronorda</i>	PF	182.54	188.76	13.92	13.92
B	<i>Menardella praemenardii</i>	PF	182.54	188.76	13.95	13.95
B	<i>Triquetrorhabdulus rugosus</i>	CN	184.42	185.12	12.81	12.81
T	<i>Sphenolithus heteromorphus</i>	CN	186.62	187.42	13.55	13.55
B	<i>Fohsella peripheroacuta</i>	PF	188.76	192.85	14.02	14.02
T	<i>Praeorbulina circularis</i>	PF	192.85	195.03	14.58	14.58
T	<i>Praeorbulina sicana</i>	PF	192.85	195.03	14.63	14.63
B	<i>Orbulina suturalis</i>	PF	195.03	196.53	14.70	14.70
B	<i>Orbulina</i> spp.	PF	195.03	196.53	14.71	14.71

Table T15 (continued).

	Datum	Type	Upper depth (mcd)	Lower depth (mcd)	Minimum age (Ma)	Maximum age (Ma)
B	<i>Praeorbulina circularis</i>	PF	196.53	198.03	15.15	15.15
B	<i>Discoaster signus</i> gr. + T acme <i>D. deflandrei</i>	CN	198.11	198.91	15.60	15.60
B	<i>Praeorbulina glomerosa</i>	PF	199.53	200.49	16.16	16.16
B	<i>Menardella archeomenardii</i>	PF	201.03	201.99	16.16	16.16
B	<i>Praeorbulina sicana</i>	PF	201.99	202.53	16.86	16.86
T	<i>Catapsydrax dissimilis</i>	PF	203.49	203.67	17.51	17.51
B	<i>Sphenolithus heteromorphus</i>	CN	210.09	210.89	17.76	17.76
T	<i>Sphenolithus belemnos</i>	CN	210.09	210.89	17.89	17.89
T	<i>Globoquadrina binaensis</i>	PF	213.60	215.06	19.08	19.08
B	<i>Globoquadrina binaensis</i>	PF	215.06	215.10	19.98	19.98
B	<i>Sphenolithus belemnos</i>	CN	216.15	216.95	18.92	18.92
T	<i>Paragloborotalia kugleri</i>	PF	219.63	224.77	21.03	21.03
T	<i>Paragloborotalia pseudokugleri</i>	PF	219.63	224.77	21.22	21.22
B	<i>Globoquadrina dehiscens</i>	PF	240.10	246.16	21.44	21.44
B	<i>Globigerinoides trilobus</i> s.l.	PF	249.52	250.75	22.87	22.87
B	<i>Paragloborotalia kugleri</i>	PF	257.65	258.90	22.87	22.87
T	<i>Sphenolithus delphix</i>	CN	257.65	258.68	23.07	23.07
T	<i>Globigerina euapertura</i>	PF	258.90	260.40	23.03	23.03
T	<i>Tenuitella gemma</i>	PF	260.40	261.90	23.54	23.54
B	<i>Globigerinoides primordius</i> (common)	PF	260.40	261.90	23.54	23.54
B	<i>Sphenolithus delphix</i>	CN	260.98	261.18	23.33	23.33
T	<i>Sphenolithus ciperoensis</i>	CN	262.64	277.86	24.23	24.23
T	<i>Sphenolithus distentus</i>	CN	277.73	278.13	25.98	25.98
B	<i>Paragloborotalia pseudokugleri</i>	PF	277.86	282.11	25.15	25.15
T	<i>Chilogumbelina cubensis</i> (common)	PF	283.98	294.42	27.92	27.92
B	<i>Sphenolithus ciperoensis</i>	CN	288.52	289.22	27.55	27.55
B	" <i>Globigerina</i> " " <i>angulisuturalis</i> "	PF	294.42	295.44	28.89	28.89
B	<i>Sphenolithus distentus</i>	CN	306.08	316.47	30.32	30.32

Notes: T = top, B = bottom, TC = top common, BC = base common. o = oldest, y = youngest. PF = planktonic foraminifers, CN = calcareous nannoplankton, PMAG = paleomagnetic reversals. This table is also available in [ASCII](#).

Table T16. Age model, linear sedimentation rates, and mass accumulation rates, Site 1264.

Age (Ma)	Depth (mcd)	LSR	Growth Factor	Corrected LSR	Dry density (g/cm ³)	CaCO ₃ (wt%)	Total MAR (g/cm ² /k.y.)	CaCO ₃ MAR (g/cm ² /k.y.)	Noncarbonate MAR (g/cm ² /k.y.)
1	5.04	5.04	1.12	4.50	1.15	93.6	0.52	0.484	0.033
2	11.96	6.93	1.12	6.18	1.22	94.6	0.76	0.716	0.041
3	20.27	8.31	1.12	7.42	1.26	94.5	0.93	0.881	0.051
4	32.33	12.06	1.12	10.77	1.28	91.8	1.38	1.265	0.113
5	66.47	34.14	1.12	30.49	1.29	95.3	3.94	3.750	0.185
6	77.24	10.77	1.12	9.61	1.26	93.8	1.21	1.133	0.075
7	89.38	12.14	1.12	10.84	1.22	96.5	1.32	1.272	0.046
8	116.67	27.29	1.12	24.36	1.20	94.7	2.92	2.762	0.155
9	125.33	8.66	1.12	7.73	1.20	88.1	0.93	0.816	0.110
10	146.42	21.10	1.12	18.84	1.27	94.5	2.40	2.268	0.131
11	169.16	22.74	1.12	20.30	1.27	94.4	2.58	2.439	0.144
12	180.33	11.17	1.12	9.98	1.18	94.3	1.18	1.109	0.067
13	185.48	5.15	1.12	4.60	1.25	94.8	0.58	0.546	0.030
14	189.89	4.41	1.12	3.94	1.22	94.1	0.48	0.452	0.029
15	195.31	5.42	1.12	4.84	1.23	93.6	0.60	0.562	0.039
16	200.62	5.32	1.12	4.75	1.23	92.5	0.49	0.456	0.037
17	205.81	5.19	1.12	4.63	1.27	94.6	0.31	0.291	0.017
18	211.11	5.30	1.12	4.73	1.23	91.3	0.93	0.848	0.081
19	217.17	6.06	1.12	5.41	1.24	92.7	0.36	0.332	0.026
20	227.62	10.45	1.12	9.33	1.35	0.00	0.11	0.000	0.106
21	238.05	10.43	1.12	9.31	1.24	94.5	0.62	0.582	0.034
22	248.11	10.06	1.12	8.98	1.27	94.4	2.69	2.541	0.152
23	258.04	9.94	1.12	8.87	1.36	94.0	1.41	1.329	0.085
24	265.95	7.90	1.12	7.05	1.35	93.1	1.20	1.116	0.083
25	272.12	6.17	1.12	5.51	1.34	92.5	0.74	0.682	0.056
26	278.06	5.94	1.12	5.30	1.28	92.0	0.68	0.626	0.055
27	284.99	6.93	1.12	6.19	1.32	94.6	0.81	0.770	0.044
28	292.07	7.08	1.12	6.32	1.36	88.7	0.86	0.763	0.097
29	299.27	7.21	1.12	6.43	1.35	91.9	0.87	0.800	0.070
30	306.62	7.35	1.12	6.56	1.34	92.5	0.88	0.811	0.066

Notes: LSR = linear sedimentation rate, MAR = mass accumulation rate. This table is also available in [ASCII](#).